

Influence of frozen ground on seismic data

Cathrine Tangerås Eide

Thesis for the degree
Master of Science



**Department of Earth Science
University of Bergen**

August 2012

Abstract

The interest for subsurface exploration in the arctic is increasing. Thus knowledge about the effects of glaciers and permafrost on seismic data is needed. This thesis focuses on five questions that are relevant in this respect:

- How do the seismic velocities of the glacier influence seismic data?
- How does the glacier thickness affect the seismic data?
- How does the permafrost affect the seismic data?
- How do thickness variations of the permafrost layer affect the seismic data?
- How do saturation and freezing conditions in the near-surface sediments influence the seismic data?

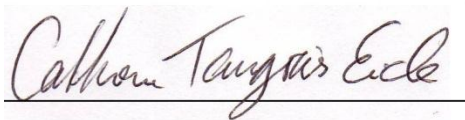
Various scenarios of glacier thickness, near-surface sediment saturation/freezing conditions and thickness variations of the near surface sediments were tested on seismic data acquired on two glaciers on Nathorst Land on Svalbard. Velocity models generated in NORSAR 2D/3D (NORSARa 2011; NORSARb 2011) and comprehensive processing using Geocluster (CGGVeritas 2008) resulted in seismic sections providing answers for the previous mentioned questions. The glacier thickness and velocities, in addition to the saturation of the near-surface sediments underneath the glacier may have a tremendous effect on the seismic data. Amplitude differences, travel-time shift and decreased continuity of the reflectors may occur if the velocity model is not in correspondence with the actual geology. When the sediments are 100% water saturated it appears as a low-velocity layer. This layer show the largest effect on the seismic data, compared to 100% ice filled sediments, if not included in the velocity model. This thesis concludes that the near-surface sediments are \approx 100% frozen.

Acknowledgement

This thesis is written at the Department of Earth science at the University of Bergen, where I've spent the last five years working towards this finished product. I wouldn't have reached this far without the help from my supervisor Professor Tor Arne Johansen and my assistant supervisor senior engineer Bent Ole Ruud. I would like to thank Tor Arne for encouragement, help and for guiding me in the right direction for creating this interesting thesis. And thanks to Bent Ole for always keeping the door open when I needed help, especially with Geocluster and NORSAR.

To all my fellow student who I've spent these year with. Thank you for all the discussions, ice creams in the sun, social gatherings and guidance. I wouldn't have made it without you, and you all have made these five years amazing.

And last but not least, I would like to thank my family for support, encouragement and always believing in me.

A handwritten signature in black ink, reading "Cathrine Tangerås Eide", written over a horizontal line.

Cathrine Tangerås Eide

August 2012

Content

Chapter 1: Introduction	1
1.1 Marine VS land seismic data	1
1.2 Frozen surface VS unfrozen surface	4
1.3 Chapter conclusion	5
Chapter 2: Acquisition	6
2.1 Exploration methods	6
2.2 Background of seismic survey	8
2.2.1 Seismic waves	9
2.2.2 Seismic parameters	10
2.2.3 Marine seismic acquisition	12
2.2.4 Land seismic acquisition	13
2.2.5 2D and 3D seismic survey	14
2.3 Acquisition on glaciers in Nathorst Land	15
2.3.1 Geological setting	15
2.3.2 Earlier work	16
2.4 Acquisition system	19
2.5 Chapter conclusion	20
Chapter 3: Seismic processing	21
3.1 Processing in general	21
3.1.1 Pre-processing	21
3.1.2 Deconvolution (inverse filtering)	22
3.1.3 Common mid-point (CMP) sorting	23
3.1.4 Muting	24
3.1.5 Velocity analysis	24
3.1.6 Normal moveout (NMO) correction	24
3.1.7 Stacking	25
3.1.8 Migration	25
3.1.9 Seismic velocities	29
3.2 Specific processing	29
3.2.1 Geocluster	30
3.2.2 NORSAR 2D/3D	32
3.2.3 Processing flow	33

3.3 Rock physics models.....	38
3.3.1 Elastic and seismic properties	39
3.4 Chapter conclusion.....	41
Chapter 4: The ice effect	42
4.1 Glacial effects	44
4.2 Permafrost effects.....	50
4.2.1 Permafrost effect; variable permafrost thickness.....	52
4.2.2 Permafrost effect; constant permafrost thickness	57
4.2.3 Permafrost effect: constant VS variable thickness.....	61
4.3 Interpretation	61
4.4 Chapter conclusions	62
Chapter 5: Discussion	63
5.1 Acquisition.....	63
5.2 Processing.....	63
5.3 Scenarios	65
5.3.1 Glacial effects	65
5.3.2 Permafrost effects	68
5.4 Chapter conclusion.....	71
Chapter 6: Conclusion.....	72
6.1 Summary and conclusion	72
6.2 Further work.....	73
References	75
Appendix A	78
Appendix B.....	85
Appendix C.....	88

Chapter 1: Introduction

1.1 Marine VS land seismic data

Seismic surveying is the most widely used geophysical method to determine the earth's properties with the help of physical principles (Park 2007). By sending a seismic (or elastic) wave down in the subsurface, a disturbance of the rock will occur. This disturbance is measured, processed and displayed, and an image of the subsurface is generated. The elastic waves are caused by a source; airgun, explosion, sledge hammer etc., as a result, multiple waves are generated; air-, direct-, surface- and body waves. Surface waves are further divided into Love and Rayleigh waves, while body waves are divided into pressure (P) and shear (S) waves.

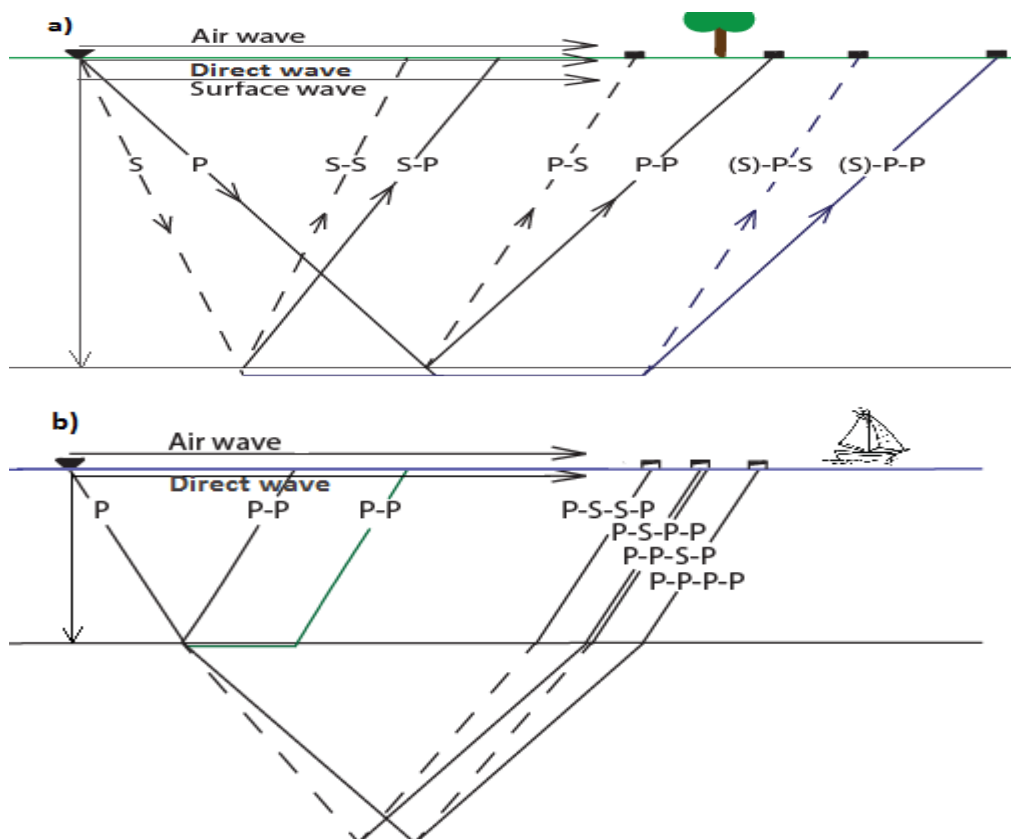


Figure 1.1: Waves generated when acquiring a) land seismic and b) marine seismic data. Both reflected and refracted waves generate P- and S- waves, while surface waves only occur on land. E.g. P-S-S-P indicates the ray path. Notice in b) the last wave is always a P-wave. The dashed line represents the S-waves, while the continuous line represents the P-wave.

Comparing marine- and land seismic data, the main difference is the free-surface in marine environments, while land seismic is masked with a variable near-surface. Acquiring data on land allows all types of waves to be registered by the geophones; direct P- and S-wave, air wave, surface and body waves (see figure 1.1 a). On the contrary, the lack of shear strength in water prevents the S-waves to propagate through the water, thus the hydrophones only register the pressure-, air- and direct waves (see figure 1.1 b). Figure 1.1 shows how the P-wave may be converted to S-waves when hitting an interface, and what may happen when the source is generating S-waves in addition to P-waves. As seen in the figure, both P- and S-waves are present in the layer beneath the sea bottom, thus a receiver on the seafloor is needed to register the generated S-waves in marine environments. Due to the different wave registration, the processing steps are quite different for the two types of data. The presence of complex surface reflectivity and ground roll, the source and receiver coupling problems, and the irregular data acquisition geometry on land, makes the pre-processing job much more important in this case, compared to the marine (Kelamis and Verschuur 2000). Comparing the traces in figure 1.2 from a) land seismic data and b) marine seismic data, apparent differences is seen. This thesis is based on land seismic data, acquired on two glaciers on Spitsbergen, and a subsequent chapter will give an overview of the comprehensive pre-processing needed.

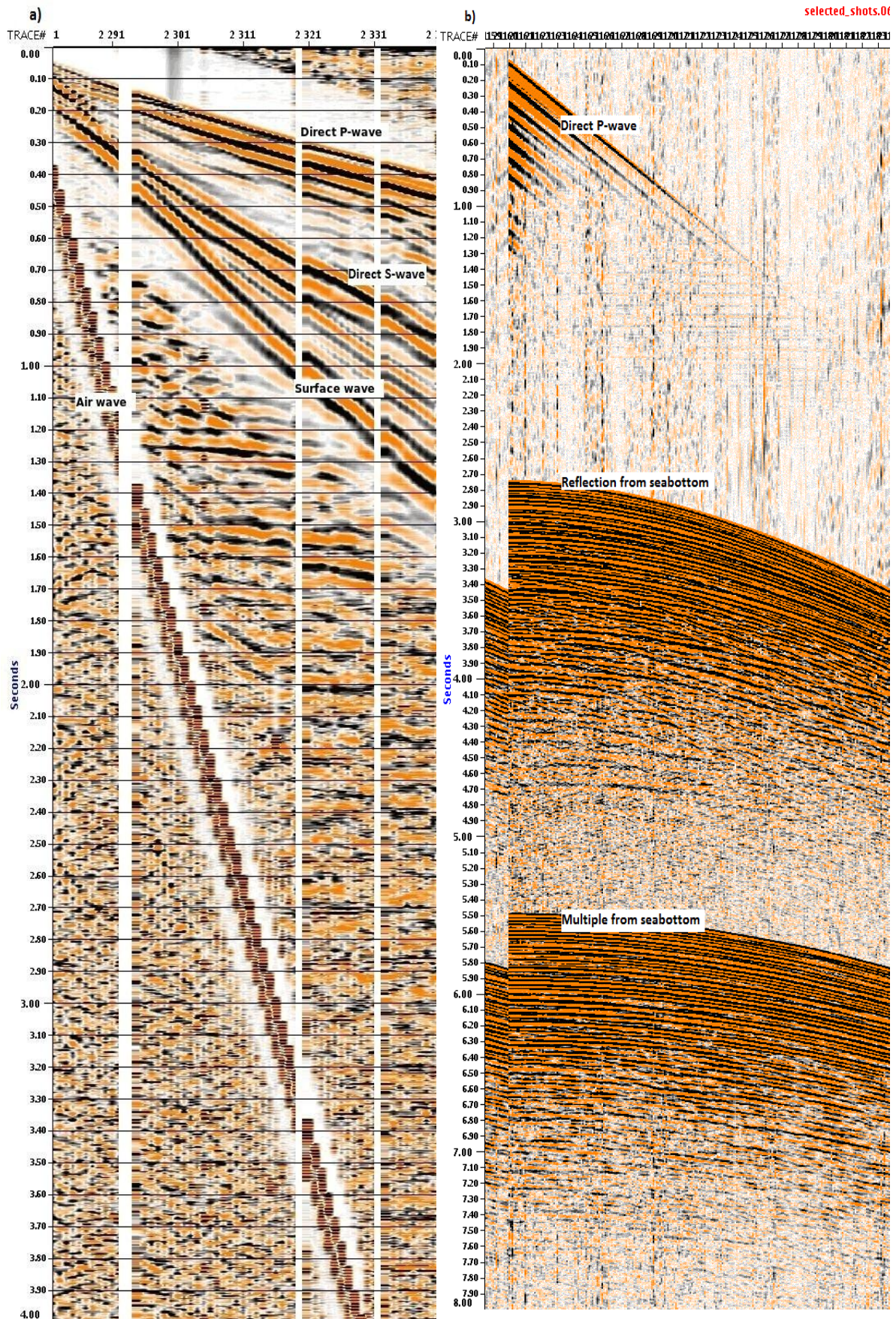


Figure 1.2: Show raw seismic data from a) land seismic and b) marine seismic. It illustrates the different waves registered in the different surveys.

1.2 Frozen surface VS unfrozen surface

In arctic environments the ground is usually dominated by glaciers and/or permafrost, which will affect the seismic data in one way or another. When the near-surface sediments are taken into account, some of the possible scenarios for the ground may be:

1. Glacier on top of frozen near-surface sediments
2. Glacier on top of partially frozen near-surface sediments
3. Glacier on top of unfrozen near-surface sediments

Velocities derived from Johansen et al. (2003) are plotted in table 1.1, which serve as basis for some of the velocity models generated for this thesis.

Table 1.1: *The seismic velocities in the subsurface corresponding to varying saturation of the rocks. Velocities derived from Johansen et al. (2003), are also shown in this thesis; figure 5.4.*

Saturation	V_p (km/s)
100% water	2.5
60% water - 40% ice	3.35
100% ice	4.28

Figure 1.3 shows examples of possible velocity profiles for three scenarios; a) marine environment, b) when the near-surface sediments are frozen and c) when the near-surface sediments are unfrozen. The profiles show how the P-wave velocities vary with depth, and indicate the strong contrast when the near-surface sediments are c) unfrozen/partially frozen, acting as a low-velocity layer, compared to the two first profiles, a) and b) where the velocity increase with depth. The results in this thesis will discuss how such varying near surface conditions affect the seismic data, also including the influence of thickness variation of the permafrost layer beneath the glacier.

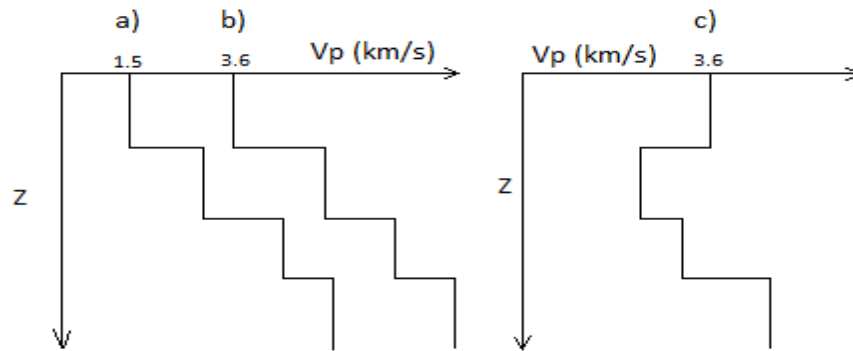


Figure 1.3: The velocity profiles for a) a marine environment, b) when the near-surface sediments are frozen and c) when the near-surface sediments are unfrozen/partially frozen. Low-velocity layers may also occur in marine environments, as beneath a glacier, but there will be no focus on marine environments in this thesis.

By combining the processing software Geocluster and the modelling software NORSAR 2D/3D, seismic models of the subsurface are studied, and interpreted with focus on variations in glacier thickness and various near-surface conditions.

The aim of this thesis is to figure out how the glacier, permafrost and the near-surface sediments are affecting the seismic data. Questions to be studied are:

- How do the seismic velocities of the glacier influence seismic data?
- How does the glacier thickness affect the seismic data?
- How does the permafrost affect the seismic data?
- How do thickness variations of the permafrost layer affect the seismic data?
- How do saturation and freezing conditions in the near-surface sediments influence on seismic data?

1.3 Chapter conclusion

The introduction chapter explains the difference between the surface-free marine seismic data and the masked near-surface land seismic data. When acquiring seismic data in arctic environments, the frozen/unfrozen ground needs to be taken into account. The main questions focused on are lined up in the end of the chapter.

Chapter 2: Acquisition

Hydrocarbons are important for the world as we know it today, so the exploration for it is a crucial part of the world's economy. The investigation of the subsurface is carried out by geophysical exploration methods, which will give information about occurring anomalies (Kearey et al. 2002) . By drilling boreholes, the same and more information may be revealed, but this method is expensive and gives information from a limited area. The seismic acquisition is just one part of the surveying; it may be divided into four stages; planning and designing the survey, data acquisition, processing and interpretation. Exploration of the subsurface is not only used in oil and gas prospecting, other areas of interest are (Asghar 2011):

- Measurement of the bedrock depth
- Ground water investigation
- Geotechnical purpose
- Investigation of lithospheric structures

This chapter will give an overview of different exploration methods, general acquisition, focused on seismic surveying, and then an introduction to the acquisition system used when acquiring the data studied in this thesis.

2.1 Exploration methods

Due to the different subsurface- and surface environments, varying local conditions within the survey area are needed to be taken into account in planning of the survey. The choice of source is made during the planning phase, in accordance to the geological features to be studied. Both the intensity and type of source depend on the strata of the subsurface due to varying near-surface attenuation conditions. The main geophysical methods applied in exploration are focusing on gravity, magnetic, electrical and seismic properties of the earth. These methods are limited by their operative physical constrains and depend on the focus of

the survey. Usually, one or a combination of these, is chosen to gather the wanted information (Kearey et al. 2002).

The operative physical property for gravity surveys is density, and it is measuring anomalies in the gravitational field of the earth. It will detect rock bodies in the subsurface with different densities than the surrounding rock, which means, on a small scale, a buried relief on a bedrock surface, while a salt dome may give rise to a large scale anomaly.

The magnetic method is detecting variations in the strength of the geomagnetic field in the subsurface, and the operative physical property is magnetic susceptibility and remanence. It may be performed in marine surveys, on land and in the air, so it is widely used both in small scaled engineering and archaeological surveys, and in large scale regional mapping of geological structures.

The electrical properties can be divided into at least five subgroups of electrical survey methods; 1) resistivity, 2) induced polarization, 3) self-potential, 4) electromagnetic and 5) radar. They have a relatively similar operative physical property, which is the electrical conductivity. Number 1, 2 and 3 utilize direct currents or low-frequency alternating currents in order to investigate electrical anomalies in the subsurface, while 4 use alternating electromagnetic fields of high frequency.

The seismic exploration method has an advantage over the other exploration methods due to its accuracy, resolution and presentation (Robinson 1988). Seismic surveying is the most frequently used exploration method today. It's measuring the travel time of reflected/refracted seismic waves passing through the subsurface. The operative physical property is the density and elastic moduli, and by combining these, the velocities of the waves are determined.

More detailed descriptions of the various methods are discussed by Kearey et al. (2002).

2.2 Background of seismic survey

During acquisition of seismic data, a source (airgun, vibrator etc.) creates energy, waves, that travel through the subsurface. These waves are reflected and reach the receivers on the surface. During land seismic acquisition, multiple waves are generated when energy is released from the source (figure 2.1-2.4); surface waves, divided in to Rayleigh- and Love waves, and body waves, divided into pressure- and shear wave (P- and S-waves respectively). Surface waves are generally denoted as noise when investigating the deep structures, and therefore removed by filtering during the processing. The P-wave is the primary wave which is the main source of information of the subsurface. The P-waves propagate about 60% faster than S-waves, and they can travel through both rocks and fluids, in contrary to S-waves that can't travel through fluids due to the lack of shear strength in the fluid. The equations for calculating the P- and S-wave velocities (equation 2.1 and 2.2) show that both waves are dependent on the effective shear, μ^* , and effective density, ρ^* , of the rock, but the V_p is also dependent on the effective bulk modulus, K^* . These parameters depend on the saturation in the rock; if the voids are dry, partially or fully saturated with water, ice or partially frozen water, the seismic parameters will change. This thesis will mainly focus on the case when the voids are fully water saturated, with three different saturations; 100% water, partially frozen water and 100% ice. The velocities and densities are defined by:

$$V_p = \sqrt{\frac{\frac{4}{3}K^* + \mu^*}{\rho^*}}, \quad (2.1)$$

$$V_s = \sqrt{\frac{\mu^*}{\rho^*}}, \quad (2.2)$$

$$\rho^* = (1 - \phi_0)\rho_G + \phi_0 S_w \rho_w + \phi_0 S_I \rho_I. \quad (2.3)$$

Equation 2.3 gives the effective density, where ϕ_0 defines critical porosity, ρ_G , ρ_w , ρ_I define the densities of grain, water and ice respectively and S_w and S_I denote the fraction of the voids that are water- and ice filled, respectively.

2.2.1 Seismic waves

Rayleigh wave is a wave that makes the ground move in a retrograde motion in the vertical plane. The top of the elliptical path is moving the opposite direction of the wave propagation, while the bottom is moving in the same direction. These waves make up the main part of the ground rolls energy, and are usually low-velocity, low-frequency and high-amplitude waves, denoted as coherent noise (Varhaug and Gillis 2012).

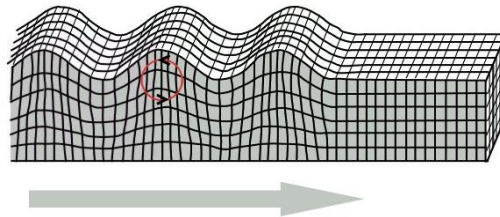


Figure 2.1: Rayleigh wave, one of the two surface waves generated. The particles move the opposite way of the energy propagation. Figure from (U.S.GeologicalSurvey and Saundry 2011).

Love waves are moving the ground from side-to-side, thus the movement is perpendicular to the direction of the wave's energy. This is the fastest surface wave, and is confined to the surface of the crust (Varhaug and Gillis 2012) .

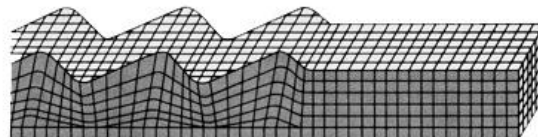


Figure 2.2: Love wave the second of the surface waves. Particles move perpendicular to the wave propagation. Figure from (U.S.GeologicalSurvey and Saundry 2011).

Pressure waves, also called primary or compressional wave are the fastest of all seismic waves. The particle movement is a pull-and-push fashion and they are moving in the same direction as the wave propagation. P-waves can propagate through both rocks and fluids, and when the incident angle on an interface is larger than normal incidence (0°), some of the P-wave energy is converted into transmitted and reflected S-waves. (Varhaug and Gillis 2012).

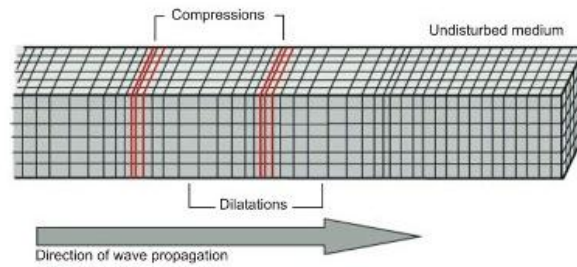


Figure 2.3 Particle motion of a P-wave. The fastest wave and the particles in the rock are undergoing compression and dilatation. Figure from (LamitCompany 2010).

Shear waves, also called secondary wave, propagate slower than the P-wave. The particle movement is perpendicular to the wave propagating, with an up-and-down, or a side-to-side movement. Contrary to the P-wave, the S-wave can only be transmitted through the rock matrix, not the fluid. By comparing the P- and S-wave of a formation, determination of rock properties; density, orientation, porosity and the fluids filling the pore space etc. may be given (Varhaug and Gillis 2012). These waves may be generated directly by the land seismic sources, but not by airguns, due to the lack of shear strength in water. The recording of S-waves is only possible when the receiver is coupled to the earth, i.e. not with a hydrophone.

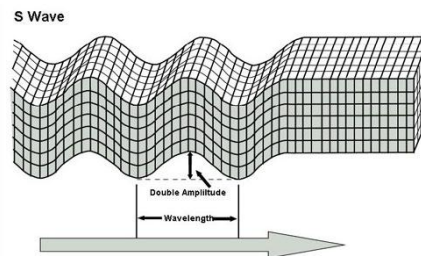


Figure 2.4: Particle motion of an S-wave. This is the slowest, and the particles move perpendicular to the wave propagation. Figure from (LamitCompany 2010).

2.2.2 Seismic parameters

When a wave hits an interface in the subsurface, it is separating layers of different acoustic impedance contrasts, which often occur when the lithology changes, and are calculated by $V_2\rho_2 - V_1\rho_1$. Some energy will be reflected (reflection seismic) and some will be transmitted before reflected towards the surface, while some waves will travel laterally along a higher velocity layer, before returning to the surface (refracted seismic). The

reflected energy is recorded and used, while the refracted is either removed or used with regards to the purpose of the survey. When the reflected energy is registered, the records the two way travel time down to the reflector. The reflector is turning up as a wiggle on the seismic trace, where the amplitude will depend on the contrast in acoustic impedance (AI).

Waves propagate spherically through the subsurface, thus the energy will hit the interface with different incident angles (θ). When the wave path is perpendicular to the interface, the reflection coefficient (R) is defines by

$$R = \frac{Z_2 - Z_1}{Z_2 + Z_1} = \frac{V_2 \rho_2 - V_1 \rho_1}{V_2 \rho_2 + V_1 \rho_1}, \quad (2.4)$$

where Z denotes the acoustic impedance, V_2 and V_1 are the velocity in the layer beneath and over the interface, respectively, and ρ is the density. When $\theta > 0^\circ$ both P- and S-waves will be generated. One approximation for the reflection coefficient, in this case the Wiggins approximation, where the assumptions are small incident angles and $V_p/V_s = 2$ are (Gelius and Johansen 2007a):

$$R_{pp}(\theta) = R_p + G \sin^2 \theta, \quad (2.5)$$

where R_p is the AVO intercept and G is the AVO gradient:

$$G = R_p - 2R_s, \quad (2.6)$$

$$R_p = \frac{1}{2} \left[\frac{\Delta V_p}{V_p} + \frac{\Delta \rho}{\rho} \right], \quad (2.7)$$

$$R_s = \frac{1}{2} \left[\frac{\Delta V_s}{V_s} + \frac{\Delta \rho}{\rho} \right]. \quad (2.8)$$

Here ΔV_p is the change in P-wave velocity from layer 1 to layer 2, R_{pp} is the reflection coefficient for a P-P wave, θ is the incidence angle and R_s and R_p is the zero-offset reflection coefficient for the S- and P-wave, respectively. AVO is the focus on amplitude VS offset, will however not be further explained in this thesis. As seen from the equations, the strength of the reflected signal is determined by the density and the seismic velocities of the media, which are the most important parameters in seismic analysis. The product of these properties gives the acoustic impedance, denoted Z in eq. 2.4, which again dictates the reflectivity.

The reflection will be negative or positive, depending on the acoustic impedance contrast. A negative reflection will occur when the upper layer has higher acoustic impedance than the lower layer, e.g. limestone over shale (negative polarity). A positive reflection occurs in case the acoustic impedance increase, e.g. gas sand above shale (positive polarity) (Cramez et al. 2007). Figure 2.5 show an example of positive and negative reflection.

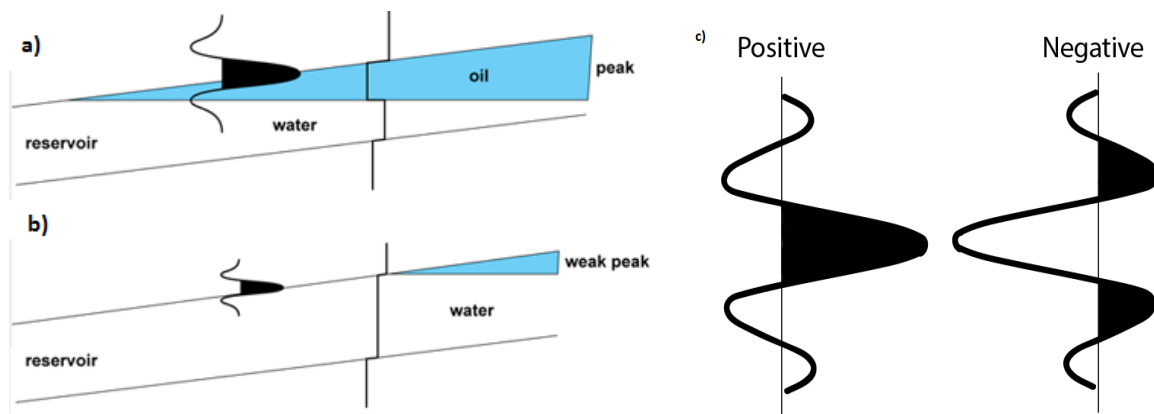


Figure 2.5: The figure (Labastie 2003) shows the change in a wiggle amplitude for various acoustic impedance contrasts. Here it is in case of a) before and b) after production. C) shows example of positive and negative polarity.

In addition to primary reflections, multiples may occur. This is energy trapped between interfaces in the subsurface. It may be multiples from the sea bottom, or in between different layers in the ground. The sea bottom multiple is very strong due to the large reflection coefficient at the seafloor. These multiples show up in the traces, and will be misleading in the interpretation of the subsurface if not removed.

To acquire seismic data, a type of source and receivers is needed, which varies from land- to marine seismic surveying. Vibrator, airgun, detonation fuse and dynamite are all standard ways to generate the necessary acoustic or elastic vibrations needed.

2.2.3 Marine seismic acquisition

Marine seismic is the main source for hydrocarbon exploration offshore. It is conducted by either placing the receivers on the sea bottom (OBS) or drag them after a marine seismic

vessel in various configurations towing cables, while generating a shockwave by firing an airgun approximately every 10 seconds (Mjelde 2010). The streamers are usually from 2500 to 12000 m long, divided into section by 100 meters, where the hydrophones are coupled in series and parallel with a group length of 6.25, 12.5, 25 or 50meters. The streamers are towed 6-9meter below the surface of the water while 10-15 'birds' on the streamers are ensuring the correct depth. Hydrophones are used in marine surveys because they detect the pressure variations in the water due to the piezo-electric plates in the hydrophones. These plates generate electricity when subjected to pressure variations (Mjelde 2010).

2.2.4 Land seismic acquisition

Land sources can be used over, on and under the surface, where the source in a borehole gives the best data (Mjelde 2008). The problem with placing a source *on* the surface, relative to within a borehole, is weaker amplitudes (figure 2.6a), stronger surface waves, strong air waves and it is difficult to get a good repeatability due to poor coupling to the ground. For acquisition on snow, detonation fuse is widely used, due to easy handling in cold and hash surroundings. Detonation fuse is referred to as an impulsive surface source; a non-impulsive surface source is Vibroseis, which is mostly used in land seismic acquisition under milder conditions (Mjelde 2008). Snowstreamers are receivers used when acquiring data on the snow, and they are built quite similar to the marine streamers; the difference is that the receivers are geophones, instead of hydrophones. The hydrophones are designed to have a good acoustic impedance match with the denser fluid, water, not air, so they will be much less sensitive in air (Mjelde 2008). The geophones are built to detect the particle movement. They have a cylindrical magnet with a coil in the middle. When the earth moves, the magnet will move in respect to the earth, and the electromagnetic induction between the magnet and the coil will generate electricity. From this electricity, the velocity of the earth movement is measured. Snowstreamers are a quick acquisition method, about 3 km/h which is 5 times faster than of the usual land technique, e.g. land cables and digital accelerometer (Mjelde 2008).

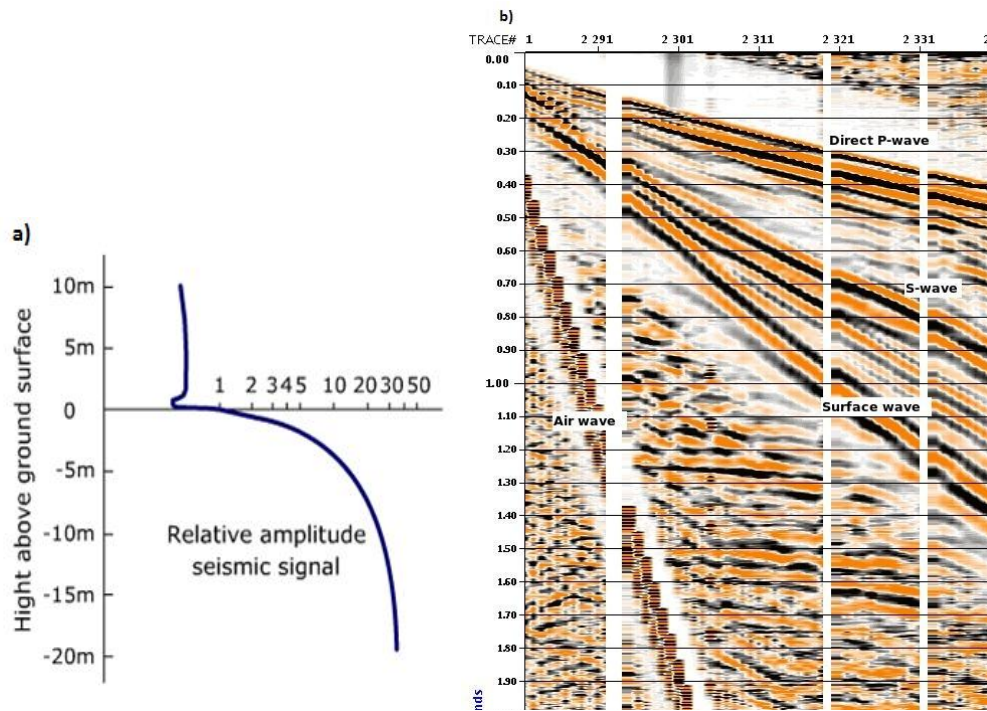


Figure 2.6: a) Shows the relative amplitude strength with the respect to the placement of the source (Mjelde 2008). B) Shows an unprocessed seismic shot gather with strong surface waves generated from the detonation source.

2.2.5 2D and 3D seismic survey

Seismic survey in two- and three dimensions are widely used. Often an acquisition survey is started with a 2D surveying in order to get an overview of the regional geological structures in the subsurface. This means a single streamer towed behind a seismic vessel, and a single source. Due to the single seismic streamer, the reflections are assumed to be just beneath the line. This may result in inaccurate and noisy results due to reflections and refractions from offline structures (RRI 2009). After the 2D survey, 3D acquisition is carried out over a known target area from the 2D survey. Since the wave front is expanding spherically, the only way to get representative illumination of an interface is to sample the entire wave front (RRI 2009). 3D are using more reflection points in an observation, which makes 3D survey much more accurate than 2D. The resulting seismic data are presented as a cube which is sampled of a range from offsets and azimuths. Figure 2.7 shows the difference between 2D and 3D surveys.

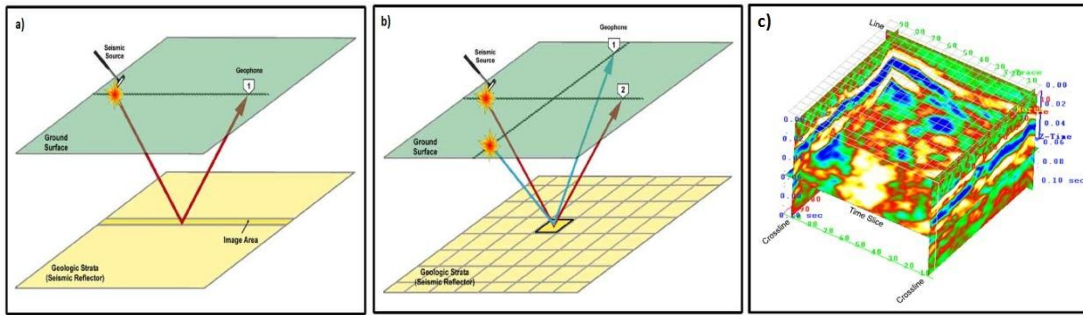


Figure 2.7: The figure show a) 2D seismic survey, b) 3D seismic survey and c) 3D resulting volume of seismic data. Figure from RRI (2009).

2.3 Acquisition on glaciers in Nathorst Land.

2.3.1 Geological setting

Svalbard is an archipelago in the Arctic Ocean at latitude 74° to 81° North and longitude 10° and 35° east, where the largest island is Spitsbergen. 60% of Svalbard is covered by glaciers, in addition to falling under the category of permanent permafrost. Nathorst Land is located in the southern part of Svalbard, and is the land between Van Keulenfjorden and Van Mijenfjorden. In the transition between Cretaceous and Tertiary, Greenland collided with Svalbard, leading to the formation of the fold and thrust belts in the west and the central basin in the east. This basin covers large part of the central-southern part of Spitsbergen, including the Nathorst Land area in the south. The rocks in the basin are of Tertiary age and a part of the Van Mijenfjorden group. This group is further divided into six formations; Aspelintoppen Fm, Battfjellet Fm, Frysjaodden Fm, Grumantbyen Fm, Basilika Fm and the oldest Firkanten Fm, and is interpreted as a regression and propagation system (Harland et al. 1997). Figure 2.8 shows a map of Svalbard, and indicates the location of the glaciers (red lines) and the borehole (red point on the close up).

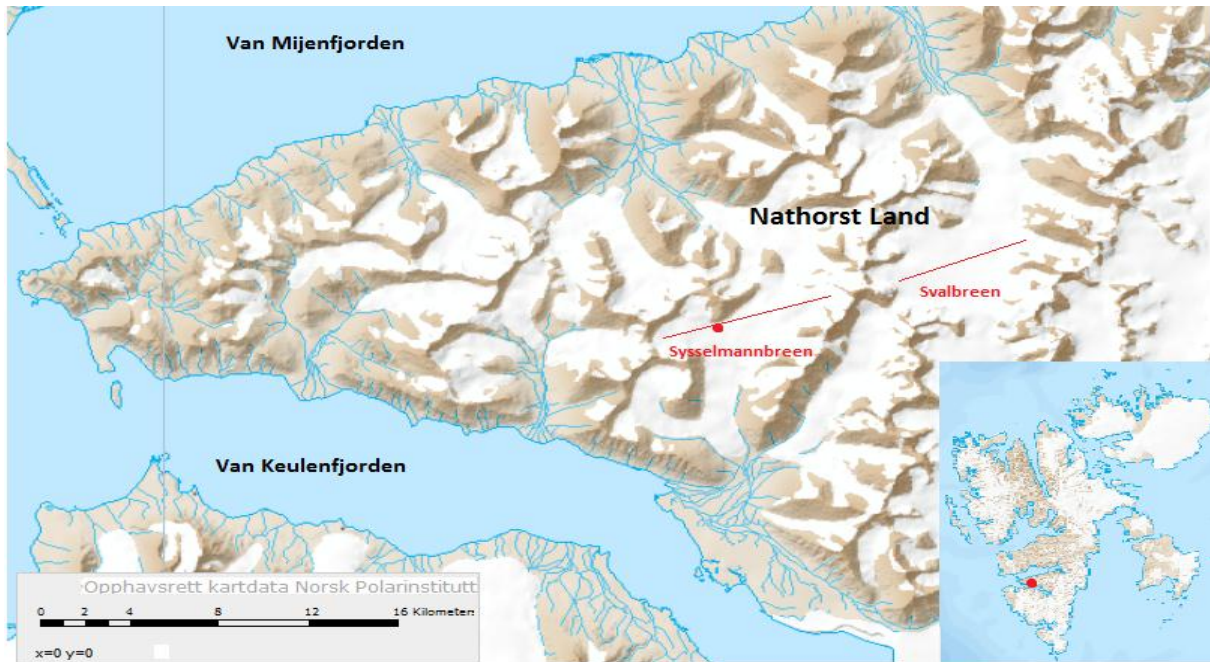


Figure 2.8: Svalbard and location of acquisition. The red lines indicate Line 1A (Sysselembreen) and Line 1B (Svalbreen). The red dot at Sysselembreen close to Line 1A shows the position of the well. Modified map from (NorskPolarinstittutt 2009)

2.3.2 Earlier work

Gautier et al. (2009) expressed in his article that about 30% of the world's undiscovered gas and 13% of the world's undiscovered oil is to be found north of the Arctic Circle (Gautier et al. 2009), this is one of the reasons why seismic acquisition in polar environments has become increasingly more interesting for oil companies. The understanding of both the development and dynamic of the upper crust in these environments is important for interpretation of the subsurface beneath the permafrost and glaciers in these areas. Even the near-surface sediments have an impact on the seismic acquisition. Johansen et al. (2003) shows that when an unconsolidated sediment, fully or almost fully, saturated with water freeze, the P-wave and S-wave velocities will have a tremendous increase and as a result the seismic resolution will decrease. The saturation of frozen ice has a larger effect on the reflectivity than the actual characteristics of the sediment, which leads to the conclusion that a combination between velocity and reflectivity is the best way to reveal saturation and freezing conditions. Freezing does two things to the seismic which is worth mentioning at this point; the first is the travel time-shift, where the reflectors appear higher in the subsurface, and the second is the reduction of the reflection coefficient. Due to the

increasing interest in the exploration for gas hydrates, the study of the actual P- and S-wave velocities have become more relevant. Other important features on Svalbard are the unique geological preservation, where the Eocene clinoforms are one of the most economically interesting preserved structures. The clinoforms in Van Keulenfjorden expose the entire deposition sequence from the basin floor shales, by the muddy slopes and all the way up to the coastal plain (Johannessen et al. 2011). This is a good example where sedimentation is taking over a passive margin, and can be used as an analogue to the Norwegian shelf and elsewhere. Information about facies and sandstone geometries in the transition between basin floors to shelf is extremely important to know when developing an exploration model. The Sysselmannbreen borehole is located north-west of Storvola and gives a complete core of the outbuilding of a clinoform. By comparing wireline logs, seismic data, cores and interpretation of outcrops from Svalbard, more precise play models may be developed and used in marine surveys. Figure 2.9 shows the log results taken from Sysselmannbreen well, including the deposition environments interpreted from the gamma-, resistivity-, and porosity-, caliper-, and density logs. This figure was used to interpret and indicate the reliability of the 'correct' model from Johansen et al. (2011) and the results found in this thesis, figure 4.13.

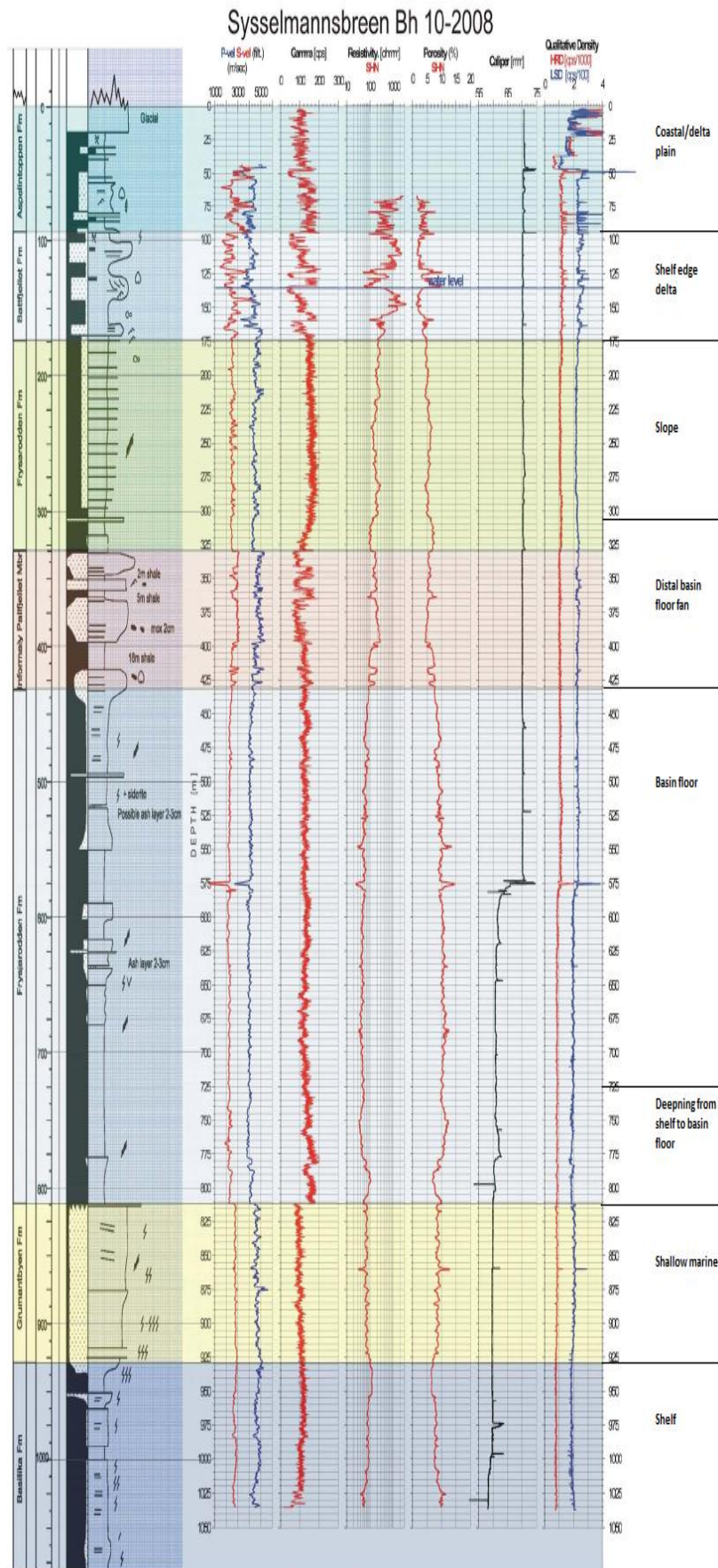


Figure 2.9: Shows a complete collection of the different logs taken from Syssemannsbreen including a deposition interpretation on the right side. Modified from Johannessen et al. (2011)

2.4 Acquisition system

Safety is the most important issue when acquiring seismic data, especially on a glacier. Crevasses and tunnel systems can occur due to melt water and ice dynamics, and can be dangerous if they're not detected. Geo-radar (Malå ProEX system) was used to monitor the glacier and create a safety zone, in addition to give important information about the thickness and shape of the glacier. This GPR is a non-destructive high resolution electromagnetic technique used to illuminate the uppermost part of the ground/glacier (Daniels 2005), before a detonation fuse is ignited to get best possible information on the subsurface beneath the glacier. The principle of geo-radar is analogous to seismic; shot energy down towards the subsurface with a source, and receivers, the snowstreamers, will receive the signal on the surface. Satellite data gave accurate GPS measurements on the elevation of the glacier. By combining satellite data and GPR data, the bottom of the glaciers elevation above the sea surface could be estimated. The thickness of the glacier was included in the initial velocity model. This information is important for later static corrections due to elevation differences between the source and receiver. Without knowing the thickness of the glacier, there may be problems interpreting the shallow structures just beneath the glacier bed. This part will be further discussed in later sections.

The seismic acquisition was carried out using a band wagon towing snowstreamers, which consisted of 60 geophone groups with eight equi-spaced 14 Hz gimbaled vertical geophones in each group. Table 2.1 gives the details of the acquisition. Detonation fuse are the most frequently used seismic source on Svalbard, this is due to its easy handling and deployment in low temperatures. In addition, the fuse is ignited in one end, so it is possible to direct the energy in the direction of interest. It also follows the strict rules on Svalbard to not leave permanent footprint in the ground. The disadvantage with placing the source on the surface is that some of the energy will go the way with the least resistance, thus out in the air, and in addition, the long duration of the source pulse will generate relative strong airwaves as seen in figure 2.6. All the information around the acquisition is from Johansen et al. (2011). Land seismic acquisition in other arctic environments, geophones and borehole sources are normally used, instead of the detonation fuse.

Table 2.1: Details about this seismic acquisition operation (Johansen et al. 2011).

Seismic acquisition	
Length of snowstreamer	1500 m
Number of geophone groups	60
Group interval	25 m
Length of geophone group	21.5 m
Distance between shots	50 m
Length of detonation cord	50 m
Weight of each shot	4 kg (\approx 6.6 kg TNT)
Near offset	125 m
Sampling rate	2 ms
Recording time	4 s
CMP fold	15
Distance between CMP points	12.5 m

2.5 Chapter conclusion

This chapter includes a description of various acquisition methods and give some background information about seismic data acquisition. GPR and GPS obtained information on the geometry of the glacier, while the detonation fuse was the source for the acquired seismic data and obtained information of the subsurface. The main difference between acquiring and processing seismic data on land and in marine environment are the more complex masked near-surface land seismic. The geological setting of the study area, Nathorst Land, and a small introduction on earlier work is presented. The specific acquisition parameters on Nathorst Land are listed at the end of the chapter.

Chapter 3: Seismic processing

To obtain a confident geological cross-section of the subsurface, a series of processing modules must be executed. No processing flow is the same; it is unique from one survey to another. However, processing should commonly consist of; pre-processing, deconvolution, velocity analysis, normal move out (NMO) correction, stacking (pre- or post-stack) and migration. This chapter will explain these general processing steps, in addition to the specific processing flow for this thesis. Subsequently sections explain the rock physic models used for deriving the velocities used in the processing of some of the resulting seismic sections in this thesis.

3.1 Processing in general

The main purpose of processing seismic data may be summed into two steps:

- Enhancing the signal to noise ratio,
- Display the results in a way so that the information of the geological structures is obtained.

3.1.1 Pre-processing

Yilmaz (2001) divides the pre-processing into five main steps, starting with demultiplexing. When the seismic data is acquired, it is stored in a multiplexing mode. The demultiplexing converts this data into another format, usually the Society of Exploration Geophysicist (SEG-Y) format, which is the common format for processing. Trace editing is the second step, which is the removal of damaged traces or traces overpowered with noise. Traces may be damaged due to problems with the receivers or other unexpected events. If there is need for a polarity inversion, it is done in this step. (Yilmaz 2001). The third step is filtering of noise. Noise is categorized into non-linear (multiples), linear (diffraction and refractions) and ambient (rain, wind) noise, which can be removed with deconvolution techniques, FK-filtering and low-pass or band-pass filters, respectively (Gelius and Johansen 2012). Forth step

is a time-variant scaling function which is used to compensate for geometrical spreading and attenuation losses. This scaling brings up the weak signals from the deep reflectors. The gain control must be used with care, since it may destroy signal character. The final pre-processing step is the merging of the field geometry and the seismic data (Yilmaz 2001). All the information on the field geometry (offset, source- and receiver locations etc.) is stored in trace-headers, which again is stored with each trace in the computer (Gelius and Johansen 2012).

3.1.2 Deconvolution (inverse filtering)

Primary reflections from deep in the subsurface may arrive at the receivers at the same time as shallow ground multiples. These multiples may have the same normal moveout and the same frequency spectrum as the primary reflectors, and will as a result, not be compressed with CDP stacking or frequency filtering (Yilmaz 2001). In order to remove these multiples from the seismic data, inverse filtering is performed. There are two kinds of deconvolution methods; spiking and predictive. Spiking deconvolution attempts to enhance the temporal resolution by compressing the wavelet in the trace, thus the output will show up as a spike. Predictive deconvolution implies the ability to predict a periodic part of the signal (e.g. the multiples), while the non-predictable parts (e.g. the primary reflections) are left, and then spiked. One important assumption for doing deconvolution is that the source wavelet is in minimum phase, otherwise a minimum phase conversion should be done in advance (Gelius and Johansen 2012). Figure 3.1 shows a flowchart for the deconvolution.

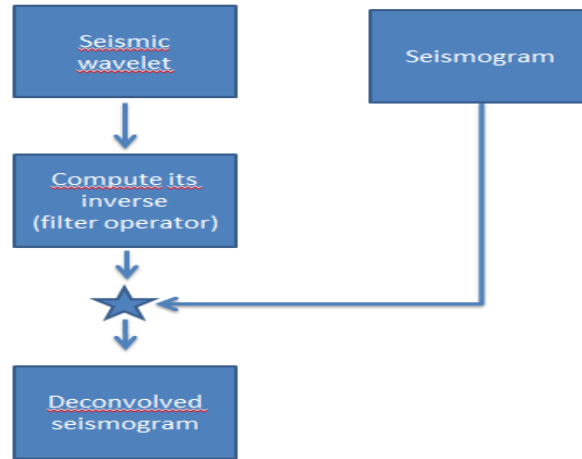


Figure 3.1: Figure from Yilmaz (2001), showing the flowchart for inverse filtering. The star denotes the deconvolution.

3.1.3 Common mid-point (CMP) sorting

During acquisition of seismic data, the traces are sorted by source and receiver coordinates. However, in order to process the data, the traces must be sorted into CMP gathers. This means that each trace is assigned to the midpoint between the source and receiver, and this is according to the geometry information in the trace headers. CMP and CDP (common depth point) is often used interchangeably, but this is only true when the reflectors are horizontal (Yilmaz 2001), see figure 3.2.

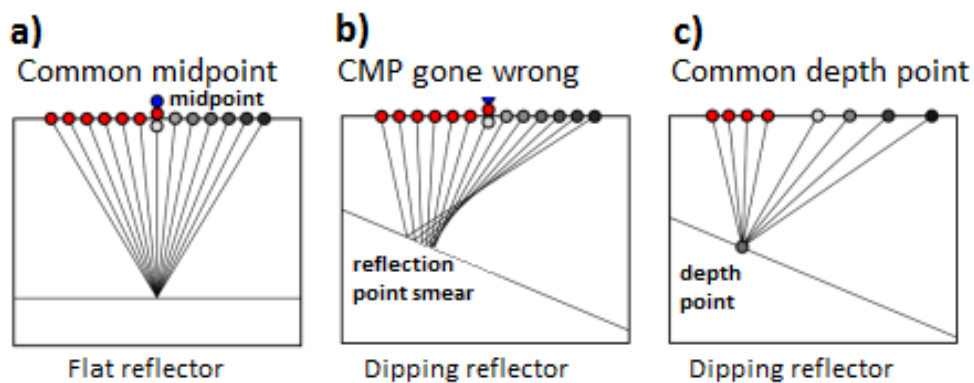


Figure 3.2: The red points represent the source, while the grey points represent receivers. a) $CMP = CDP$, while b) $CMP \neq CDP$ due to the dipping reflector and c) CDP. Figure from (Bianco and Hall 2011)

3.1.4 Muting

This step set the beginning of selected traces to zero, in order of removing noise preceding the first arrivals. The muting will remove energy from the direct wave, the water layer and the refracted waves (Gelius and Johansen 2012), and is an effective method for removing noise.

3.1.5 Velocity analysis

Before stacking the CMP gathers, a velocity analysis and normal moveout correction is necessary. The velocity analysis may be conducted in different ways (BPI 2005); (t^2-x^2) -analyse, constant velocity panel (CVP), constant velocity stack (CVS) or by an analysis of the velocity spectrum. The focus here will be on the velocity spectrum analysis, where velocity spectra is derived from selected CMP gathers and analysed. Assuming a horizontal layered earth model, the reflectors will appear as hyperbolas. The spectra will indicate the primary reflectors with high amplitudes, and the user is able to pick the correct velocities in order to remove the hyperbolic effects. This leads to the removal of hyperbolic events, and give a straight reflector. This velocity is used for the NMO correction.

3.1.6 Normal moveout (NMO) correction

The offset (distance between source and receiver) will increase from trace to trace during acquisition. This increase will cause a shift in travel time curve of the reflector for different offset. When the travel time changes for a single reflector, the reflector will show up as a hyperbolic event. The NMO correction has the purpose of removing this hyperbolic effect by correcting all the traces to a zero-offset. NMO is a dynamic correction, which means that the value of a single trace will be shifted with a different amount. This leads to increased stretching effect of the traces with offset, and an artificial increase of wavelength will occur (Yilmaz 2001). This stretching can be removed by muting before stacking (figure 3.3)

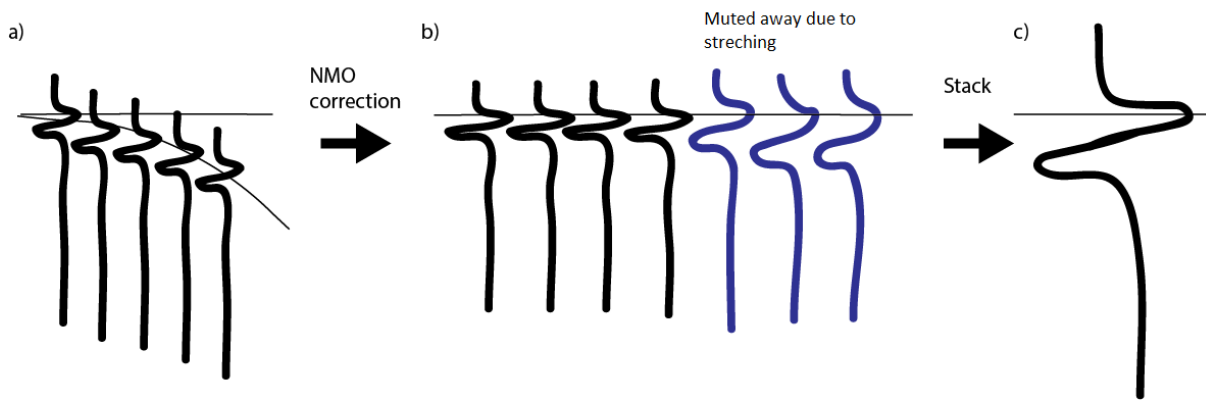


Figure 3.3: a) Hyperbolic event, when the traces reaches the receiver with increasing offset, b) NMO corrected traces where the blue traces indicate the stretched traces that must be muted away before, c) the traces get stacked.

3.1.7 Stacking

Stacking is the summations of all the NMO corrected traces in a CMP gather (figure 3.3c). This will increase the signal-to-noise ratio, and is the best way to remove multiples. The latter is dependent on a good velocity analysis.

3.1.8 Migration

Migration is the final step in the processing. This is the step that will place all dipping reflectors back to the correct location in the subsurface, and collapses the diffractions. It will increase the spatial resolution, and a seismic image of the subsurface is generated. When energy hits an edge (e.g. a fault) in the subsurface, the energy will get spherically spread and the reflections will hit the “wrong” receivers. This spreading is termed diffraction, and needs to be collapsed. In addition to diffractions, the reflections from dipping reflectors will not be registered correctly on the surface, due to the lack of CMP (figure 3.2b). Migration will correct these effects, and it may be performed both pre-stack and post-stack. Pre-stack will give the best results, but it is much more expensive and time consuming than the post-stack. This is due to the migration of every trace in the pre-stack migration, compared to the post-stack data which are stacked together in a CMP gather, and appears as a single trace. When performing pre-stack migration, the most frequently used migration method is Kirchhoff, while for post-stack, the finite difference method is usually used. One reason Kirchhoff is

used for pre-stack is due to its ability to handle a large amount of input data (Audebert 2001). The finite-difference method is based on traces in zero-offset when migrating, which is not the case during pre-stack migration. The output of a migration process is supposed to give a geological cross-section, but it is often displayed in time as for the stacked input section. To correct this, a depth conversion is carried out, and the time section is transformed to a depth section (Yilmaz 2001). There are two fundamental migration algorithms that are usually used. The algorithms are defined by the domain in which they are applied; either in the time or in the depth domain, depending on budget, time restrictions and subsurface geology structures. Kirchhoff migration is usually used when migrating in the depth domain, while Finite-difference is the main method when performing time migration (Yilmaz 2001). In order to explain these migration methods, some other concepts must be included, and Yilmaz (2001) explained this in his book.

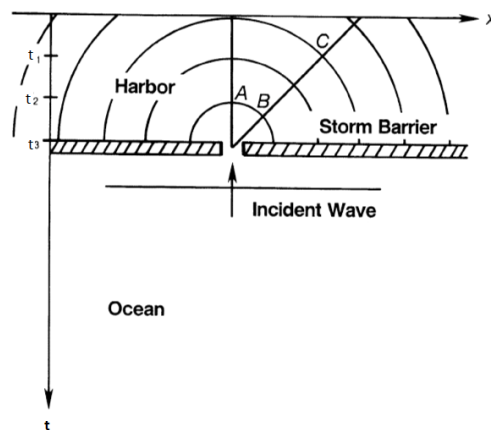


Figure 3.4: The harbour/beach example, where a plane incidence wave is hitting the storm barrier and the wave is diffracting towards the beach. Figure from Yilmaz 2001.

The beach example (figure 3.4) shows how a plane incidence wave is spreading out into semicircles when passing through a gap in the storm barrier. This gap will act as Huygens' secondary sources, which will respond as diffraction hyperbolas in x-t plane. By comparing this example to the subsurface, a reflection point on the reflecting horizon act as a gap in the storm barrier. When the reflecting points (gaps) is close enough to each other, the hyperbolas show up as the actual reflecting interface (figure 3.5 c and d). It is the same as assuming that the barrier is wiped out, so the primary wave reaches the beach/receivers. Only the diffractions on the outer edges are still apparent, which is equivalent to fault diffractions (figure 3.5 d). There are two migration methods that may be performed; one is

based on the superposition of semicircles (outdated), and the other is summation of amplitudes on a hyperbolic path (diffraction summation method) figure 3.6.

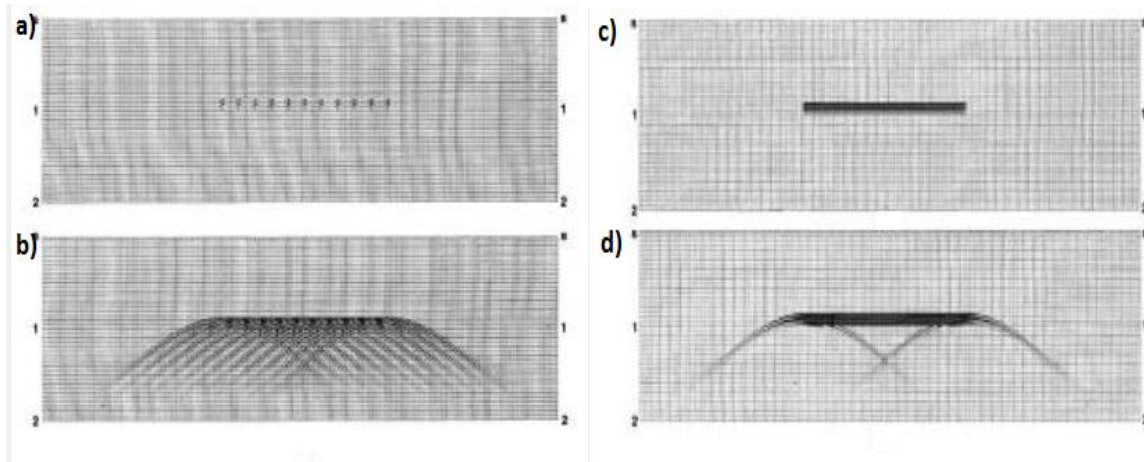


Figure 3.5: b) Superposition of a discrete number of the reflection points in a) while d) is a superposition of a continuum reflection points as in c) Figure from Yilmaz 2001.

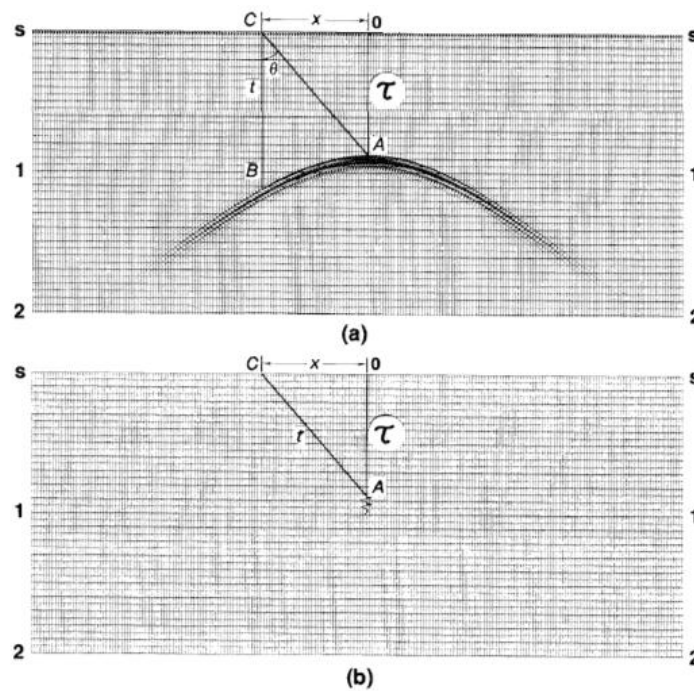


Figure 3.6: The diffraction summation method. A hyperbola is formed in a) and the energy of the hyperbola path is summed and placed on the apex. This figure is used to express the summation equation 3.1. Figure from Yilmaz 2001.

The diffraction summation method is based on finding intersect point of the hyperbola on the traces, take the amplitude at the intersect point for all the traces, and sum together. The summation is mapped onto the x-t plane. From figure 3.6 an equation for the summation is found:

$$t^2 = \tau^2 + \frac{4x^2}{v_{rms}^2}; \quad 3.1$$

where t , τ and V_{rms} are input time, output time at the apex of the hyperbola, and the root-mean-square velocity, respectively.

When a plane incident wave hit the gap and a diffraction hyperbola is formed, there are three factors that must be taken into account.

- The first is the oblique factor: since the wave front is not isotropic, the amplitude is angle-dependent. This must be corrected by taking the cosine of angle θ in figure 3.6a.
- The second is the spherical spreading factor. The further away from the source, the weaker the amplitude. This factor is proportional to $\sqrt{\frac{1}{vr}}$ for 2D- and $\frac{1}{vr}$ for 3D propagation, where v and r is velocity of the wave and distance from source to wave front, respectively.
- The third is the wavelet shaping factor. A wavelet from a hyperbolic path has a unique phase and frequency characteristic. The resulting waveform must restore both phase and amplitude after summation.

When including these three factors in the diffraction summation, it is called the Kirchhoff summation. The migration method based on this summation is called the Kirchhoff' migration. This migration method is performed by multiplying the input data with the oblique- and the spherical spreading factors, before applying a filter (pre-defined specifications) and sum along the hyperbolic path with equation 3.1. The v_{rms} velocity is typically the output time sample: apex time τ of the hyperbola.

Finite difference is explained with the same beach/storm barrier example. But instead of summing the amplitudes on a diffraction path in order to collapse the diffraction as in Kirchhoff, the hyperbola is measured from the beach. The recording cable is moved from the beach, toward the barrier in intervals. Continue to move the cable until the distance between the recording cable and barrier is zero ($t=0$), and then the hyperbola will collapse.

3.1.9 Seismic velocities

Knowledge of different velocities is important for the understanding of seismic data. Some of the most used velocities are (Kearey et al. 2002; Varhaug and Gillis 2012):

- Root-mean-square (RMS) velocity which is used when the subsurface layers consist of different interval velocities along a specific raypath. It is defined as

$$V_{rms,n}^2 = \frac{\sum_{i=1}^n (V_n^2 t_n)}{\sum_{i=1}^n t_n}; \quad (3.2)$$

where V_{rms} is the interval velocity for an n layered model and t is the two-way travel time. RMS is often much larger than the average velocity.

- The average velocity of the top n layers is the depth divided by the traveltime. It is the measurement vertically down from the surface to the reflector, and is defined as

$$V_{av} = \frac{\sum_{i=1}^k h_n}{\sum_{i=1}^k t_n}; \quad (3.3)$$

where h_n is depth, t_n is two-way travel time and $n=1,2,3\dots,k$.

- The interval velocity is the velocity within a specific layer and chosen time interval

$$V_{int} = \frac{h_n}{t_n - t_{n-1}}; \quad (3.4)$$

where t_n is the two-way travel time down to the chosen layer, while t_{n-1} is the layer above.

- Stacking velocity V_{st} is defined as the velocity value that gives the maximum amplitude when stacking traces:

$$t^2 = t_0^2 + \frac{x^2}{V_{st}^2}; \quad (3.5)$$

where t_0 , x and t is the zero-offset traveltime, the maximum offset value and the two-way traveltime to the reflecting event on the trace, respectively (Kearey et al. 2002).

3.2 Specific processing

The acquired seismic data is processed with the software Geocluster, which is a product of CGG Veritas. Geopad is the most used application in Geocluster, which is a file manager program where the different jobs are made and executed (figure 3.7). The creation of the velocity models was performed in NORSAR 2D/3D. Figure 3.11 gives an overview of the jobs that has been executed, and which output is which input in what job.

3.2.1 Geocluster

This thesis is based on the processing and interpretation of seismic data from the arctic environment. The acquired seismic data is processed with the software Geocluster 5.0, which provides a set of processing modules and applications that can be used in all aspects of processing, and can execute both single and complex functions on a seismic flow (batch mode). Batch mode is a function that will execute a command or job on a group of files all in one, instead of opening, editing and saving one file at a time, without any human intervention. Geocluster also perform interactive operations, where human and computer commands are interleaved after each single run, such as flow design, velocity analysis, and parameter definition and so on (CGGVeritas 2008). Creating a job flow is done from the Geocluster desktop, with a graphically function called XJob (figure 3.8), and it is possible to generate and submit a group of jobs related to the same survey. Subsequently section describe all the workboxes used in the jobflows and their functions.

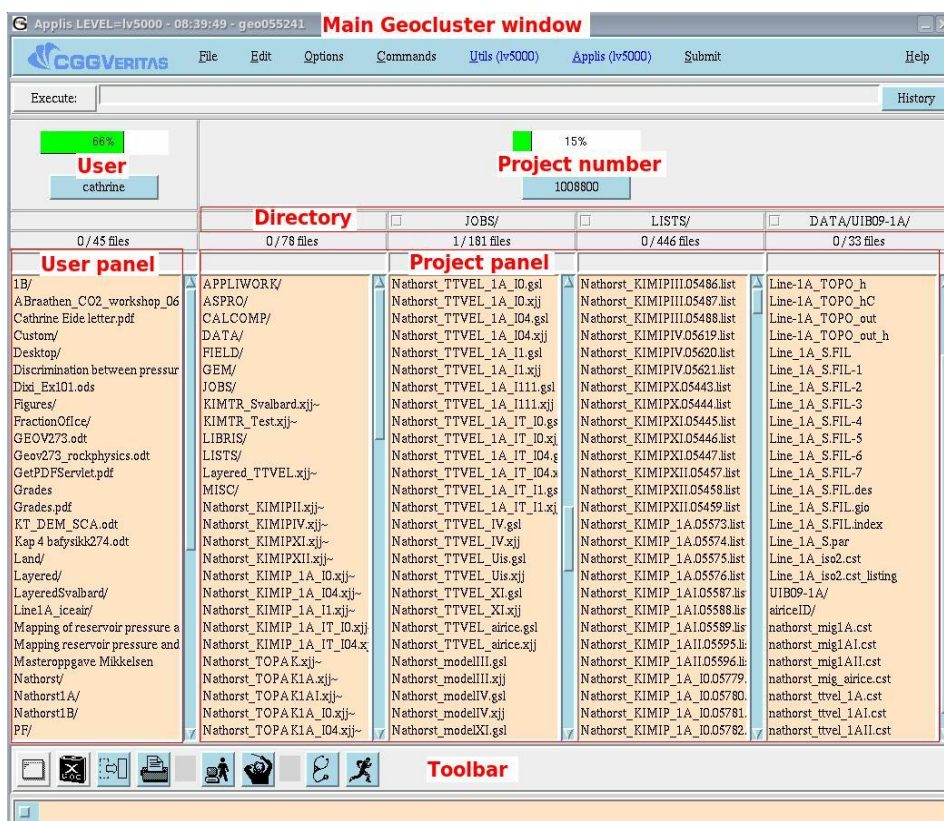


Figure 3.7: Geocluster working window.

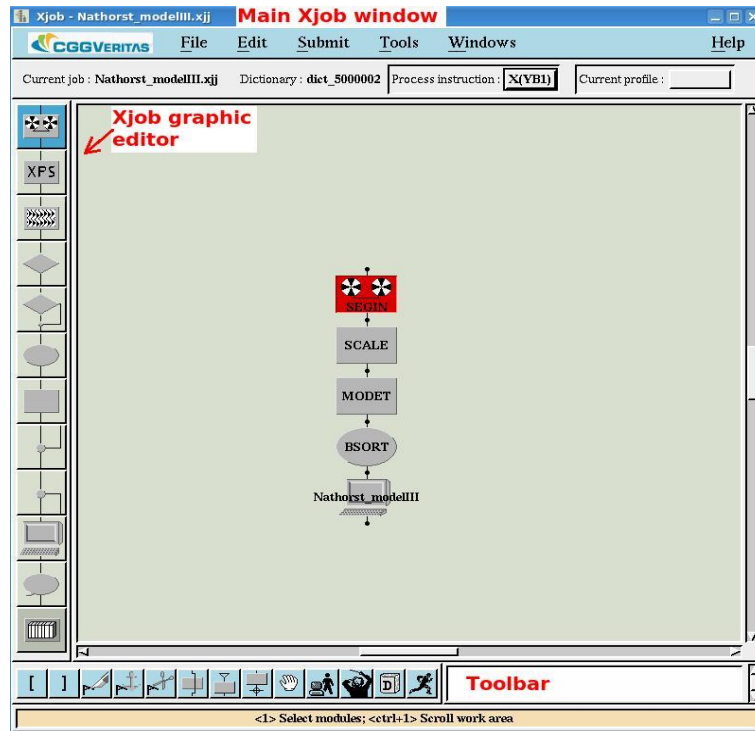


Figure 3.8: Xjob working window

Teamview (figure 3.9) displays the result after a jobflow. This module is designed for data analysis and presentation, and gives the possibility to pick horizons, water-bottom and multiples, in addition to estimation of time-shift at selected line intersections (CGGVeritas 2008).

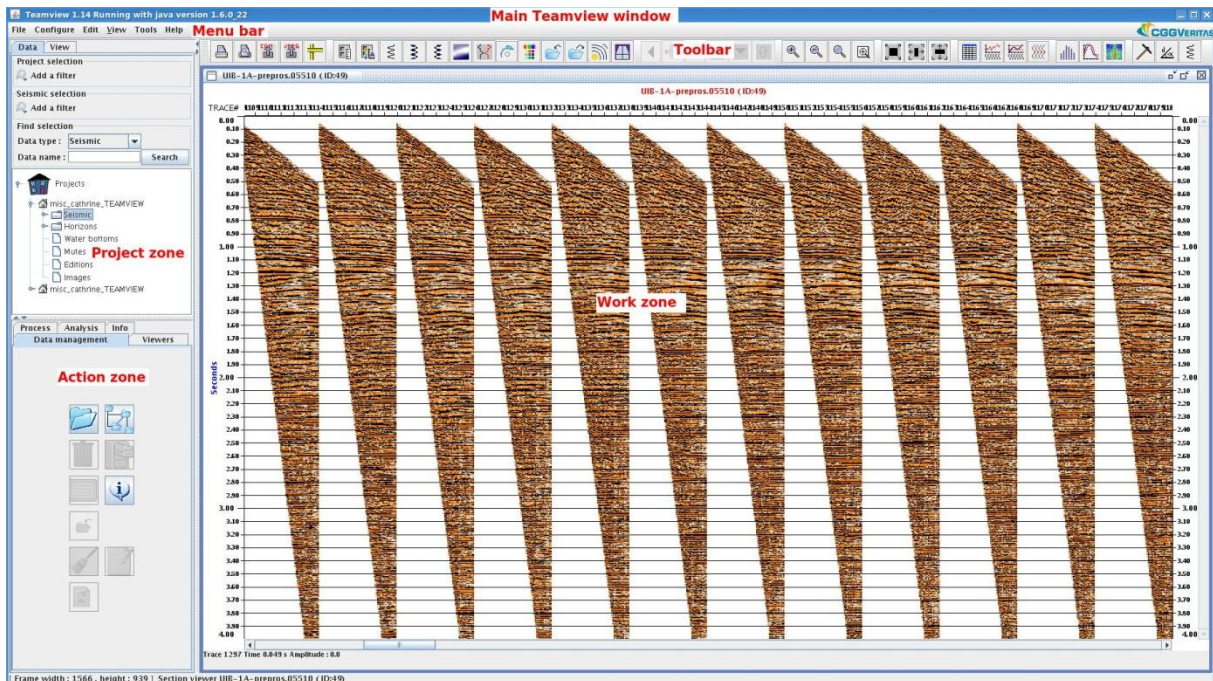


Figure 3.9: Main Teamview working window.

3.2.2 NORSAR 2D/3D

NORSAR is software used to get a better understanding of the seismic data. It has many attributes within seismic modelling and ray tracing, but for this thesis, the use is limited to model builder. In the model builder a model of the glacier is generated and appropriate velocities are assigned the layers. Two files with the .Sxyz suffix are imported to N2D; ice and topo in order to make the model geometry. Topo gives the topography of the glacier surface, given by GPS satellite measurements, while ice is the bottom of the glacier given by GPR measurements. These two interfaces create three closed apartments, and each of these apartments gets assigned a block. Figure 3.10 shows the geophysical model made after importing the interfaces for Line 1A and Line 1B with the mathematical functions representing the geophysical parameter V_p assigned to each block.

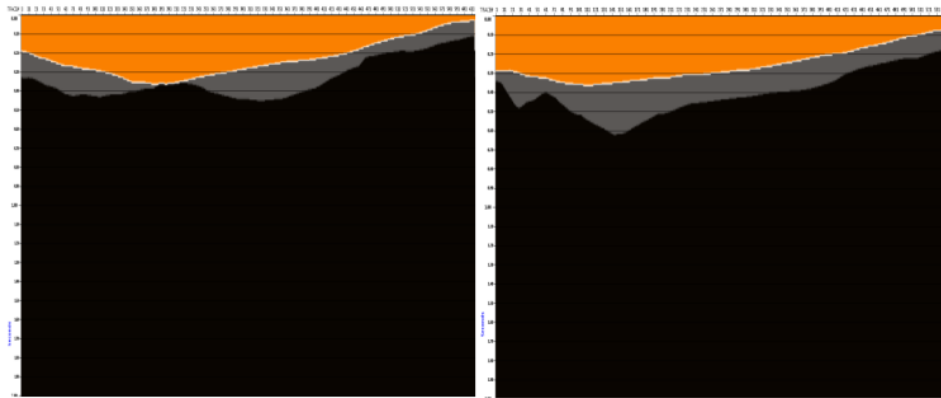


Figure 3.10: Basic models of the glaciers, Line 1A to the left and Line 1B to the right. Orange, grey and black represents air, ice and rock, respectively.

Orange, grey and black colour represents air, ice and rock respectively, with P-wave velocities 1.5km/s, 3.6km/s and 4.1km/s respectively. Model dimensions are made in “model box” which limits the model within a rectangular in the XZ-plane, horizontally and depth respectively, both measured in km (NORSARa 2011). This geophysical model of the glaciers is generated due to later pre-stack depth migration. The entire model, containing both geometry and property information, is exported and used in N3D by converting it to a seismic model interchange file (SMIF), which is an ASCII file. After importing the SMIF file into N3D, a 2.5D NORSAR-3D model is made. A 2.5D model is made by placing a number of identical 2D lines after each other (appendix B, figure 2B), creating a relatively good approximation to a 3D profile. This mean that the model varies in the x-direction, but not in the y-direction since it is not a real 3D model (NORSARa 2011). This model is now gridded to

convert the 2D data into a dense, evenly spaced 3D data volume (Lin and Holloway 1988), before a 3D working cube is defined. Table 3.1 displays the values of the 3D cube for Line 1A and Line 1B. The #Nodes gives the number of points in a 3D grid, thus $NX \times NY \times NZ$. The values are defined by taking the difference between the last- and the first CDP and adding incrementing CDP, example from line 1A: $1039 - 390 + 1 = 650$ for the X-axes. The grid dimensions have to be correct in order for the velocity model to be correctly exported into Geocluster. The last step is the exporting of the velocity model from N3D to Geocluster as a SegY file.

Table 3.1: The 3D cube properties. Line 1A to the left, and line 1B to the right.

Axes	X	Y	Z	Axes	X	Y	Z
	(km)	(km)	(km)		(km)	(km)	(km)
Low	5.02	0	0	Low	4.875	0	0
High	13.125	2.4	5	High	11.875	2.4	5
Increment	0.0125	0.1	0.005	Increment	0.0125	0.1	0.005
#Nodes	650	25	1001	#Nodes	561	25	1001

3.2.3 Processing flow

Figure 3.12 show the pre-processing flow, which is the longest and most comprehensive flow in this thesis. It also shows how the job processing window will look like when some of the steps are skipped. These skipped steps are shown with a vertical black line, for example the first HISTA job. Detailed review of the pre-processing job is found in appendix A, while Appendix B shows the resulting figure after the modelling job (table 3.4). The different jobs are explained in the tables 3.2 to 3.7. Figure 3.11 show the entire job flow, and give the overview of input and output.

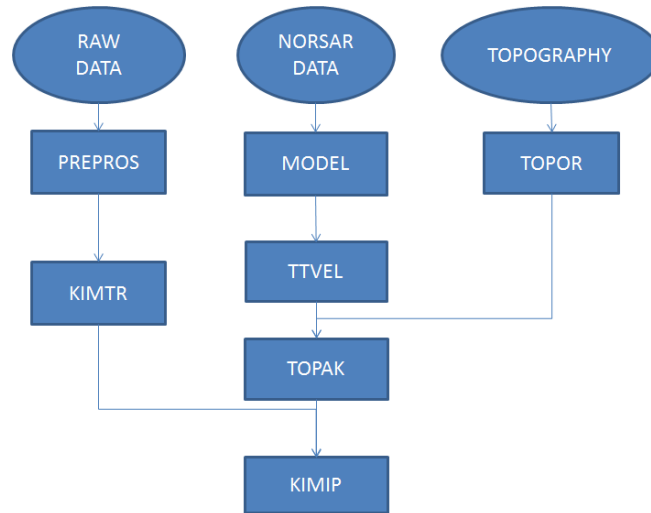


Figure 3.11: Overview of the job flow

Pre-processing:

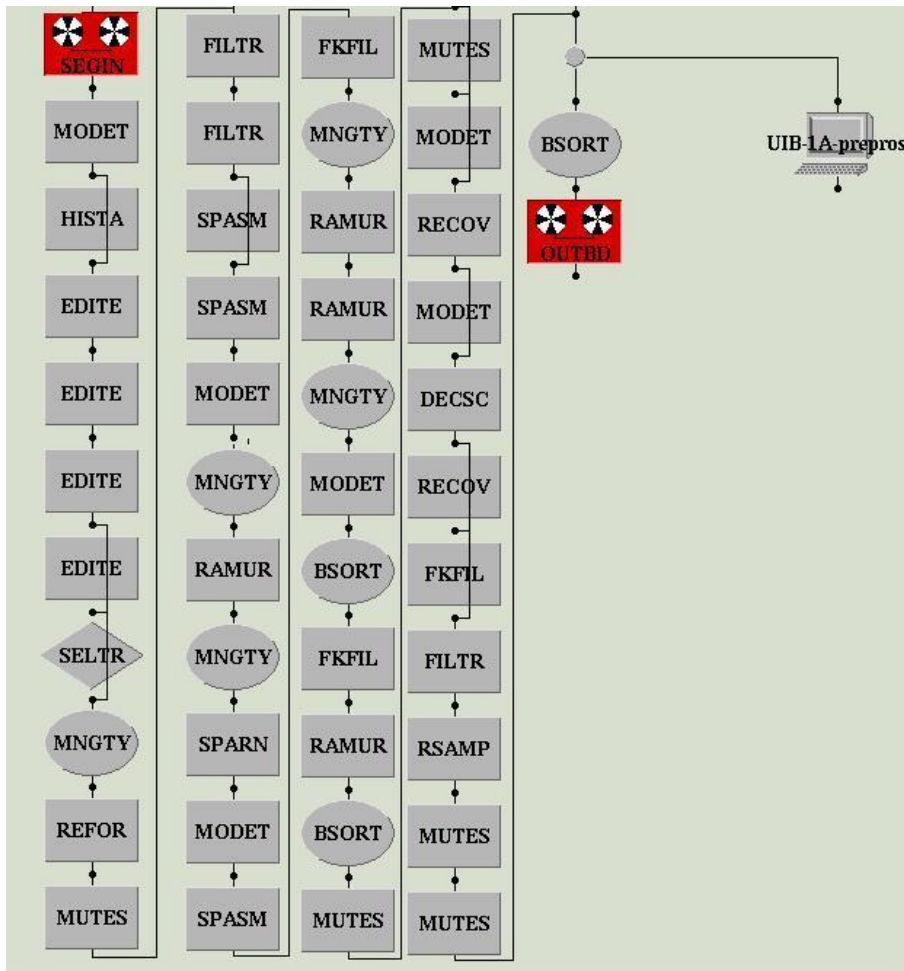


Figure 3.12: An example on how a job flow may look like; in this case it is the comprehensive pre-processing flow for the land seismic data collected for this thesis.

Table 3.2: Brief explanation for the different job boxes.

No.	Module	Purpose
1	SEGIN (Input/Output)	Reads the SEG Y data files, and transforms these into a Geocluster format.
2	MODET (Data management)	Mathematical function in order to modify a trace header word.
3	EDITE (Data scaling or editing)	This module is editing the traces according to pre-defined parameters; removing bad traces, up-scaling traces etc.
4	MNGTY (Flow management)	Traces are divided into groups, and this step marks the end of the group with a flag.
5	REFOR (Time gain function)	Multiply the amplitude by $(T/250)^1$, where T is the time of the sample in ms.
6	MUTES (trace muting)	Setting traces to zero to remove disturbing traces; airwaves, noise etc.
7	FILTR (Filtering)	Applying filter operators, with or without spatial interpolating.
8	SPASM (Amplitude)	Spatial smoothing of traces within a gather.
9	RAMUR (Anti-multiple)	High resolution, de-aliasing multiple or noise attenuation in the Radon (τ, p) domain.
10	SPARN (Noise attenuation)	Signal preserving attenuation of random noise in the f-x domain
11	FKFIL (FK filtering)	Filtering traces in the FK domain.
12	BSORT (Trace sorting)	Sorting the traces in accordance to header words.
13	RECOV (Amplitude recovery)	Amplitude recovery. Increase the amplitude of the traces due to the weakening after processing.
14	DECSC (Deconvolution)	Surface consistent pre-stack spiking deconvolution

15	RSAMP (Trace resampling)	Resampling traces at a different sampling rate than on the input by using a band-limited sampling filter.
16	OUTBD (Output)	Controls that the output of the seismic traces are in Geocluster format.

The comprehensive pre-processing job is necessary for the land seismic data. Trace headers include information about the field geometry (offset, source- and receiver locations etc.). Some of the job boxes are repeated several times (figure 3.12), which underlines the complexity of the job. More details are out of the scope for this thesis.

KIMTR:

Table 3.3: Module explanation for migration preparation flow.

No.	Module	Purpose
1	INPTR	Reads the trace input from the pre-processing job. The length of the trace to be processed is 4000ms with the sampling interval at 4ms.
2	MODET	Modify the trace header. Here the mathematical function sets the 3D line number to 13.
3	KIMTR	Creates files to be migrated in later section. The library file gives the information about the acquisition geometry.

MODEL:

Table 3.4: Module explanation for model flow.

No.	Module	Purpose
1	SEGIN	Reads the SEG Y files made in N3D, so the generated velocity model can be processed. Trace length and sample interval; 5005 and 5 respectively.
2	SCALE	Gain application as a function of time. The model in NORSAR is made with velocities in km/s, while Geocluster needs it is m/s, so a scaling factor = 1000 is set.

3	MODET	A mathematical function adds 389 to the CDP number set in NORSAR in order to correlate this with the CDP number set in Geocluster.
4	BSORT	The output data from NORSAR show the seismic line as cross line, so the data is sorted into inline data in this step.
5	Output	The output file.

TOPOR:**Table 3.5:** Module explanation for topography flow.

No.	Module	Purpose
1	TOPOR	Smoothing and interpolating topography data collected during acquisition of the seismic data. This job is typical for land seismic data due to the topography difference for the acquisition line. By including the topography, the source and receivers are migrated back to their real position during the Kirchhoff migration (table 3.8).

TTVEL:**Table 3.6:** Module explanation for Travel time flow.

No.	Module	Purpose
1	RUNET	Reads the seismic data and transform it to a local format suitable for Geocluster. The input is in GCT format, which is the output format from the model job (table 3.4)
2	TTVEL	This module select and resample (in z direction) interval velocity parameters (the model job), and computes travel times for the Kirchhoff's pre-stack depth migration. The output is velocity parameters in binary format.
3	WUNET	Output in Geocluster format.

TOPAK:**Table 3.7:** Module explanation for travel time map flow.

No.	Module	Purpose
1	TOPAK	Computes travel time maps in the KIMIP Kirchhoff's depth migration flow. The input consists of velocity model and anisotropic parameters.

KIMIP:**Table 3.8:** Module explanation for migration flow.

No.	Module	Purpose
1	KIMIP	Kirchhoff pre-stack 3D depth migration. The input is the TOPAK travel time map.
2	WUNET	Output in Geocluster format.

Due to the nature of the migration program, the required input details are massive. With a 2D time migration program, the velocity model in NORSAR would not be necessary, and stacking velocities derived from a velocity analysis would be good enough. Kirchhoff pre-stack depth migration demands the interval velocities, which are set during the model made in NORSAR 2D/3D.

3.3 Rock physics models.

The purpose with a rock physical model is to bridge the macroscopic observations such as seismic, to the microscopic structure of the rock. The model must be able to describe how the seismic parameters (V_p , V_s , K and μ) are affected by the reservoir parameters (rock composition, porosity, pore fluid, saturation etc.) (RockPhysics 2012). If we are able to find the seismic parameters V_p , V_s , K and μ , we will be able to construct a model of the subsurface (Johansen 2011).

3.3.1 Elastic and seismic properties

The near-surface sediments beneath the glaciers in this thesis assumed to have a critical porosity, ϕ_0 , at 38%, and the elastic properties of a granular rock. By combining several rock physic theories (Johansen et al. 2003), the seismic parameters (bulk- and shear modulus) may be found for different saturation conditions, and then the P- and S-wave velocity is easily found with the help of equation 2.1 and 2.2. The Hertz-Mindlin contact theory (CT) is used in the case of dry voids. The assumptions behind the CT approach are that the grain aggregate is stabilized and the foundation is built up of identical spherical grains in a random packing (Gelius and Johansen 2007b). The equation 3.6 and 3.7 gives the effective bulk, $K^*=K_{CT}$, and shear modulus, $\mu^*=\mu_{CT}$, respectively, based on the CT approach (Dvorkin et al. 1999):

$$K_{CT} = \left[\frac{C_0^2 (1 - \phi_0)^2 \mu_s^2}{18\pi^2 (1 - \nu_s)^2} P \right]^{\frac{1}{3}}, \quad (3.6)$$

$$\mu_{CT} = \frac{5 - 4\nu_s}{5(2 - \nu_s)} \left[\frac{3C_0^2 (1 - \phi_0)^2 \mu_s^2}{2\pi^2 (1 - \nu_s)^2} P \right]^{\frac{1}{3}}; \quad (3.7)$$

where the C_0 is the average number of contact point between the grains, ϕ_0 is the fractions of the voids that are without ice, μ_s is the shear modulus for the solid parts, ν_s is the Poisson's ratio of the grains and P is the hydrostatic differential pressure.

When water enters the system, the bulk modulus changes, while the shear is unaffected by the input of non-viscous fluid, $\mu^*=\mu_{CT}$. The Gassmann theory (1951) consider the dry rock elastic properties, K_{CT} and μ_{CT} , and estimate the effective bulk modulus for a fully water saturated, K_{satW} , rock to be (Dvorkin et al. 1999):

$$K_{satW} = K_S \frac{\phi_0 K_{CT} - (1 + \phi_0)^2 K_W K_{CT} / K_S + K_W}{(1 - \phi_0) K_W + \phi_0 K_S - \frac{K_W K_{CT}}{K_S}}, \quad (3.8)$$

K_W is the bulk modulus for water and K_S is the bulk modulus for the solids. Further on, cementation (in this case, the ice) in the voids will affect the seismic velocities as well. Contact cement theory (CCT) may be used to find the K^* when there is small amount of cement in the composite, but when the volume fraction of cement is increased, new methods must be taken to use. There are different types of cement in the voids, one case is when grains are in contact before the cement is induced, and it is denoted contact cement. This type of cement compared to the pore-filling cement will have a larger effect on the

stiffness of the rock. Due to this, the contact cement theory (CCT) needs to be combined with an effective medium theory (EMT), in this case; self-consistence approach (SC) (Dvorkin et al. 1999) in order to take the microstructure of the composite in to account. CCT gives the effective property when there is small amount of cement in the voids, i.e. high porosity, while the combination with the EMT will give rise to the opportunity to obtain the elastic moduli at 100% cement concentration. This procedure has to be divided into three steps in order to find the K^* for different cement stages (Dvorkin et al. 1999).

The first step is to find the effective elastic modulus with CCT when there is small amount of cement. The effective compressional- (M_{CCT}), the bulk- (K_{CCT}) and the shear (μ_{CCT}) moduli are found by using equations 3.9, 3.10 and 3.11 respectively.

$$M_{CCT} = K_{CCT} + \frac{4}{3}\mu_{CCT}, \quad (3.9)$$

$$K_{CCT} = \frac{C_0(1 - \phi_0)}{6} M_c S_n, \quad (3.10)$$

$$\mu_{CCT} = \frac{3}{5} K_{CCT} + \frac{3C_0(1 - \phi_0)}{20} \mu_c S_\tau; \quad (3.11)$$

where M_c and μ_c is the compressional and shear moduli of the cement, respectively. S_n and S_τ are further discussed in Dvorkin et al. (1999). Then the second step is to look at the three-phase system (grains, cement and voids) as a two-phase system (voids and homogeny matrix), before using EMT to find the elastic properties. The output expressions are combined with the CCT expressions, obtaining two equations and solve these to find the elastic properties for the matrix.

$$K_{EMT}(\phi) = K_{CCT}(S_{CI}); \mu_{EMT}(\phi) = \mu_{CCT}(S_{CI}), \quad (3.12)$$

S_{CI} is the fraction of the void that is cemented with ice. The matrix is assumed to be identical to a pack with 100% cemented concentration, when the voids in the matrix are completely cemented.

$$\frac{1}{K_{CCT} + \left(\frac{4}{3}\right)\mu_{CCT}} = \frac{1 - \phi}{K_s + \left(\frac{4}{3}\right)\mu_{CCT}} + \frac{\phi}{\left(\frac{4}{3}\right)\mu_{CCT}}, \quad (3.13)$$

$$\frac{1}{\mu_{CCT} + Z} = \frac{1 - \phi}{\mu_s + Z} + \frac{\phi}{Z}; \quad (3.14)$$

where $Z = \frac{\mu_{CCT}(9K_{CCT}+8\mu_{CCT})}{6(K_{CCT}+2\mu_{CCT})}$. By solving these in terms of the K_s and μ_s , unique results will

be provided. The third step is to calculate a modulus when all the inclusions are cemented

(eq. 3.15 and 3.16) and one when some of the voids are cemented and some are empty (eq. 3.17 and 3.18) (Dvorkin et al. 1999):

$$(1 - \phi)(K_s - K_{fill})P_s + \phi(K_s - K_{fill})P_c = 0, \quad (3.15)$$

$$(1 - \phi)(\mu_s - \mu_{fill})Q_s + \phi(\mu_s - \mu_{fill})Q_c = 0; \quad (3.16)$$

where K_s are the bulk modulus for the solids, K_{fill} are the bulk modulus for the fully cemented matrix and the complete formulas for P_s , P_c , Q_s and Q_c are described in Dvorkin et al. (1999) p. 467.

$$(1 - \phi)(K_s - K_{eff})P_s + (\phi - \phi_e)(K_c - K_{eff})P_c - \phi_e K_{eff} P_0 = 0, \quad (3.17)$$

$$(1 - \phi)(\mu_s - \mu_{eff})Q_s + (\phi - \phi_e)(\mu_c - \mu_{eff})Q_c - \phi_e \mu_{eff} Q_0 = 0. \quad (3.18)$$

When the effective bulk- and shear moduli were found, Johansen et al. (2003) used these results, performed a numerical modelling and seismic interpretations of different scenarios. Table 5.1 Defines the properties of three granular materials; M1, M2 and M3. This thesis is focusing on material M2 with 100% water saturation.

3.4 Chapter conclusion

This chapter contains detailed description of general- and specific processing steps carried out in this thesis. The geometry and velocities in the glacier and permafrost is included in the velocity model in order to get reliable data. Different scenarios for saturation/freezing conditions in the permafrost layer was processed and compared to the correct model. Kirchhoff pre-stack depth migration was performed for get the best data. In addition, an explanation of the rock physical models used to derive the fundamental velocities used in some of the resulting seismic section in this thesis.

Chapter 4: The ice effect

10% of all land area on earth is covered with glacier ice. There are different types of glaciers; mountain-, valley- and cirque glaciers etc., in addition one can distinguish cold-, thermal- and poly-thermal based glaciers. The glaciers move due to a combination of the gravity and the weight of the glacier pushing it down causing a plastic deformation/movement (NSIDC 2012). The cold-based glaciers are frozen to the ground, while beneath a thermal glacier the water is at pressure melting point, so the glacier has a slippery surface to slide on. This causes the glacier to move faster, and crevasse may occurrence easier. It also means that the melt water underneath the glacier may keep the near-surface sediments unfrozen, which may affect the seismic data. On the contrary to seismic acquisition on land, the glacier (and marine water) is a homogeneous body which doesn't diffract and decreases the seismic energy, thus allows good seismic data to be acquired.

Permafrost is another important factor to account for when shooting seismic in arctic environments. Glaciers behave as an isolating cover on the ground, so the thickness and continuity of the permafrost is depending on the location; by the coast the thickness is much smaller than in the highlands, and it is depending on glaciers, vegetation and snow cover (Ingólfsson 2008). There are also cases when the isolation from the glacier will prevent freezing, and there might be flowing water underneath the glacier.

Scenarios with alternating glacial- and permafrost conditions are processed, and presented in this chapter. The achieved results are compared to the 'correct' model, figure 4.1a) and b). The correct model will be used throughout this thesis to refer to the model processed with the same velocity model as the resulted seismic section from the published article of Johansen et al. (2011). This is done in order to have a reliable model to compare with resulting models found in this thesis. This correct model is processed with the velocities estimated during the acquisition of the seismic data. Then by comparing it with the results achieved in this thesis, an interpretation of the glacial- and permafrost effects on the seismic is performed. Figure 4.1 shows the seismic section of the correct models for a) line 1A and

b) line 1B, where the red and green lines represent the top and bottom of the glaciers, respectively.

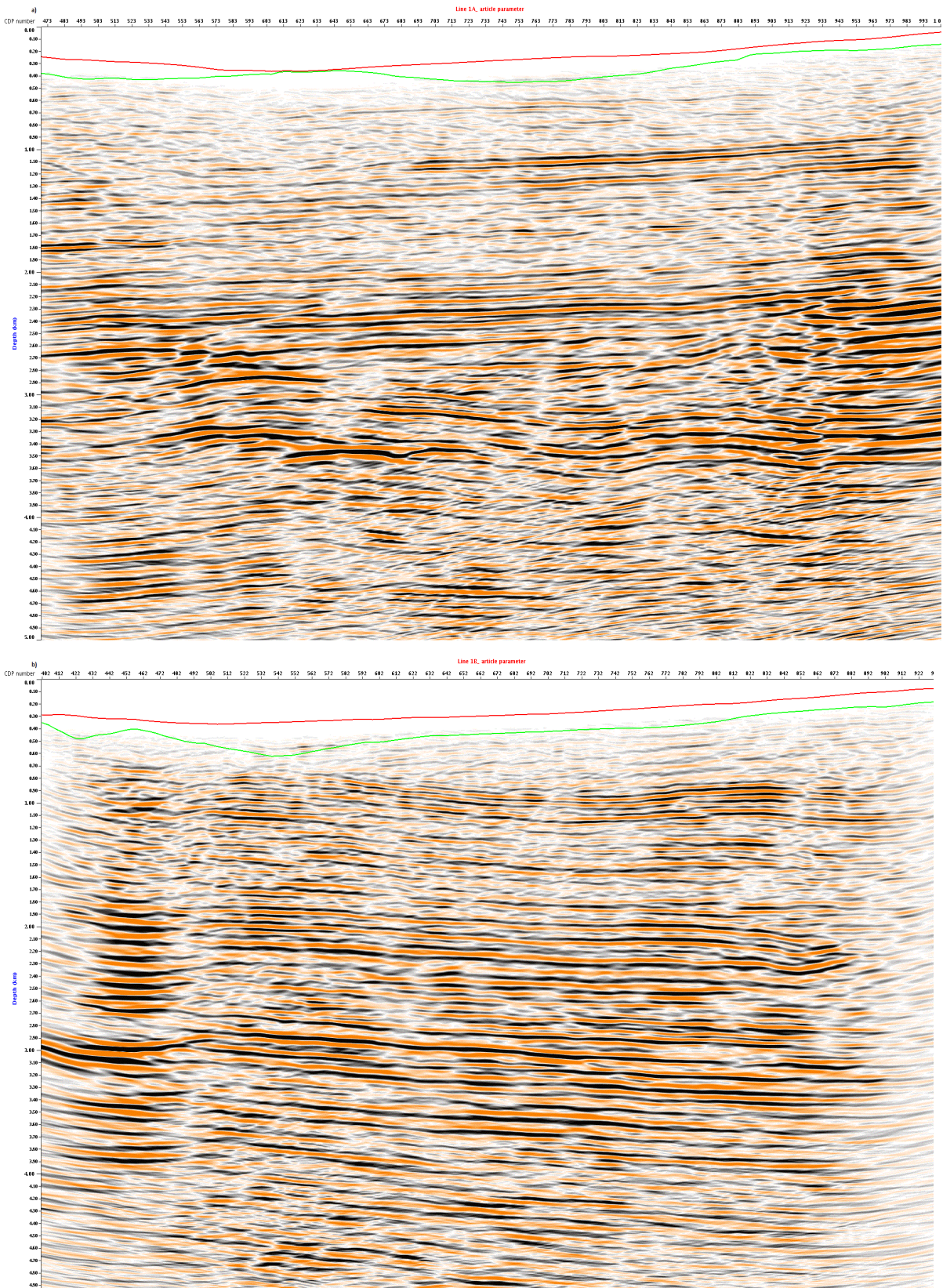


Figure 4.1: The correct seismic section of a) Line 1A, b) Line 1B. The red and green line indicates the top and the base of the glacier, respectively.

4.1 Glacial effects

Glaciers in the acquisition area may become a problem when acquiring seismic data. Velocities will differ from the glacier to the bare surrounding landscape, and will show up on the seismic section as travel-time shifts, amplitude changes or both. In this case, Line 1A and Line 1B is located on top of the glaciers Sysselembreen and Svalbreen, respectively, and the glaciers are approximately from 8m to 200m (1A) and from 125m to 300m (1B) thick. The thickness and velocities for the correct model was found during the acquisition spring of 2009 (Johansen et al. 2011). Table 4.1 gives the model parameters for Line 1A and Line 1B when modelled with three different scenarios;

1. The correct model
2. When the glaciers is neglected
3. When the glacier is 250m thicker then above

All the figures in teamview are displayed with the same scaling factor, 0.5, which is derived from the RMS values for all the amplitudes to all the traces. When applying amplitude gain control (AGC), the primary reflectors are difficult to interpret, so it is not applied to any of the resulting figures.

Table 4.1: Velocities in the different layers at the different scenarios in figure 4.2 to 4.5. The correct scenario is the values used in the actual acquisition described in the article of Johansen et al. (2011). V_{air} , V_{ice} and V_{rock} is the P-wave velocities in air, ice and rock, respectively.

Scenario	V_{air} (km/s)	V_{ice} (km/s)	V_{rock} (km/s)	Ice thickness (m)	Figure name
1	1.5	3.6	4.1	125	Correct
2	1.5	4.1	4.1	0	No ice
3	1.5	3.6	4.1	375	Thick ice

The purpose of processing the data with different scenario parameters is to see how the seismic data are affected by the neglecting of a glacier or by increasing the thickness of it, in addition to changing the velocities in the glacier when acquiring the seismic data. Figure 4.2 to 4.5 shows the finished processed result after Kirchhoff's pre-stack depth migration of Line 1A and 1B with the different scenarios. All of the comparisons show the same changes;

amplitude difference, travel time-shift and the reflectors changing shape. Figure 4.2 compares line 1A, the correct model to the no ice scenario, using the arrows and horizontal black lines to indicate the differences. When removing the 'low velocity' glacier layer ($V_{\text{ice}} = 3.6\text{km/s}$ compared to $V_{\text{rock}} = 4.1\text{km/s}$), the shape of reflectors change, and a travel time-shift occurred. To the right of the top arrow, the two close shallow structures in (a), shows up as a single reflector in (b). The top arrow indicates a reflector which has changed shape and has experiences a travel time-shift. It appears a continuity improvement when neglecting the glacier in (b), indicated with the bottom arrow. After the migration of the 'no ice' result, the waves travelled further down in the subsurface with a half a period of travel time-shift, indicated by the black horizontal lines. The reflectors in (b) appear straighter then in (a), which probably is due to the difference in velocities.

Figure 4.3 compares the Line 1A correct scenario with the case of a 250m thicker glacier. This comparison shows that when the thickness of glacier is not taken into account, the resulting figure is lacking a great deal of the reflectors. The shallowest structure, indicated by the top arrow, is non-existing in (b), in addition to the bottom arrow indicates the strong reflector which is almost vanished in (b). The amplitudes and continuity of the bottom reflector is not of good quality, and this figure is not usable for reliable interpretation of the subsurface. The black horizontal lines indicate a travel time-shift of one period, and the reflectors are moved to a shallower depth due to a thicker low-velocity layer.

Figure 4.4 is comparing the first two scenarios for line 1B. a) Shows the figure with the correct parameters, while (b) has no glacier. Looking at the middle arrow, this reflector is much more curved towards the left in (a) than (b). This straightening of the reflectors is corresponding to figure 4.2, when comparing the same scenarios at line 1A. A travel time-shift of a half a period is apparent here as is figure 4.2.

The last comparison for the glacial effects is figure 4.5, comparing the correct scenario with the thicker glacier. As for line 1A, this thick glacier scenario is not usable for a good interpretation. Most of the reflectors have disappeared and the remaining reflectors are moved one period to shallower depth.

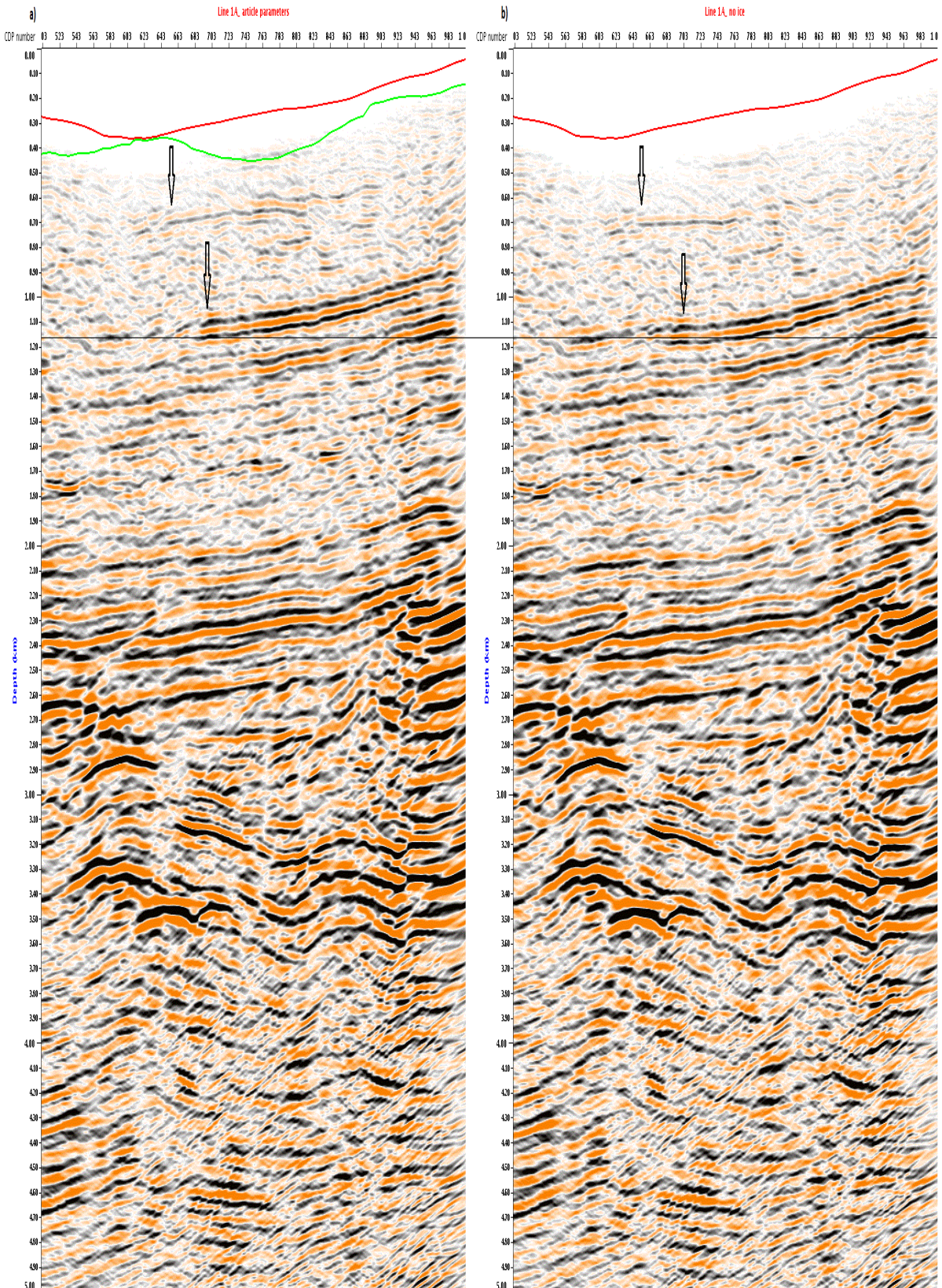


Figure 4.2: Line 1A, a) is migrated with the parameters corresponding to Johansen et al. (2011). The red and green lines indicate the top and bottom glacier respectively. b) is migrated 'without ice', so the red line is the surface where the acquisition was done. The arrows show the apparent differences, while the black lines indicate the travel time-shift.

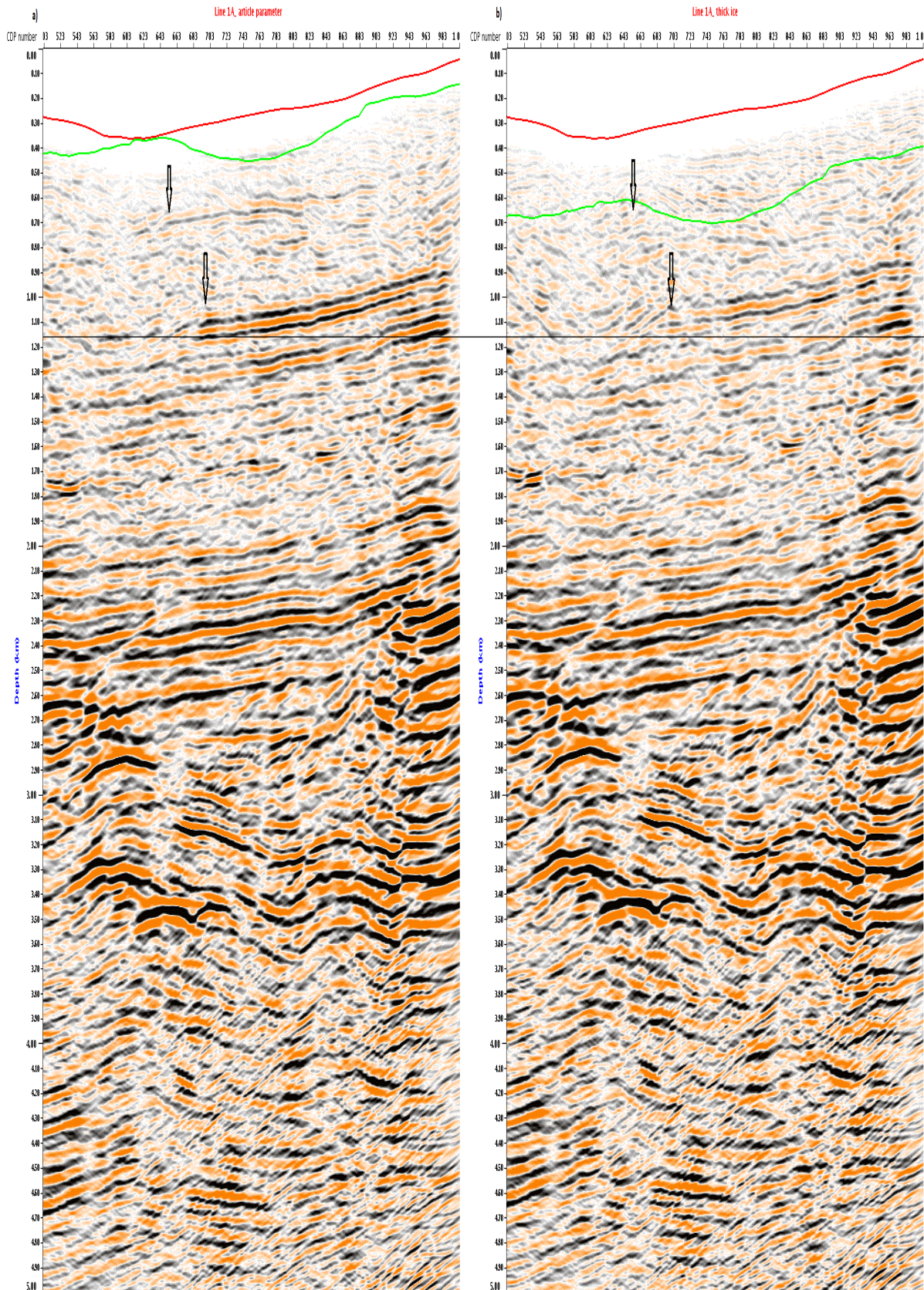


Figure 4.3: Line 1A. a) Is the correct model and b) is migrated with 'thicker glacier'. The arrows points at differences in events and the black lines show the travel time-shift. Red and green line indicates the top and bottom of the glacier respectively.

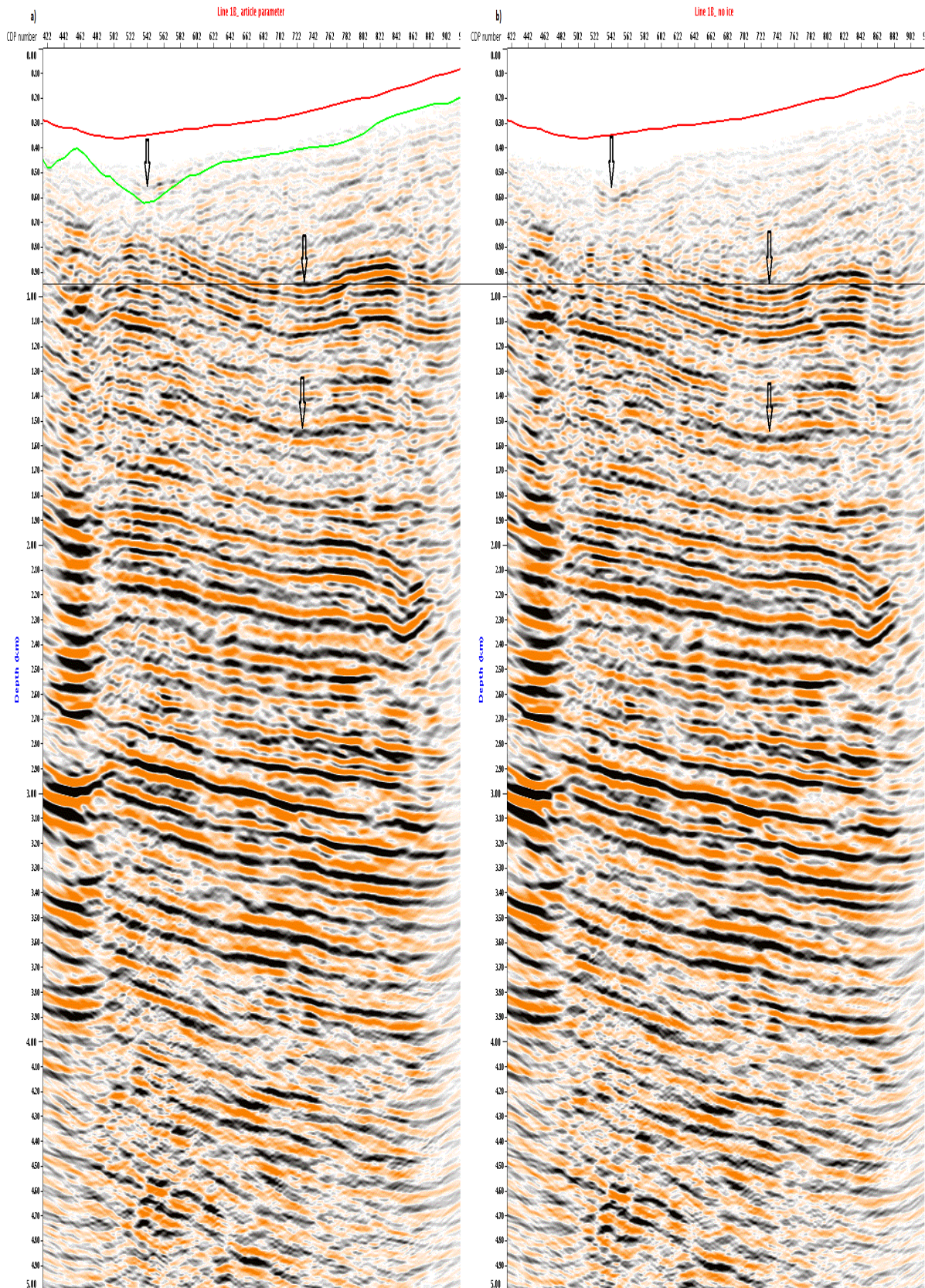


Figure 4.4: Line 1B. a) Is the correct model, b) is migrated 'without ice'. The arrows show the differences, while the black lines indicate the travel time-shift. Green and red line indicate the top and bottom glacier respectively.

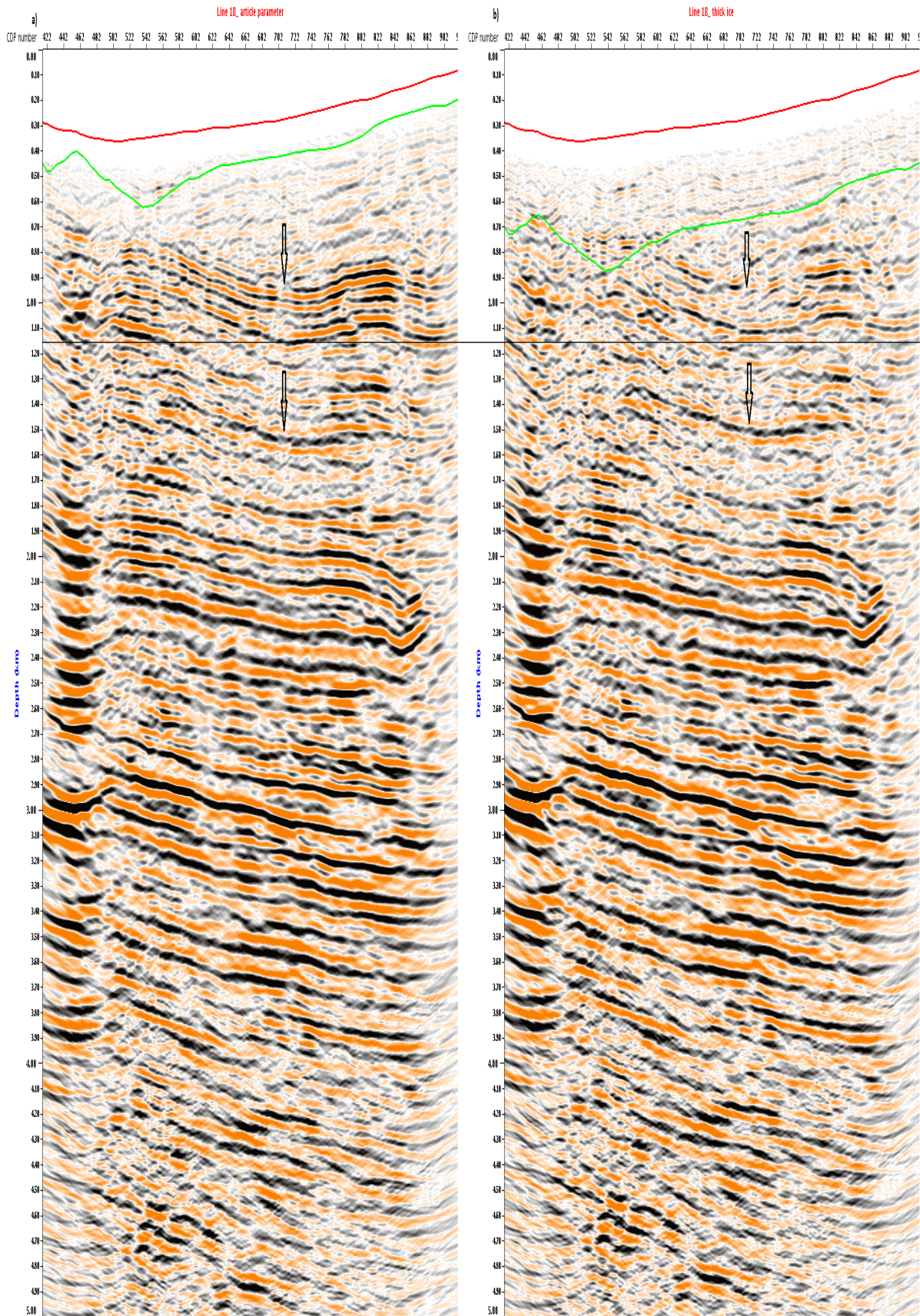


Figure 4.5: Line 1B. a) Is the correct model and b) is migrated with 'thicker glacier'. The arrows points at differences in events and the black lines show the travel time-shift. Red and green lines indicate the top and bottom glacier respectively.

4.2 Permafrost effects

This section will deal with different pore saturation/freezing conditions and how it will affect the seismic data. Johansen et al. (2003) is the source for the velocities used to figure out the saturation effects. The assumptions behind the picking of exactly these velocities are that the voids in the rock are 100% saturated and the critical porosity in the rock is $\phi_0 = 0.38$ (38%). The velocities in the air (orange), glacier (grey) and rock (black) is as before; 1.5km/s, 3.6km/s and 4.1km/s, respectively (see figure 4.6).

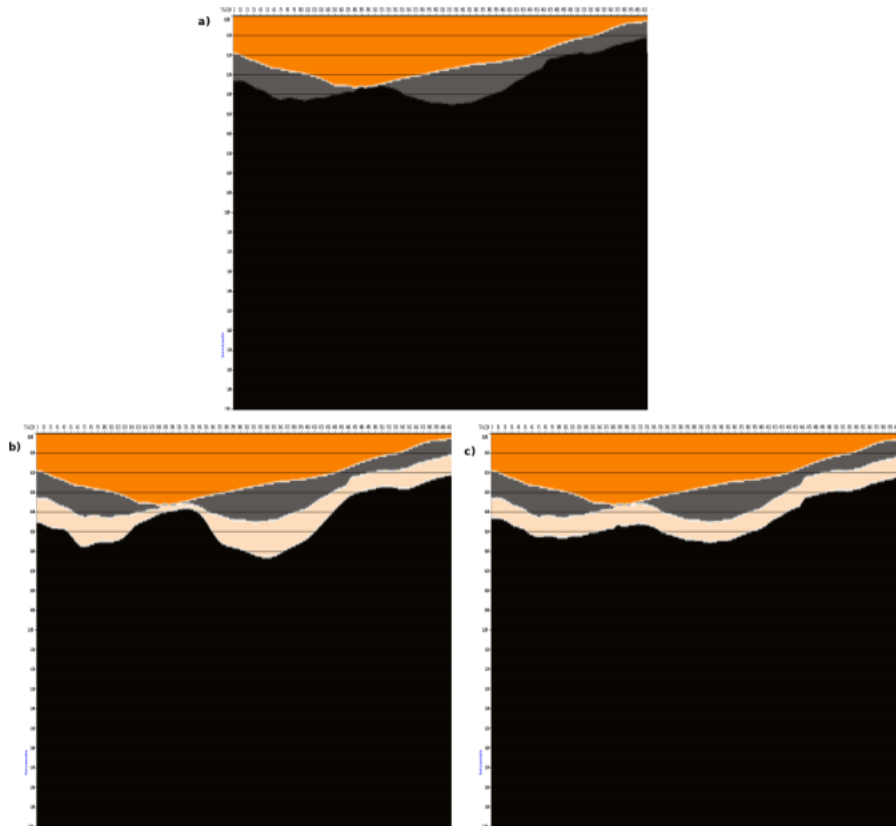


Figure 4.6: a) Show the topography of the glacier (Line 1A). B) and c) show the 100m layer beneath the glacier that is affected by the permafrost. b) show a layer with various thickness, while c) indicate a layer with continuous thickness.

Tsuji et al. (2011) wrote an article about the degree of freezing of the subglacial sediments, and how the V_s is affected by this. When looking at the surface waves (Rayleigh), the S-waves are the primary wave to focus on due to the large effect the V_s have on the surface waves, compared to V_p . Thus he used surface waves and focused on the V_s , in contrary to this

thesis's focus on V_p . He discuss two scenarios, 1) when only the glacier thickness is fixed, thus there is a lateral variation in V_s and 2) when the glacier thickness, V_s , V_p and ρ are all fixed. With fixed values in the glacier, more continuous V_s structures can be estimated in the subglacial sediments. Tsuji et al. (2012) concluded that the thickness of the glacier affects the thickness of the permafrost. It is significantly lower V_s beneath thick sections of the glacier, thus less frozen beneath thicker parts, and more frozen sediments beneath thinner parts of the glacier (see figure 4.6b). Two different scenarios are tested in this thesis; the first scenario is based upon a model where the thickness variations are taken into account. As seen in figure 4.6b, the near-surface sediments (the pink layer) are thicker beneath the thicker part of the glacier, compared to the thin layer underneath the thin part of the glacier. In contrary, the second scenario will be with a continuous permafrost thickness (figure 4.6c) and the horizon of bottom ice is copied and moved 100m down in the subsurface. These two cases were processed with variations in velocity depending on the saturation of the voids. The first is 100% water saturation in the voids of the rock and the velocity here is 2.5km/s. The next scenario is 60% water and 40% ice with a velocity at 3.35km/s. The last case is when the voids are occupied with 100% ice, here the velocity is 4.28km/s. Table 4.2 show the velocities in each of the saturation scenarios, where the velocities are derived from figure 5.3. Figure 4.7 show the velocity profile of the velocity models including the different scenarios. The comparisons will be between the correct model, and the three scenarios. This is due to figure out which figure gives the best reflectivity, continuity and overall, best information of the subsurface, and from there, figure out which scenario is most fitted for use and interpretation.

Table 4.2: Gives the velocities and names for the different saturations in figure 4.8 to 4.13.

Saturation	V_p (km/s)	Name
100% water	2.5	Topography / no topography
60% water - 40% ice	3.35	Topography / no topography
100% ice	4.28	Topography / no topography

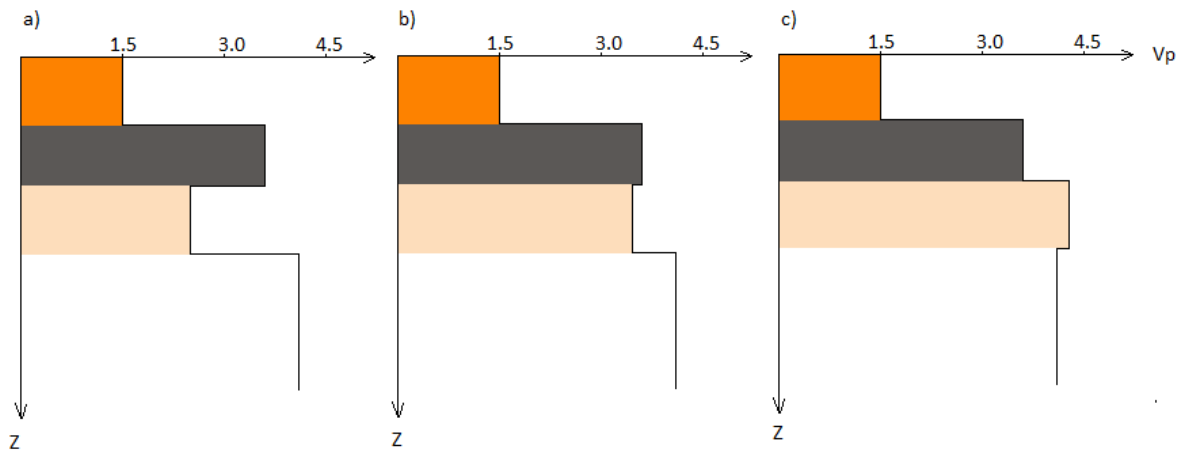


Figure 4.7: Velocity profiles for the three scenarios when included in the velocity model, see figure 4.6. a) correspond the scenario with 100% water, b) 60% water 40% ice, and c) is 100% ice.

4.2.1 Permafrost effect; variable permafrost thickness

Figure 4.8 to 4.10 compare the correct model for Line 1A, (figure 4.1a) to the three different saturation scenarios (table 4.2) in the case when there is a variable permafrost thickness. Figure 4.8 compares the correct Line 1A, with the case of 100% water filled voids beneath the glacier. As under the glacial effect section, here the differences are emphasized by arrows and horizontal black lines. The top arrow shows the top reflector in figure 4.8a) that is lacking in b). The middle arrow in b) indicates a geologically impossible structure, this artefact is not present in a). Comparing the overall structures in b) to a), it is an elevation in the middle of the figure, which is probably due to the velocity model in 4.6b). This 100m layer of 100% water filled voids ($V_p = 2.5\text{km/s}$) leads to a travel time-shift of one period towards the shallower subsurface. The two arrows furthest down indicate 'holes' in the sections that are just beneath the thickest part of the glacier, thus the thickest part of the water filled layer. As seen in the figure, the continuity is missing, the amplitudes have decreased and it is difficult to interpret the structures in this sections.

Further on, the next comparison is between the correct model and the scenario where the layer beneath the glacier is filled with 60% water and 40% ice, figure 4.9. The shallowest reflection is still not apparent in b), but the middle arrow indicates the strong reflection that has a good continuity and approximately the same amplitude strength in both seismic sections. The two bottom most arrows indicate the same 'holes' as in figure 4.8, and the

partially water filled scenario has weaker amplitudes and poorer continuity than the correct model. The saturation of 60% water and 40% ice ($V_p = 3.35\text{km/s}$) causes a travel time-shift of about a half a period, where the reflectors are shifted towards shallower ground. By comparing figure 4.8b and figure 4.9b, the latter one has more realistic shape of the reflections and the continuity and amplitudes has improved.

The last comparison is between the correct model and the scenario with a 100% frozen voids beneath the glacier (figure 4.10). There is not much difference between these figures, which is due to the small velocity differences in the ice filled layer ($V_{p_{ice}} = 4.28\text{km/s}$) and the rock beneath the glacier in the correct model ($V_{p_{rock}} = 4.1\text{km/s}$). This small velocity difference is the reason for the lack of travel time-shift in this comparison. Both of the shallowest reflectors are visible, the strong reflector with a good continuity at the middle arrow is apparent, and the two sections with decreased amplitude at the deepest arrow are not apparent. One small difference is the reflector at the bottom arrow in b) has larger amplitude than in a).

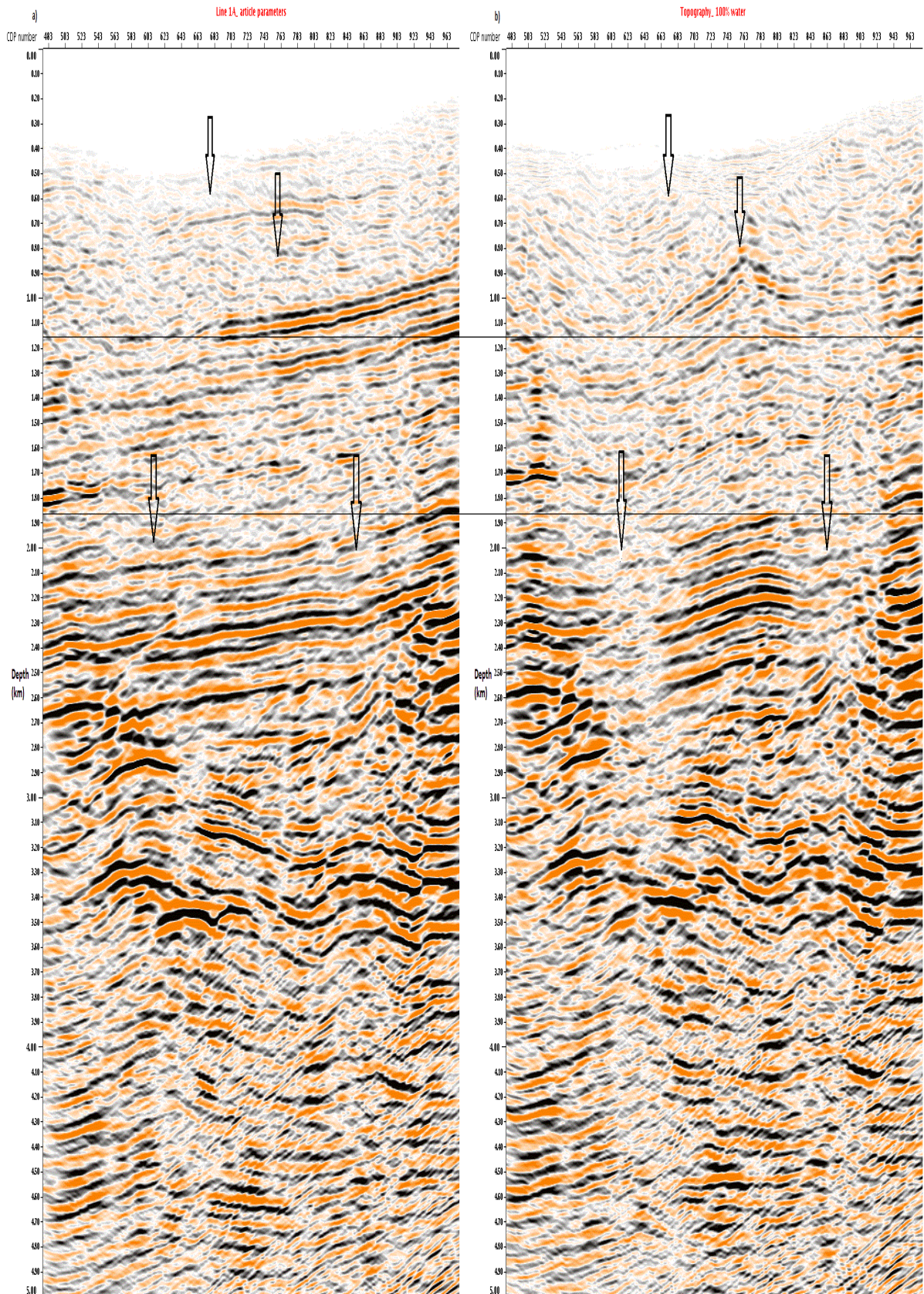


Figure 4.8: Comparison of a) the correct modelled Line 1A from Johansen et al. (2003) article, and b) the scenario when the voids are saturated with 100% water. The permafrost has a thickness variation.

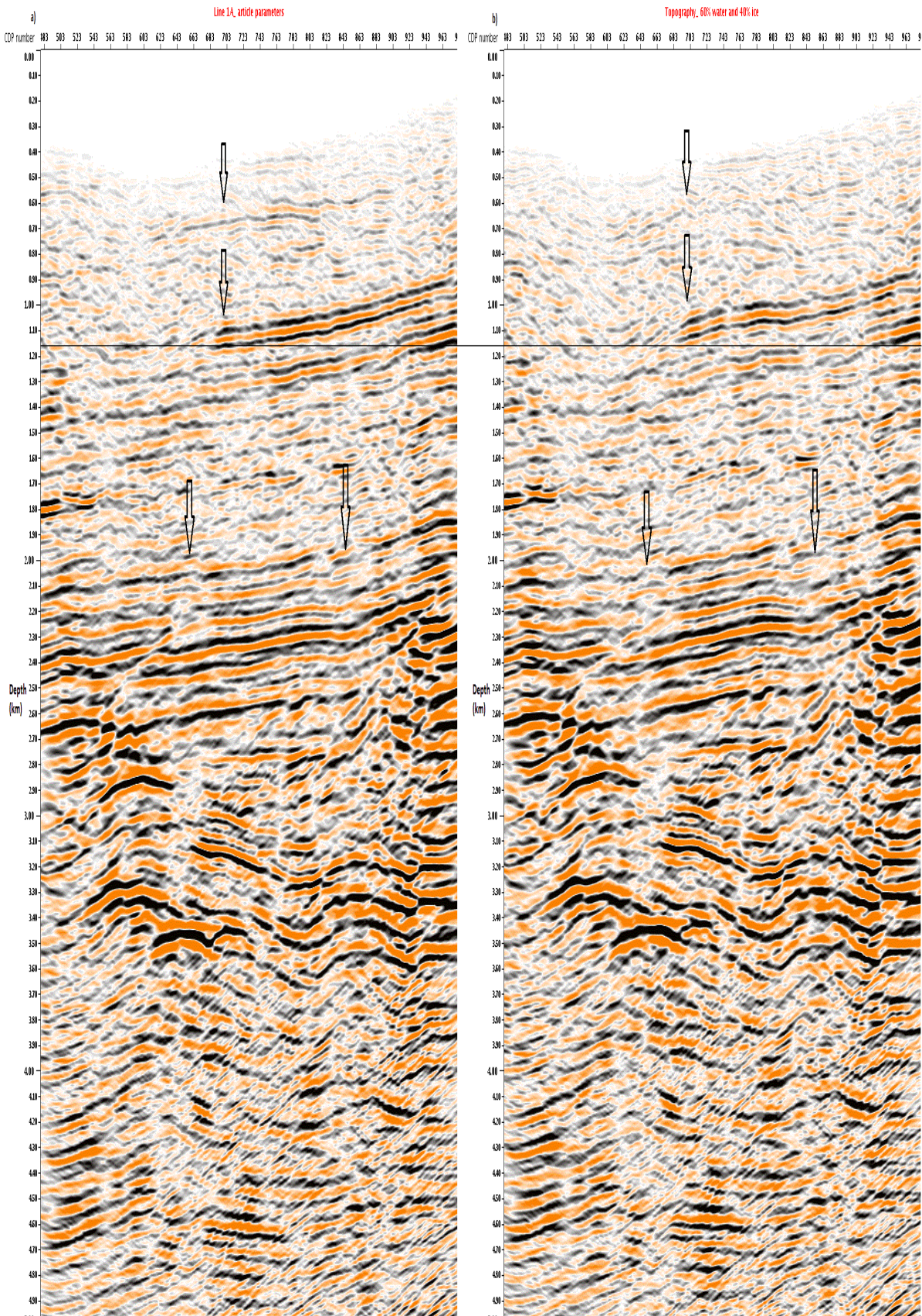


Figure 4.9: a) Is the 'correct' model, while b) is when the layer beneath the glacier is saturated with 60% water and 40% ice. The thickness of the layer is varying. Arrows and black horizontal line indicates differences.

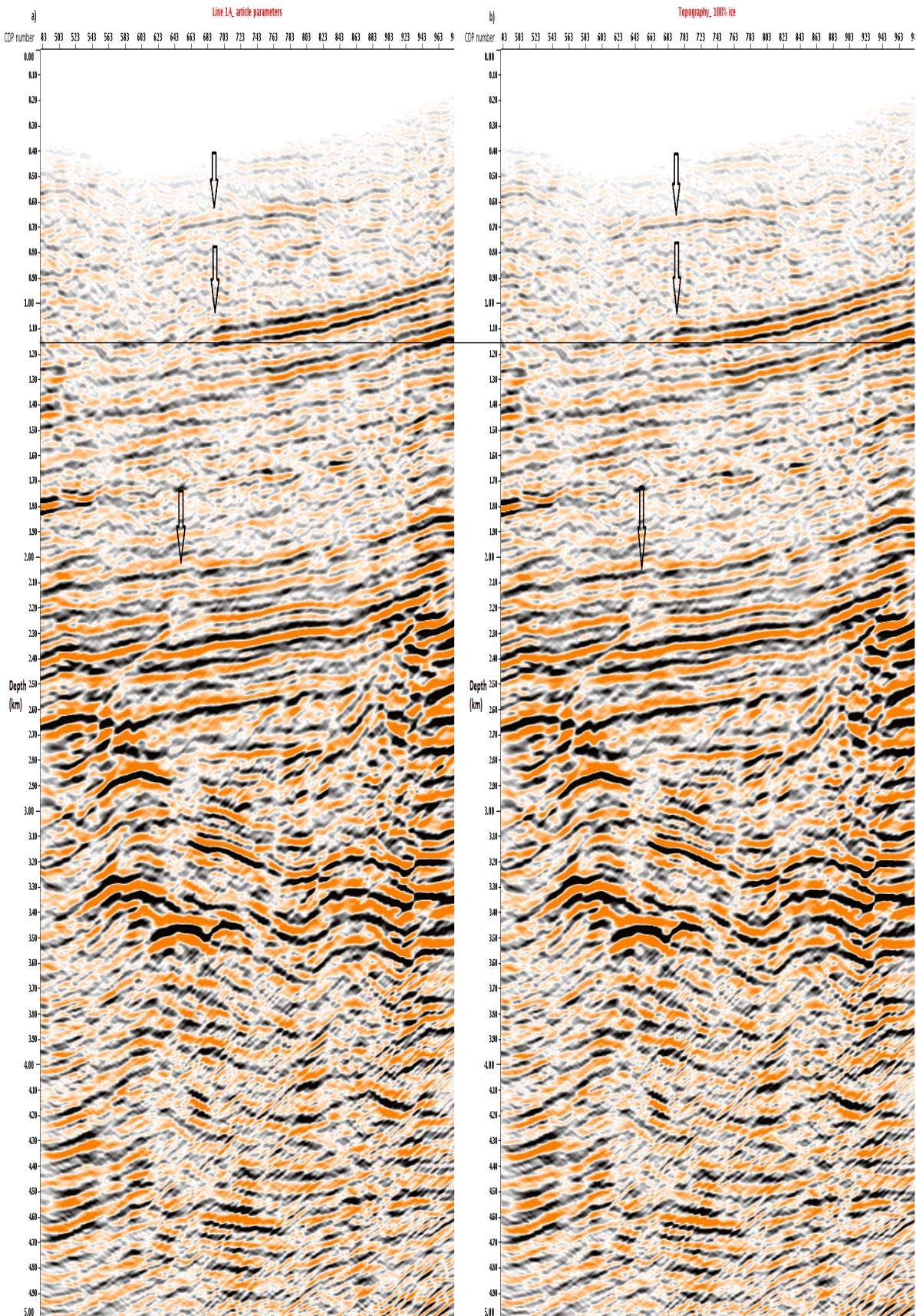


Figure 4.10: a) Is the correct model, while b) is when the layer beneath the glacier is saturated with 100% ice. Arrows and black line is indicating the differences, and the thickness of the permafrost is varying.

4.2.2 Permafrost effect; constant permafrost thickness

Figure 4.11 to 4.13 compare the correct model for Line 1A, (figure 4.1a) to the three different saturation scenarios (table 4.2) in the case when the permafrost thickness is constant. Figure 4.11 shows the comparison between the correct model and the case with 100% water saturated layer beneath the glacier. Neither the reflector in the shallow surface, nor the strong reflector indicated by the top and middle arrow respectively is apparent in b). The low velocity water layer ($V_p = 2.5\text{km/s}$), prevents the waves to travel as far down in the surface as for the correct model. The first clear continuous reflector is at about 2.5km depth (bottom arrow). The low velocity water layer causes a travel time-shift of one period towards shallower ground.

By comparing the correct model with the layer saturated with 60% water and 40% ice the strong reflector at the middle arrow appears in b) (figure 4.12). It is not as strong as is a), but the continuity is reasonably good. The shallow reflector at the top arrow is not continuous, but it is possible to see an indication of it. The travel time-shift is at about a half a period, a half a period less than in figure 4.11, which is due to the higher velocity in the water/ice mixed layer.

The final comparison is between the correct model and the 100% ice filled layer figure 4.13. Here both of the close shallow reflectors are visible (top arrow), in addition to the strong continuous reflector at the middle arrow. The amplitude strength and the continuity of the reflectors are good and much the same in both a) and b). There is no remarkable travel time-shift, or any other differences between the correct model and the case with 100% ice. This is again due to the small velocity differences in the layers beneath the glacier.

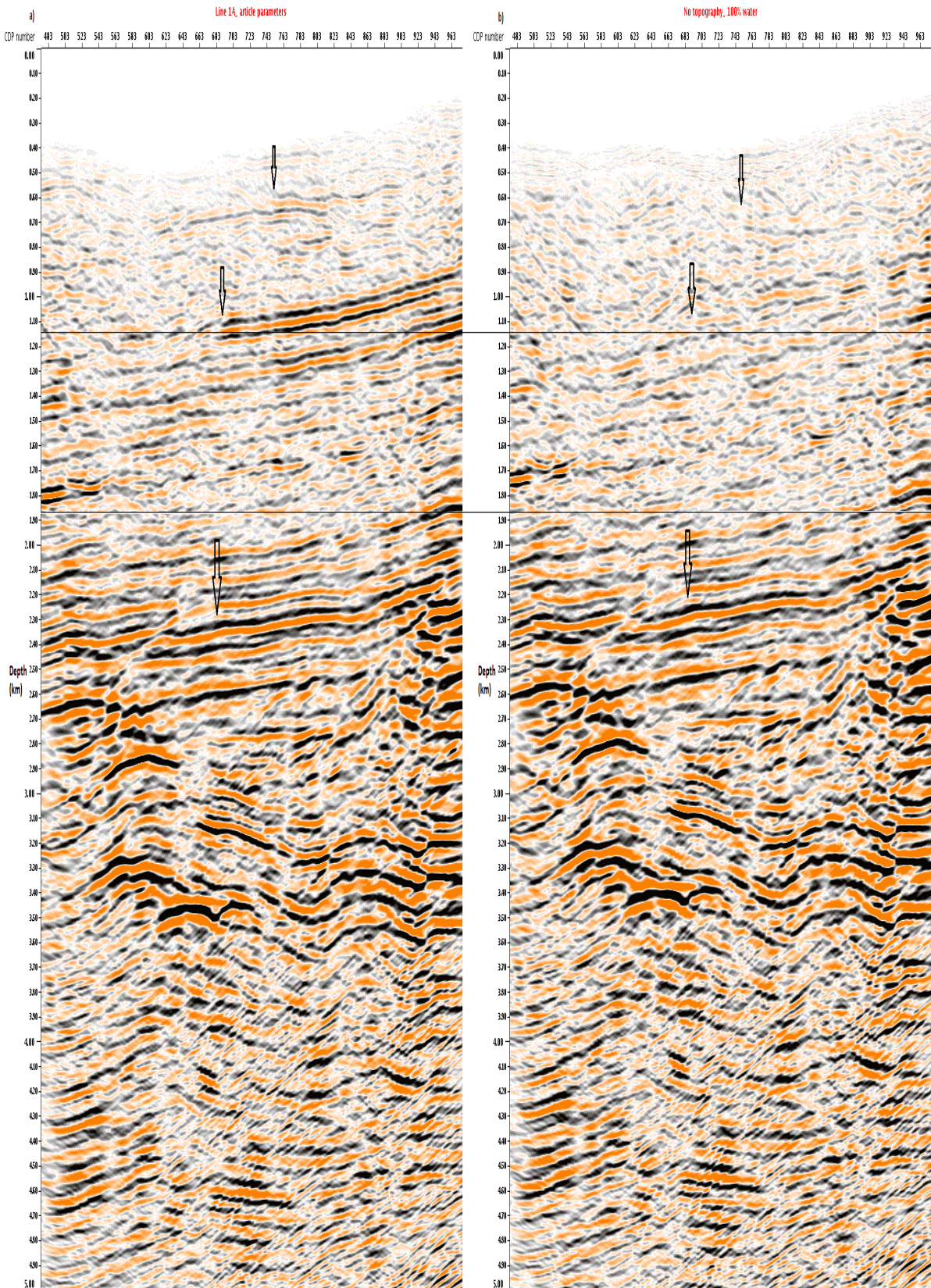


Figure 4.11: Comparison of a) the correct modelled Line 1A from Johansen et al. (2003) article, and b) the scenario when the voids are saturated with 100% water. Here there is a constant thickness of the layer.

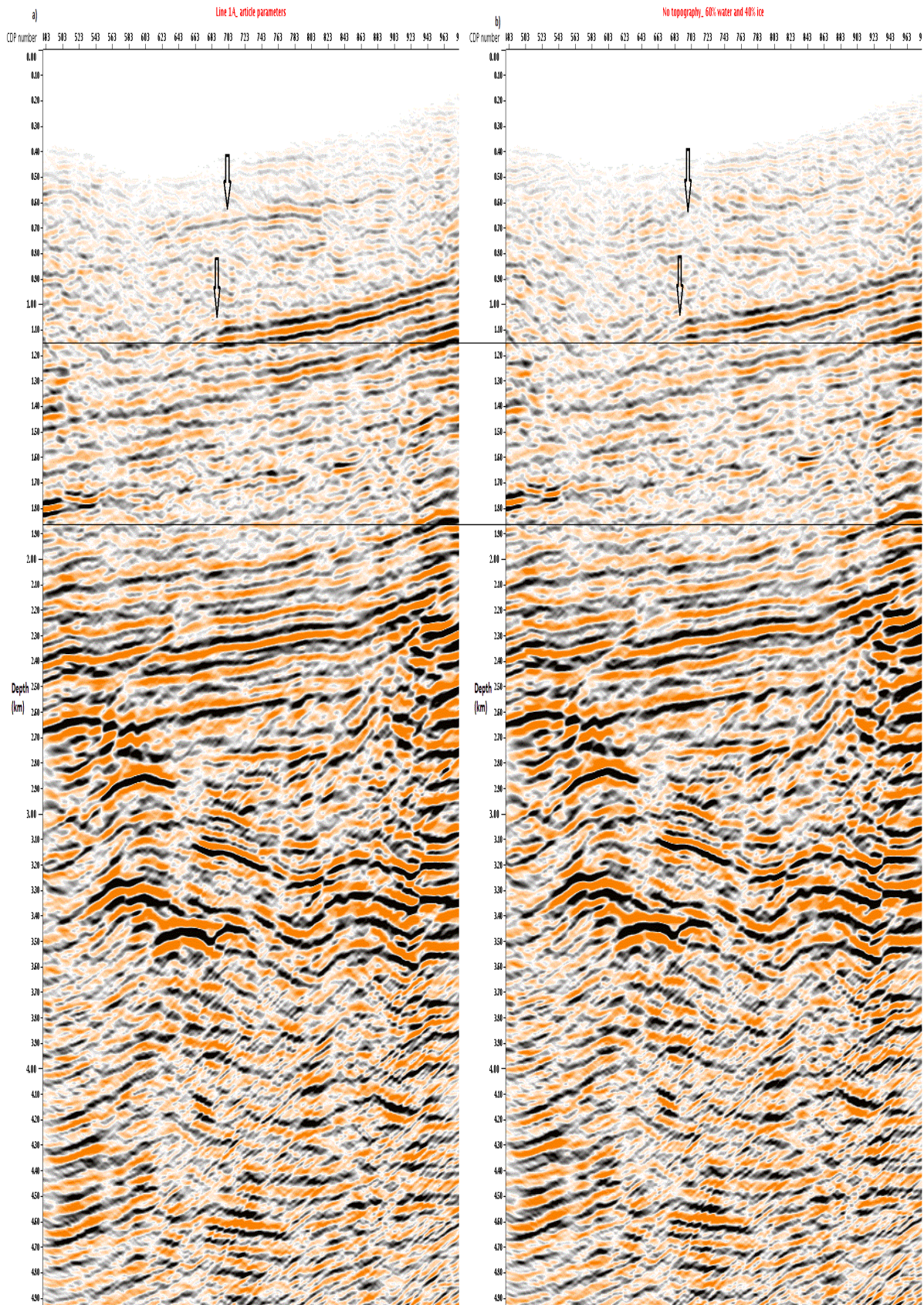


Figure 4.12: a) Is the correct model, while b) is when the layer beneath the glacier is saturated with 60% water and 40% ice. The thickness of the layer is constant. Arrows and black horizontal line is indicates differences.

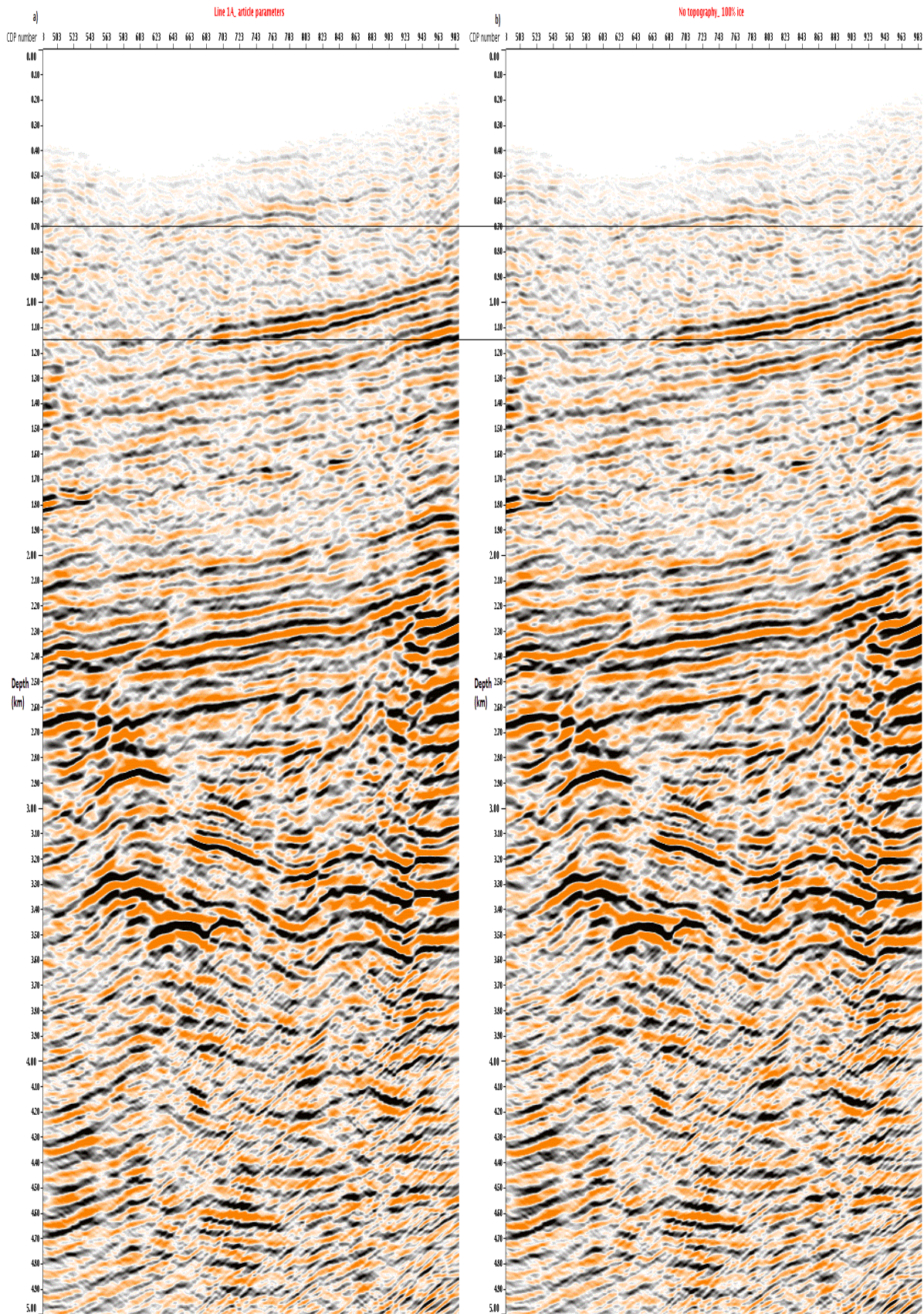


Figure 4.13: a) Is the correct model, while b) is when the layer beneath the glacier is saturated with 100% ice. Arrows and black line is indicating the differences, and the thickness of the layer constant.

4.2.3 Permafrost effect: constant VS variable thickness

By comparing the seismic section when the thickness of the permafrost layer is included and not, the most distinct differences are when the sediments are 100% water saturated. Appendix C shows the comparison between these sections, where arrows and horizontal line indicate the main differences.

For the 100% water filled scenario, the largest difference is underneath the thinnest and thickest part of the glacier. The continuity of the reflectors indicated by the bottom most arrow are nearly vanished and impossible geological structure at the reflector indicated by the top arrow.

For the case with 40% ice and 60% water saturated and 100% ice filled sediments there are not much difference between the sections.

4.3 Interpretation

Correlation between the lithological log (Johannessen et al. 2011) and the migrated result of Line 1A in this thesis, leads to an interpretation of the subsurface, figure 4.14. The red line indicates the top of the glacier, while the green is the glacier bed. The purple line indicates the unconformity, the Pallfjellet member, which divides the Frysjaodden formation. Yellow and blue marks the top and bottom interface of Grumantbyen formation, respectively.

The lithological log is the result after the drilling on Sysselembreen; it is about 1000m deep in the subsurface. Figure 1.3 shows the entire log which is the background for the interpretation done in Johannessen et al. (2011). The log correlated to the migrated Line 1A is a good match. The two most distinct reflectors are in good correlation to the top and bottom interface of the Grumantbyen formation, in addition to the Pallfjellet member reflector. These correlations reinforce credibility of the interpretation of the subsurface, in addition that the correct model is a good model.

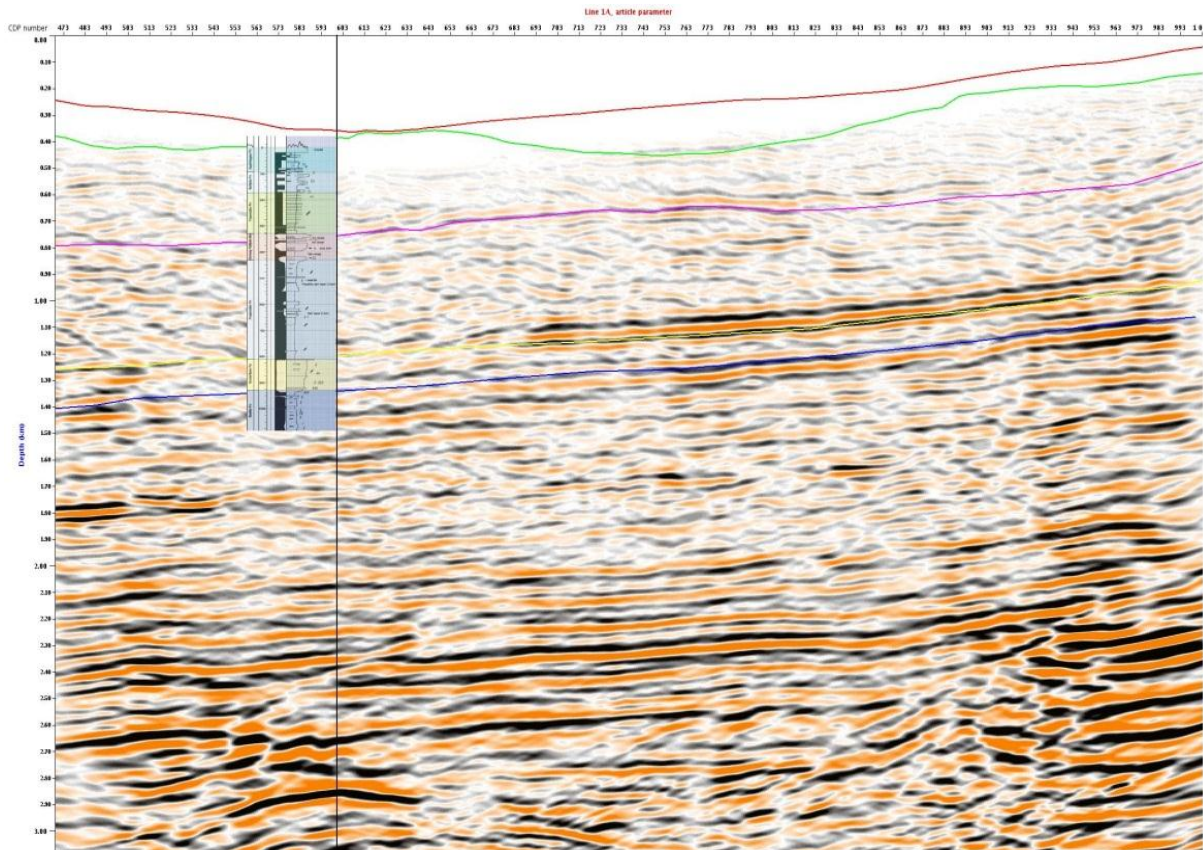


Figure 4.14: This is a finished processed picture from the data acquired on Line 1A. The red and the blue line indicate the top and bottom of the glacier, respectively. In addition, the bore hole drilled in Syssemannbreen is here marked with a black vertical line, as well as the interpretations of the subsurface. These interpretations is done by correlating the litological log (figure 1.3) to the core and seismic data. The purple line indicates the unconformity, the Pallfjellet member, which divides the Frysjaodden formation. Yellow and blue marks the top and bottom interface of Grumantbyen formation, respectively.

4.4 Chapter conclusions

This chapter presents how the glacier and the permafrost are affecting the seismic. By changing velocities and thickness of the glacier, the reflections are changing in continuity, shape, amplitude and travel time. In terms of the permafrost, the near-surface sediments may be frozen, thawed or partially frozen, which will affect the seismic in different ways. When the sediments are 100% water filled, the seismic data is most affected. In addition, by comparing the constant permafrost thickness, against a various permafrost thickness indicate that this has an effect on the seismic data as well, and should be accounted for. The good correlation between the log and correct model indicate that the correct model is generated with good velocities for the illumination of the subsurface in this area.

Chapter 5: Discussion

5.1 Acquisition

When the interstitial water in the subsurface freezes, it is the elastic moduli and electrical conductivity that changes the most (PERMAFROST 1966). Thus, the best method for mapping the permafrost distribution is either with seismic- or electromagnetic methods. Seismic acquisition was used on Nathorstland, where the detonation fuse was the chosen source, even though a large amount of the energy would disappear out in the air, and result in strong airwaves. Nevertheless, by combining all the factors of the environments, location, strict rules in the area and the goal of the study; this is cheaper than borehole study, more time saving and best seismic source to acquire the necessary data. However, in areas with complex subsurface structures the borehole source may be necessary. When the source is lowered in a borehole, it generates the best possible data. The downside is that it is an extremely time-consuming and expensive acquisition method.

The electromagnetic survey may be another geophysical method to map the distribution of the permafrost. Time Domain Electromagnetic (TDM) method is a non-invasive and effective method used in Antarctica to determine the distribution of subglacial and subsurface hydrology, permafrost and salinity etc. (Mikkelsen 2012). By combining electromagnetic- and seismic surveying, more detailed information on the permafrost may be achieved. For the good data collected on Nathorstland, this extensive work may not be necessary, but in areas with bad quality data, complex subsurface structure and unknown near-surface sediment saturation/freezing conditions, more detailed information may be crucial for the resulting seismic section.

5.2 Processing

During acquisition, information about the glaciers geometry and velocities was collected with the help from GPS, GPR and seismic. This information is included in scenario one and three, but neglected in scenario two when studying the glacial effects. Figure 5.1 shows a close-up part of line 1B, comparing a) the correct model with the b) 'no ice' model. There are

clear differences in continuity and shape of the reflectors. By including the geometry and velocity in the glacier, the reflections are greatly improving, indicating the importance of getting as much information as possible on the acquisition area before shooting the seismic.

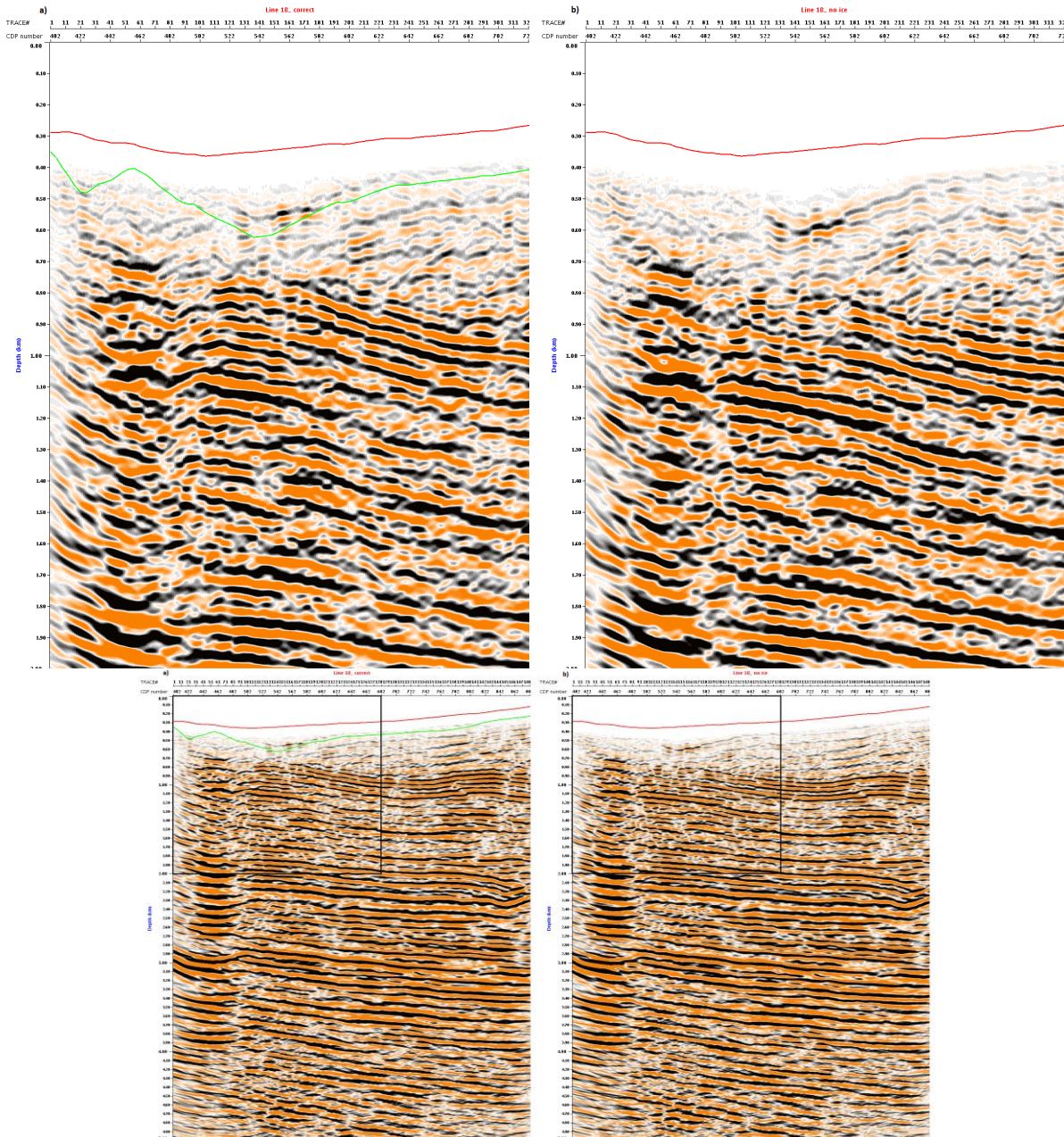


Figure 5.1: Close-up of a part of line 1B, showing the importance of glacial geometry and correct velocity in the velocity model. A) is the correct model, while b) is without the glacier.

This thesis has focused on two migration methods; the Kirchhoff pre-stack depth migration and post-stack finite-difference. The choice fell upon Kirchhoff due to a possibility to migrate the data pre-stack, on contrary to the post-stack, usually done with the finite-difference method. The choice of performing pre-stack migration is due to the major elevation

difference on the glacier; ranging from about 145 to 745 meters above the sea. When migrating before stacking of the data, the resulting seismic section is more consistent and realistic. It would be possible to do post-stack migration on this data as well, but the results would be based on much more approximations, and would not give as good and reliable results.

5.3 Scenarios

5.3.1 Glacial effects

The three scenarios was made in order to figure out how important the correct velocity and thickness of the glacier is for the seismic sections. The velocities in the correct model was derived from the slope of the P-wave reflections, and compared to other velocity models generated for this thesis. When the velocity and geometry of the glacier were not included in the velocity model for the 'no ice' scenario for line 1A, the continuity of the reflector increased compared to the correct model (see figure 5.2). However, this is not the case for line 1B (see figure 5.1), so it is not an unambiguous result. This increased continuity is vertically just beneath the thinnest part of the glacier (when included), and the three reflectors are indicated by arrows. An explanation for this may be that the TOPAK job that calculates the travel time map for the migration is not suited for the thin glacier layers. The thinnest part is about 8m thick and the sampling rate is set to 5m in NORSAR, meaning the glacier is registered on the thinnest section. This may contribute to the fact that it is the TOPAK job that is not suitable for such small thicknesses. There was not possible at the time of this thesis, to verify that the TOPAK job was able to create a map for such thin layers.

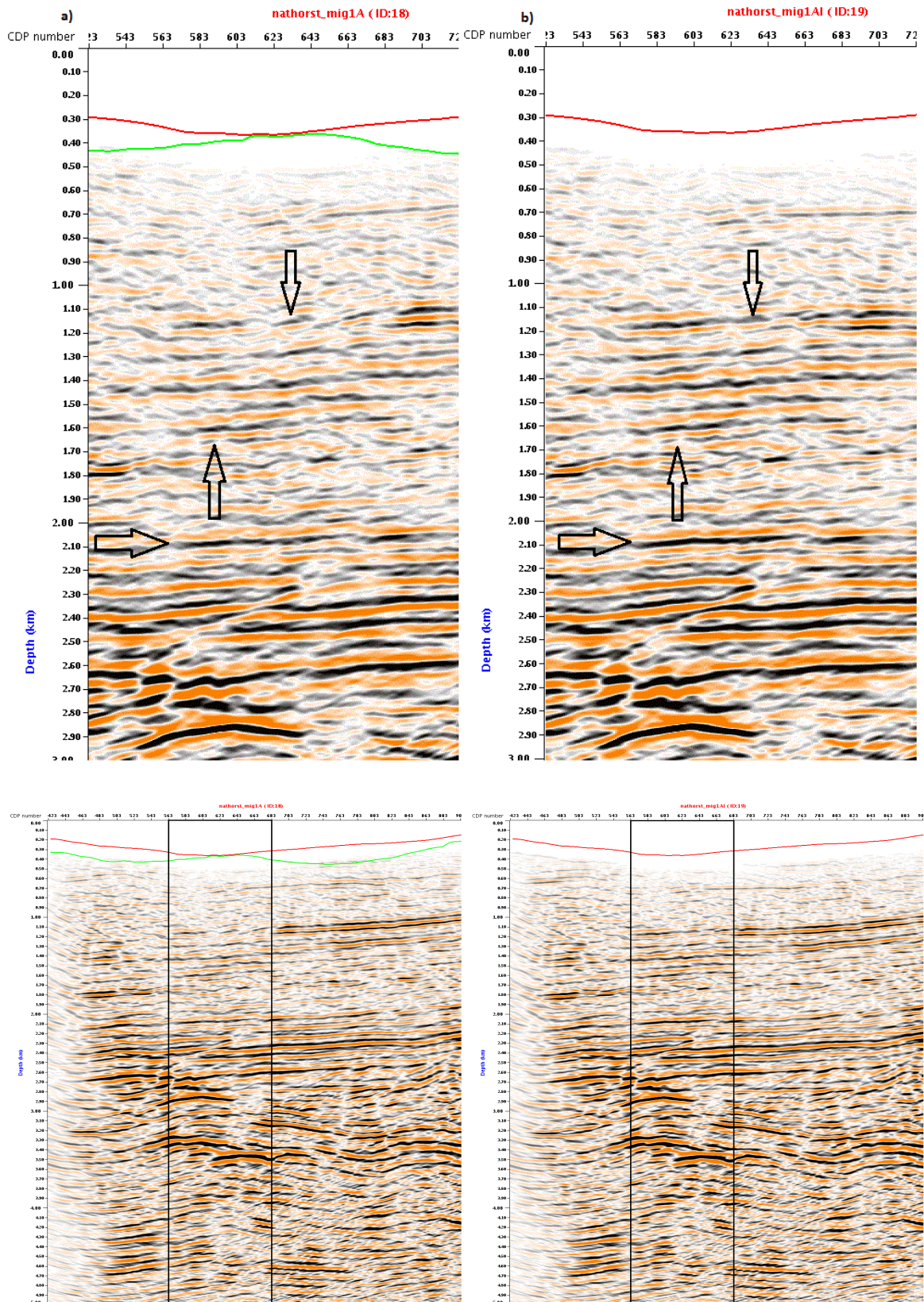


Figure 5.2: Close up on the part of the line 1A glacier (figure 4.2) which shows increase continuity in b) no ice compared to a) the correct model.

When the glacier was neglected, the glacier velocity was set to the same velocity as in the rock beneath the glacier; 4.1km/s. This is due to the importance of having the correct velocity in the subsurface in order to see the reflections. One may think that the velocity in the glacier and in the subsurface could be set to 3.6km/s (which is the velocity in the glacier), but then the velocities would be too low in the rocks, and the seismic section would not give any information on the top two kilometres (see figure 5.3).

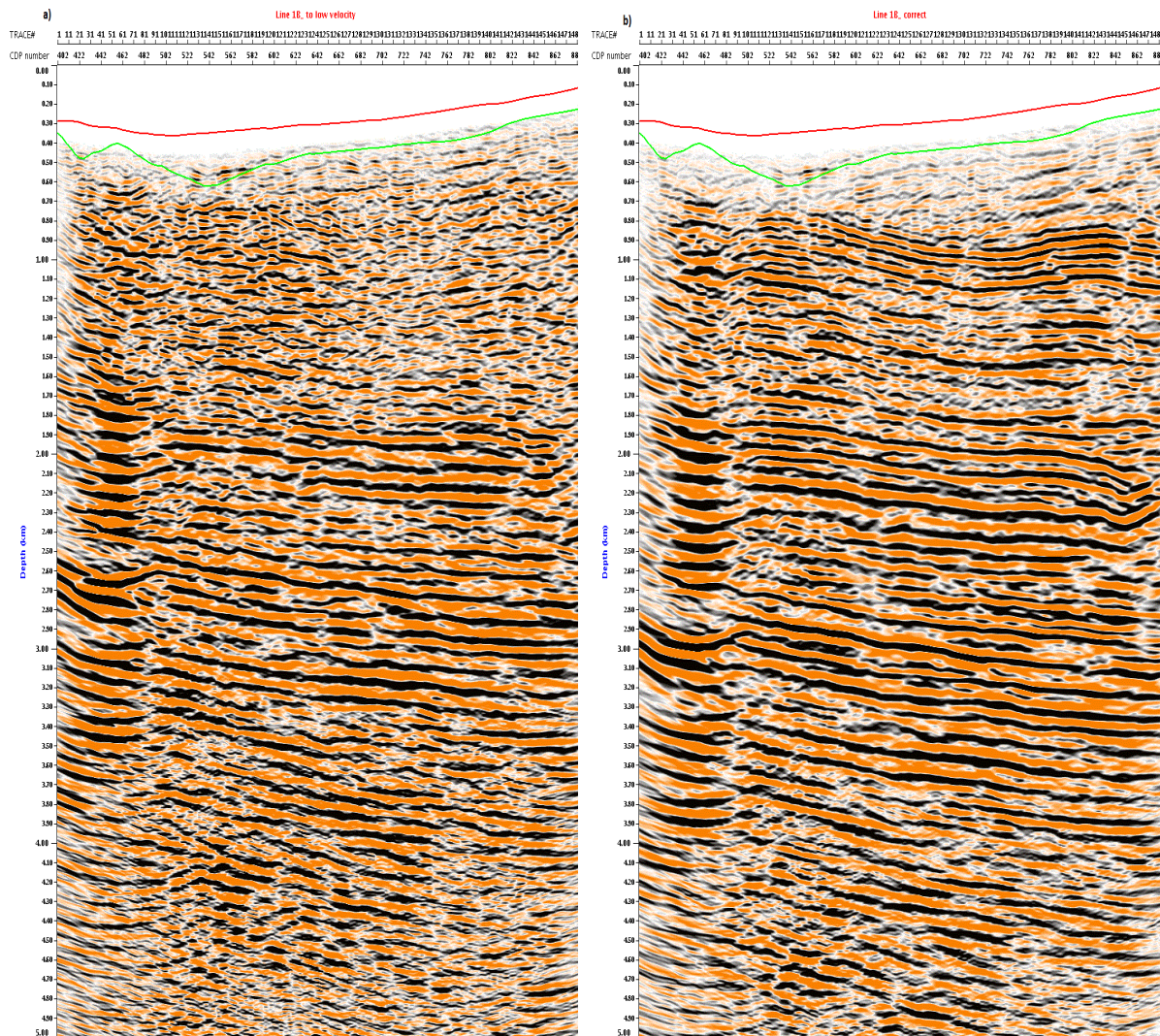


Figure 5.3: a) With too low velocities in the glacier and in the underlying rock, the two top km is impossible to interpret, while b) show the correct model.

The evident decrease in data quality in the case of a thicker glacier than expected, shows how important it is to collect information on the glacier geometry before shooting the seismic survey. If the glacier had been thicker than expected, the seismic section would not image the subsurface in a reliable way, especially not the shallowmost structures. The large

increase, 250m, was chosen to ensure the resulting seismic section gave a clear picture of the importance of this information.

Another fact to discuss is the constant velocity set for the glacier in this thesis. Cracks and melt water in the glacier may decrease the velocity both laterally and vertically. Combining surface waves and GPR measurements, both melt water and fractures in the glacier may be observed, mapped and taken into account in order to estimate these velocity variations. By including these variations, more accurate determination of the velocity in the glacier may be set.

5.3.2 Permafrost effects

The velocity models for this scenarios were generated with velocities and parameters taken from Johansen et al. (2003), displayed in table 5.1 and figure 5.4, which is a theoretically model of the velocity changes due to fraction of ice in the near-surface sediments. One important fact to notice is that the results from Johansen et al. (2003) are obtained in Adventdalen, an area without glaciers. In addition, this is a theoretical model, which makes it difficult to conclude that this is 100% correct. However, the objective of their survey was to map near-surface sediments in permafrost environment, which is the underlying reason that these velocities were used in this thesis. The velocities derived from figure 5.4 indicate that for 100% frozen voids, the velocity in the near-surface layer are 4.28km/s. The correct model in this thesis indicates that the layer has a velocity 4.1km/s. The small difference in the velocities, indicate that the velocities in figure 5.4 is a good approximation, and that the near-surface sediments underneath the glacier in Nathorst Land is \approx 100% saturated with ice.

Table 5.1: Model parameter.

Layer	Thickness (m)	Critical porosity (ϕ_0)	No. of contact point (C_0)
M1	100	0.40	8.2
M2	10	0.38	8.6
M3	—	0.36	9.0

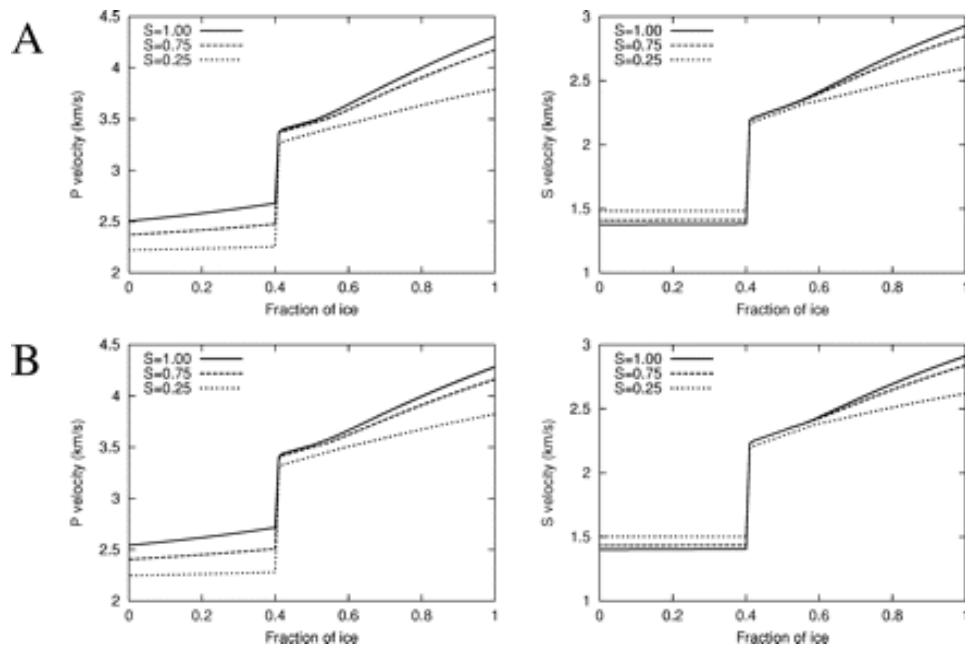


Figure 5.4: V_p and V_s variations with the degree of freezing and water saturation, S , varying from 1.0, 0.75 and 0.25. (a) for sediment M2 and (b) for sediment M3 (Johansen et al. (2003)). V_p and V_s are drastically increasing when the water freezes, and the voids consist of 40% ice.

Johansen et al. (2003) presents three granular materials, table 5.1, where V_p and V_s are modelled in figure 5.4 (neglecting V_s in this thesis). Comparing A) and B), the velocity differences are negligible, thus the M2 and M3 give relatively the same results, and M2 is used in this thesis. Johansen et al. (2003) discusses the velocity changes due to the saturation amount in the rock voids, ranging from 100%, 75% and 25% saturation (figure 5.4), where the lower the saturation, the lower the velocity in the near-surface sediments will be. By combining the velocity and the reflection coefficient, the saturation of the voids may be found. This comparison was not done in this case, but the 100% saturation was selected due to the information gathered from Johansen et al. (2003) discussed earlier in this section. Velocities from 0%, 40% and 100% ice saturation was picked to generate the resulting seismic sections in this thesis, in order to get a picture of the extreme end-points and at the point where the largest change in velocity occur; when the water freezes. The resulting seismic sections indicate the importance of information about the near-surface sediment saturation/freezing conditions. For example, in the case of 100% water saturated voids, the velocities are substantially lower than the other scenarios. This layer act as a low-velocity layer, and the illumination of the subsurface would be significantly decreased if not considered. Figure 4.7 show three velocity profiles for the three saturation conditions. The

near-surface sediments are acting like a low or high velocity layer, resulting from the chosen velocities for the velocity model and affect the seismic data in different amounts.

Tsuji et al. (2012) derived the S-wave velocity from surface-waves in order to estimate the V_s distribution beneath the Line 1A glacier, concluding with partially unfrozen sediments underneath thicker part of the glacier, on contrary to more frozen sediments underneath the topological highs. They focused on two scenarios: 1) when only the glacial thickness was fixed, and 2) when the glacial thickness, in addition to the V_p, V_s and density was fixed. Scenario 2) gave the most accurate estimation of the V_s distribution, and concluded that there is clearly a low-velocity layer beneath the thicker part of the glacier (Tsuji et al. 2012). This conclusion apparently contradicts the results in this thesis. This thesis focuses on the P-wave velocities, and clearly indicates that the sediments beneath Line 1A and Line 1B are (almost or completely) frozen and there are no presences of a low-velocity layer. These discrepancies are probably due to the differences in velocity used in the velocity model. Table 5.2 show the velocities that were used to provide the best results in both cases. Note that Tsuji et al. (2012) uses S-wave velocities, while this thesis uses P-wave velocities. Tsuji et al. (2012) is divided into a) and b) which correspond to the sediments beneath the thickest and the thinnest part of the glacier, respectively, thus, b) is more frozen than a). Another reason for the contradicting results may be that Tsuji et al. (2012) have found a more accurate near-surface sediment distribution, compared to this thesis. .

Table 5.2: Velocities in the velocity model that gave the best result when estimating the distribution of the near-surface sediments. Tsuji et al. (2012) uses S-wave velocities, while this thesis uses P-wave velocities. A) and b) indicate the sediments beneath the thickest and thinnest part of the glacier, respectively.

Article	Air	Glacier	Near-surface sediment	Rock
Tsuji et al. (2012)a)	-	1839	1300	1839
Tsuji et al. (2012)b)	-	1839	1800	1839
This thesis	1500	3600	4280	4100

The last comparison was done in order to see the difference in the seismic section when the permafrost layer varies in thickness (figure 4.6b) and when it is constant (figure 4.6.c). As mentioned in the last section, Tsuji et al. (2012) discussed that the thickness of the

permafrost is varying with the thickness of the glacier. The velocity model for this scenario was generated by taking the thickness of the glacier, and makes the permafrost layer approximately the same thickness (figure 4.6.b). This is only an approximation of the variations, so it is not an accurate image of the subsurface. Appendix C compares the two cases, including the different saturation/freezing conditions. C1 is for the 100% water saturated voids, and show large differences in the continuity and shape of the reflectors. C2 show the figures when the voids are 40% and 100% filled with ice, where the differences are not so prominent. Due to the fact that this is only an approximation of the distribution of the permafrost, it is not certain if the results are adequate. However, from these results, it indicates that the more water saturated the voids are, the more the permafrost distribution affect the data. The fact that when it is water saturated this layer act as a low-velocity layer, compared to the overlying glacier and underlying permafrost, may substantiate this statement. By study the surface waves, information of the distribution of the permafrost may be revealed. This would give a better indication of how the seismic section really is affected by the freezing conditions of the near-surface sediments and better images of the subsurface is generated.

5.4 Chapter conclusion

For acquisition of seismic data on Nathorst Land, the detonations fuse is the best choice of source. However, by combining seismic survey with an electromagnetic method, one would be able to get more information on more complex structures in the subsurface. During the processing step, the Kirchhoff pre-stack depth migration is the most suitable migration method due to the major elevation difference on the glacier. When focusing on the glacier and permafrost effect on the seismic data, it is clear that the thickness, velocity and the geometry of the glacier is important to include in the velocity model in order to get reliable data. Also, the degree of freezing in the near-surface sediments, including the varying/constant thickness of this layer is an important part of the need-to-know information before acquiring in order to be sure the reliability of the data. Contradicting results in this thesis compared to Tsuji et al. (2012) may be due to the focus on V_p in case of this thesis and V_s in case of Tsuji et al. (2012), in addition to more accurate near-surface sediment distribution in the latter case.

Chapter 6: Conclusion

6.1 Summary and conclusion

The interest for subsurface exploration in the arctic is increasing. To figure out how the glacier and permafrost are affecting the seismic data five questions was raised in the beginning of this thesis.

Velocity models for different scenarios including various conditions for the glacier, permafrost and near-surface sediments were generated. Comprehensive processing of raw seismic data collected from two glaciers at Nathorst Land on Svalbard was conducted. Resulting seismic section processed with the same parameters as the section from Johansen et al. (2011) is the comparison basis for this thesis resulting seismic section.

The main results can be summarized:

- GPR and GPS are important in order to obtain information on the glacier geometry, while the detonation fuse gives good seismic data on Nathorst Land.
- Knowing the glacier thickness is important for optimum processing of the seismic data. In order to obtain the best possible seismic section of the subsurface, glacier geometry and velocity must be included in the velocity model.
- Kirchhoff pre-stack depth migration provides the best results due to the large elevation differences on the glacier.
- The velocities derived from Johansen et al. (2003) gave a good and reliable foundation for generating the velocity model in order to determine the permafrost effect.
- The saturation/freezing conditions of the near-surface sediments beneath a glacier have a major influence on the seismic data. The more water saturated the sediments, the lower the velocity is in this layer. Generally speaking, if this low-velocity layer is not included in the velocity model, the top km of the seismic section will be significantly worsened. However, when 40% or more of the sediments freezes, the velocity drastically increases and approaches the velocity in the rock beneath the

near-surface sediments. This increase leads to minimum impact on the seismic data; however most of the shallowest reflections would get affected if the layer is not included in the velocity model.

- For this thesis an approximation of various distributions of the permafrost was generated resulting in three seismic sections for three different scenarios. For the case with 100% water filled voids the results differs the most from the correct model. From 40% to 100% ice filled sediment, the differences decreased along with the increase in freezing/increase in velocity.
- When the near-surface sediments are 100% water filled, all the scenarios are affecting the seismic data tremendously, thus needs to be taken into account when generating the velocity model for a good result. Thus, knowledge about the saturation/freezing condition for this layer is very important for seismic acquisition, which is also stated in Tsuji et al. (2012).
- The voids in the near-surface sediments underneath the Sysselembreen and Svalbreen on Nathorst Land are \approx 100% frozen.

6.2 Further work

- Verification of the TOPAK job should be done to be sure that this job is reliable for all thicknesses of the glacier.
- The discrepancies between using V_s and V_p for estimating the near-surface sediment freezing conditions should be further investigated.
- More investigation on the varying thickness factors effect on the seismic data.
- Investigate the internal variations of freezing conditions in the near-surface sediments, and what kind of affect these have on the seismic data.

References

Asghar, A. (2011). Processing and interpretation of multichannel seismic data from isfjorden, Svalbard. Petroleum geoscience, University of Bergen. **Masterdegree**.

Audebert, F. (2001). "3-D prestack depth migration: Why Kirchhoff?" Stanford Exploration Project(80): 1-18.

Bianco, E. and M. Hall (2011). G for gather. Agile geoscience.
<http://www.agilegeoscience.com/journal/2011/9/14/g-is-for-gather.html>.

BPI (2005). PDF: Seismic velocity analysis. Baird Petrophysical International, inc.
www.bairdpetro.com: 58-62. Date accessed: 27.04.2012.

CGGVeritas (2008). Geocluster Release Note

Cramez, C., P. Vail and S. Wu (2007). Seismic-Sequential Stratigraphy.
<http://homepage.ufp.pt/biblioteca/Seismic/Index.htm>.

Daniels, D. (2005). Ground penetrating radar, Wiley Online Library.

Dvorkin, J., J. Berryman and A. Nur (1999). "Elastic moduli of cemented sphere packs." Mechanics of Materials **31**(7): 461-469.

Gautier, D. L., K. J. Bird, R. R. Charpentier, A. Grantz, D. W. Houseknecht, T. R. Klett, T. E. Moore, J. K. Pitman, C. J. Schenk and J. H. Schuenemeyer (2009). "Assessment of undiscovered oil and gas in the Arctic." Science **324**(5931): 1175-1179.

Gelius, L. J. and T. A. Johansen (2007a). Seismic attributes.
http://www.unigeo.no/class/new_geoclass_embed.html: 10.

Gelius, L. J. and T. A. Johansen (2007b). Rock physics.
http://www.unigeo.no/class/new_geoclass_embed.html: 77-83.

Gelius, L. J. and T. A. Johansen (2012). Basic seismic signal theory and processing.
http://www.unigeo.no/class/new_geoclass_embed.html: 81-87.

Harland, W. B., L. M. Anderson, D. Manasrah and N. J. Butterfield (1997). The geology of Svalbard, Geological Society.

Ingólfsson, Ó. (2008). Outline of the Physical Geography and Geology of Svalbard.
https://notendur.hi.is/oi/svalbard_geology.htm.

Johannessen, E. P., T. Henningsen, N. E. Bakke, T. A. Johansen, B. O. Ruud, P. Riste, H. Elvebakk, M. Jochmann, G. Elvebakk and M. S. Woldengen (2011). "Palaeogene clinoform succession on Svalbard expressed in outcrops, seismic data, logs and cores." first break **29**(2): 35-44.

- Johansen, T. A. (2011). Lecture; Reservoir Geophysics 274. University of Bergen 2012.
- Johansen, T. A., P. Digraanes, M. Van Schaac and I. Lonne (2003). "On seismic mapping and modeling of near-surface sediments in polar areas." Geophysics **68**(2): 566.
- Johansen, T. A., B. O. Ruud, N. E. Bakke, P. Riste, E. P. Johannesen and T. Henningsen (2011). "Seismic profiling on Arctic glaciers." first break **29**(2): 65-71.
- Kearey, P., M. Brooks and I. Hill (2002). An introduction to geophysical exploration, Blackwell publishing.
- Kelamis, P. G. and D. J. Verschuur (2000). "Surface-related multiple elimination on land seismic data—Strategies via case studies." Geophysics **65**(3): 719-734.
- Labastie, A. (2003). Time-lapse seismic reservoir monitoring. AccessScience.
<http://www.accessscience.com/search.aspx?topic=ENG:OTH:PETROL&term=Time-lapse+seismic+reservoir+monitoring> figure 1.
- LamitCompany (2010). Initiation in primary seismology and the SOS-LIFE Earthquake Alarm working principle. Lamit Company. <http://www.lamit.ro/earthquake-early-warning-system.htm>.
- Lin, J. W. and T. C. Holloway (1988). 3-D Seismic Gridding. Offshore Technology Conference. Houston, Texas,
<http://www.onepetro.org/mslib/servlet/onepetroreview?id=OTC-5645-MS>.
- Mikkelsen, P. (2012). Antarctica. Hydrogeophysics Group. Department of Geoscience
<http://geofysiksamarbejdet.au.dk/en/projects/antarctica/>.
- Mjelde, R. (2008). Land Seismic Acquisition. <http://learninggeoscience.net/>.
- Mjelde, R. (2010). Seismic Equipment. <http://learninggeoscience.net/>.
- NORSARa (2011). Norsar 2D ray modelling; User's guide.
- NORSARb (2011). "Norsar 3D; User's guide."
- NorskPolarinstitutt (2009). Map of Svalbard. Norsk Polarinstitutt, Latitude Geographics Group Ltd.
- NSIDC (2012). All about glaciers. National Snow & Ice Data Center.
<http://nsidc.org/cryosphere/glaciers/questions/move.html>.
- Park, C. (2007). What is a seismic survey? <http://parkseismic.com/Whatisseismicurvey.html>.
- PERMAFROST, S. V. I. N. (1966). Geophysical methods for delineating permafrost, National Academies.

Robinson, E. S. (1988). Basic exploration geophysics, Somerset, NJ (US); John Wiley and Sons, Inc.

RockPhysics (2012). Rock physics. <http://www.rockphysicists.org/>.

RRI (2009). Resolution resources international. 3D acoustic imaging for the environment. <http://www.rri-seismic.com/Frame%20Pages/Tech%20Pages/Seismic/seismic.htm>.

Tsuji, T., T. A. Johansen, B. O. Ruud, T. Ikeda and T. Matsuoka (2012). "Surface-wave analysis for identifying unfrozen zones in subglacial sediments." Geophysics **77**(3).

U.S.GeologicalSurvey and P. Saundry (2011). Seismic waves. The Encyclopedia of Earth. http://www.eoearth.org/article/Seismic_Wave.

Varhaug, M. and G. Gillis (2012). Oilfield glossary Schlumberger. G. Gillis. www.glossary.oilfield.slb.com.

Yilmaz, ö. (2001). Seismic data analysis. Processing, Inversion, and Interpretation of Seismic Data. Volume I. USA, Society of Exploration Geophysicist.

Appendix A

Pre-processing flow, step by step

Amplitude scaling factor for all figures are 1. The scaling amplitude limitations for figure A1 – A4 a) and b) is minimum -1000 and maximum 1000, while A4c) and A5 has minimum and maximum value of -100 000 and 100 000, respectively.

The arrows are indicating the differences between the processing steps.

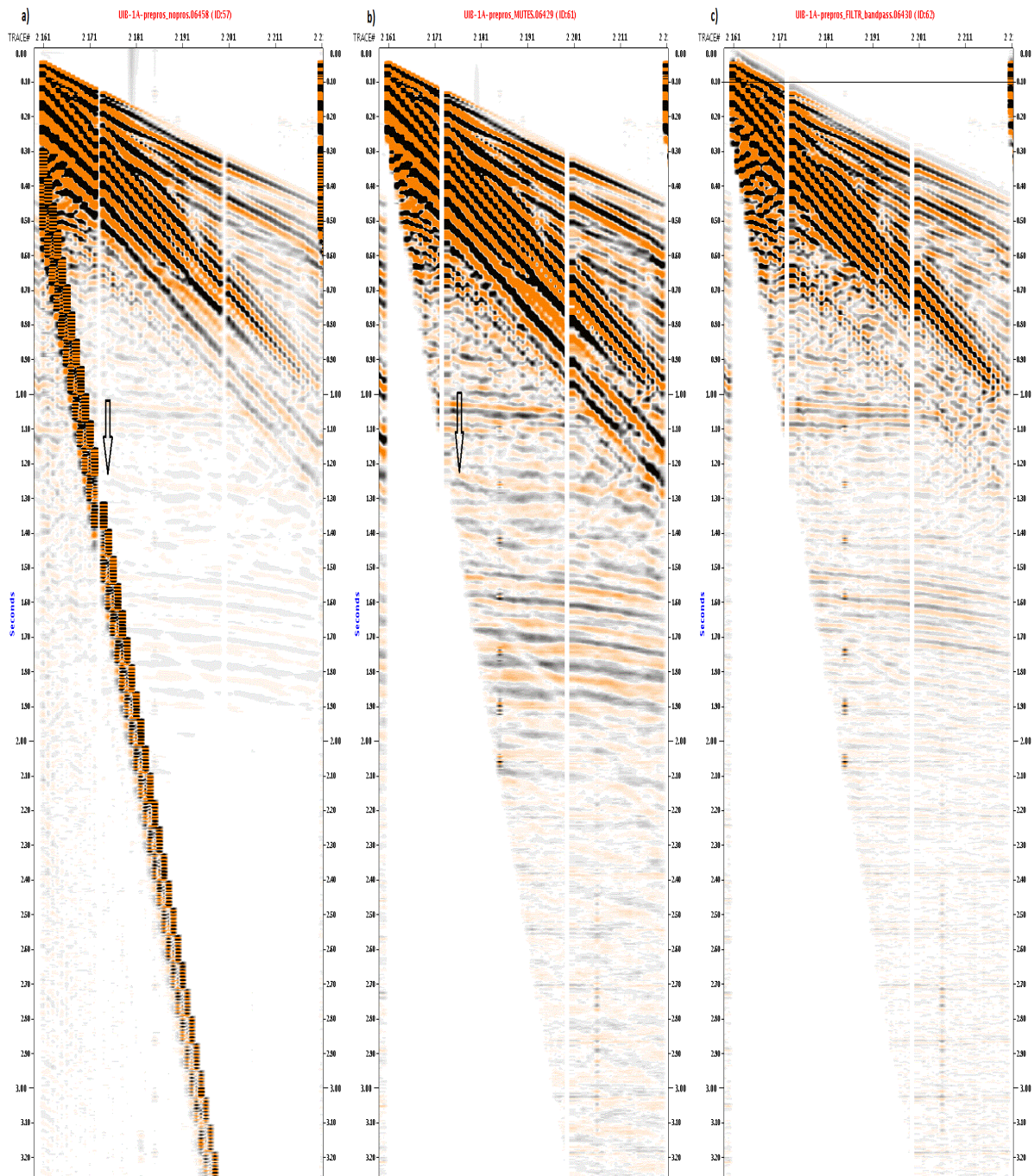


Figure A1: Compare three stages in the processing. A) is the raw data, without any processing. B) is the same trace, where the main difference from a) is the muting of the airwave (MUTES). Before the muting the trace has undergone modification, editing and time-gain function where the amplitudes were multiplied by $(T/250)^1$. C) is filtered by a time-variant band-pass filter (FILTR). A general parameter is the sampling interval which is at 2ms, and operator length is 200ms. The filter limitation is 10-30-120-160, which means that the amplitude is equal to zero for frequencies lower than 10 and greater than 160, and constant and maximum between 30 and 120.

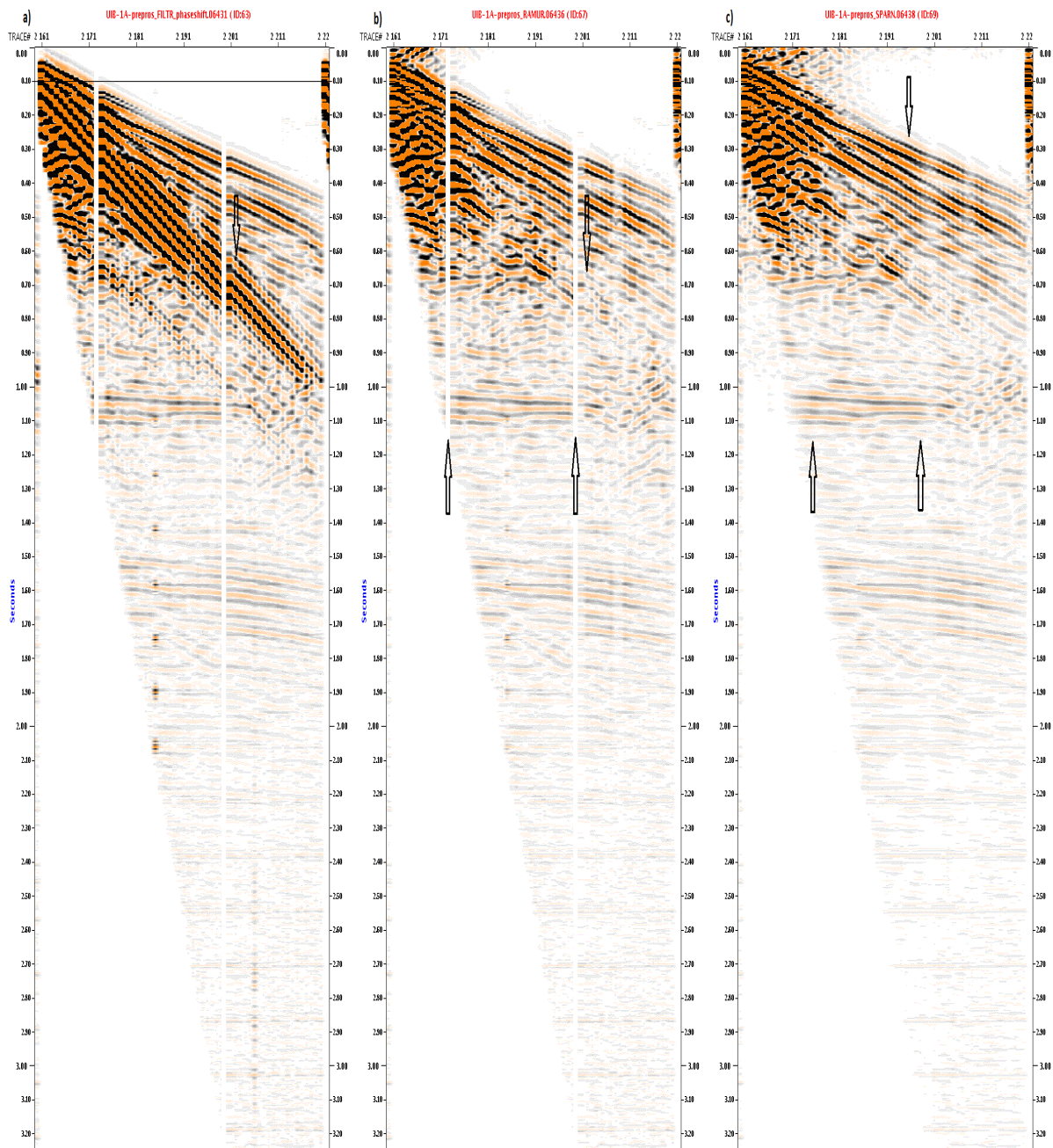


Figure A2: Starts with a phase-shift filter (FILTR), which also is a time variant filter. The minimum frequency for this filter is 10ms, and the phase shift angle is 140° . This value means that the phase shift is a positive pick towards smaller times. 3.13b) has undergone a linear noise attenuation (RAMUR), and the surface waves are clearly attenuated. This is a high resolution de-aliased multiple/noise attenuation done in the Radon (τ, p) domain. Maximum shot distance is 1600m, and is used as a reference when computing the Radon model. Maximum coverage is 60 shotpoint gathers. Before the RAMUR was used, a spatial amplitude smoothing and some modifications were done. C) Show the result after noise attenuation in addition to trace restoration (SPARN). This filter is a

projective filter that is calculated from an auto-deconvolution prediction error filter. This gives the opportunity to restore missing traces, indicated by the arrows pointing upwards. This prediction ensures that the signal is preserved, in addition to attenuating random noise.

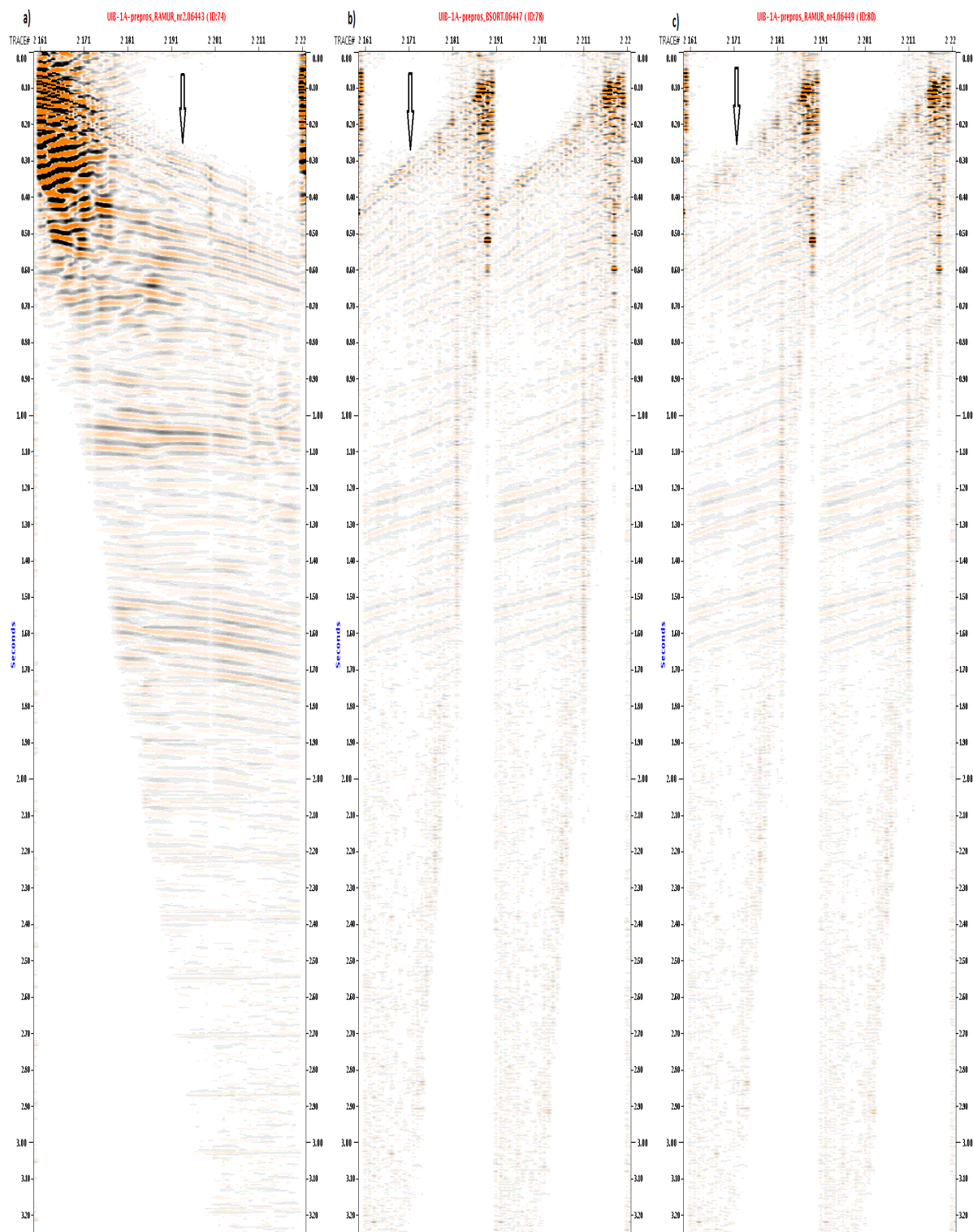


Figure A3: a) Has undergone a RAMUR, linear noise attenuation, clearly seen, indicated by arrows, and is performed with the same values as in 3.13b. b) the traces are sorted by first and second order; receiver position and physical shotpoint number respectively. This means that the traces first get sorted by the receiver position, and then the traces with the same receiver positions get ordered by the physical shotpoint number. Then a RAMUR is set on figure c).

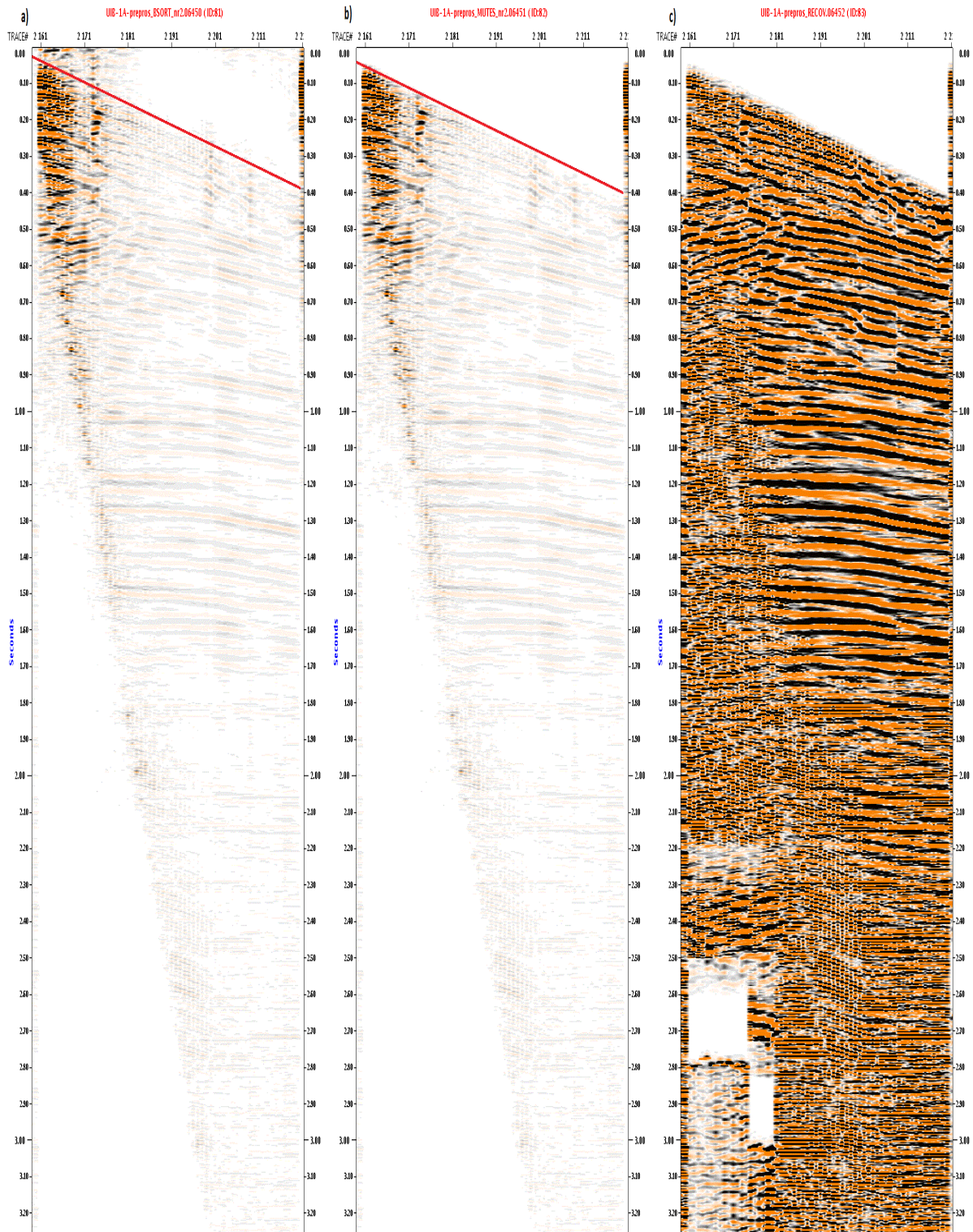


Figure A4: The traces are then sorted again with BSORT after the physical shotpoint number as first level, and by trace number as a second level in a). b) The traces are muted, and MUTES is defined according to the CDP number. The time-distance pairs are 4ms and 0ms mute time and distance respectively, in addition to 400ms and 1600ms. C) is defined by the RECOV, which is a amplitude recovery function. The muted part executed in figure A1a) is filling up with small amplitude noise during the processing step. The recovery job enhances all these small amplitudes.

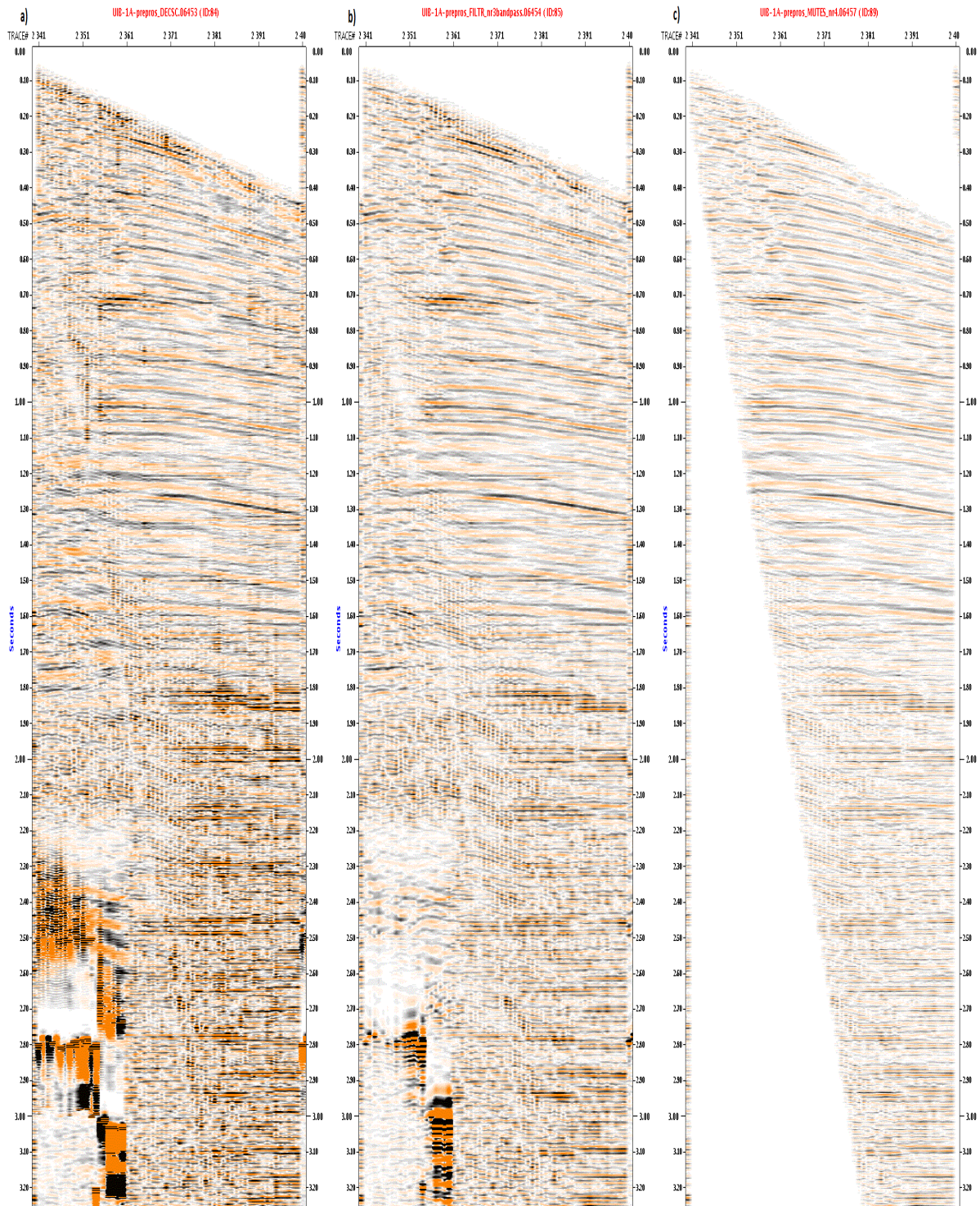


Figure A5: In a) a bandpass filter is applied, with the filter limits 10-20-100-120, and operator length is 300.) b) is a surface consistent deconvolution, which is a prestack 2D deconvolution method. The maximum number of traces to process is 9000, number of CDPs are 602, number of shotpoints and receivers are 150 and 300 respectively. C) The last processing step is muting mute pair (4-0), (4-40), (450-175) and (4000-1325). These are then sorted into CMP gather before used as input in KIMTR.

Appendix B

Processing flow

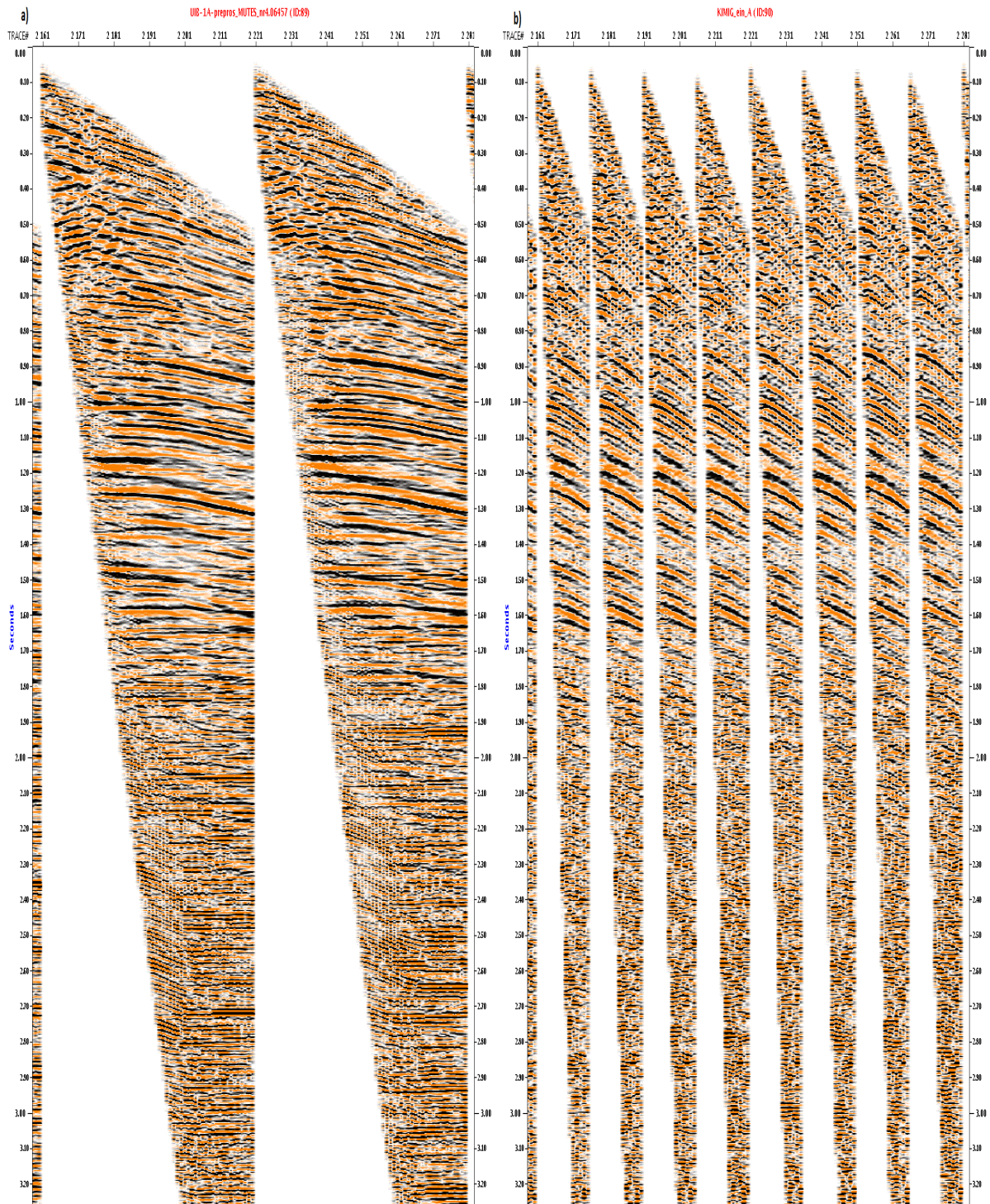


Figure B1: Shows a) the output from the pre-processing job, which is the input in the KIMTR job, and b) the output file KIMIG, from the KIMTR job. KIMTR is a process that creates data files that can later be migrated by KIMIP. There are no trace sorting done by the KIMIP, but the input data are split into several subsets. Each of these subsets is processed by a single KIMTR job, such that all KIMTR jobs can run simultaneously. This KIMIG file is the input to the last migration job KIMIP. Scaling limitation is minimum -20 000 while maximum is 20 000.

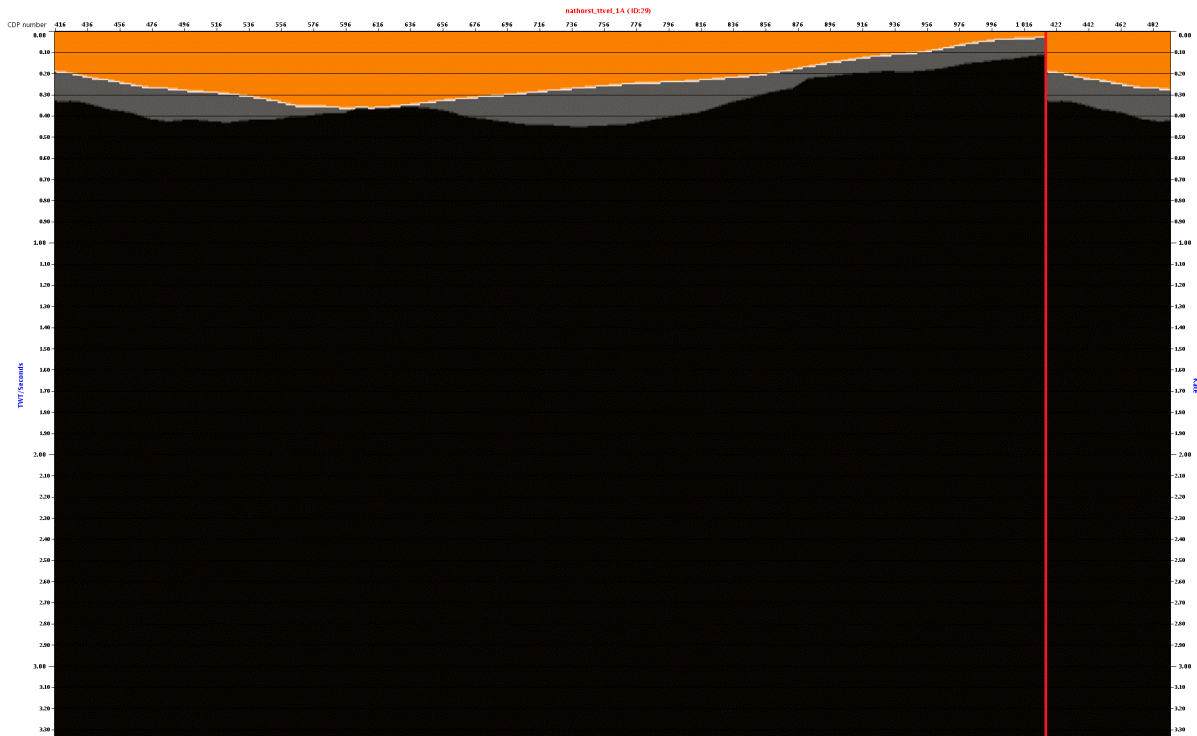


Figure B2: A model from NORSAR 2D/3D is the input in this job (Model). This input is scaled and modified. This header modification is the following calculation:

$$CDPnumber = CDPnumber + 389.$$

This modification is needed for correcting the CDP numbers from the velocity model with the migrated section. Then it's sorted by shot distance and this is the output model.

The red line indicates the end of the 2D image, and the starting picture to the right for the line is an identical 2D line. This show how the 2.5D line is displayed in teamview.

Appendix C

Permafrost thickness variation VS no variation

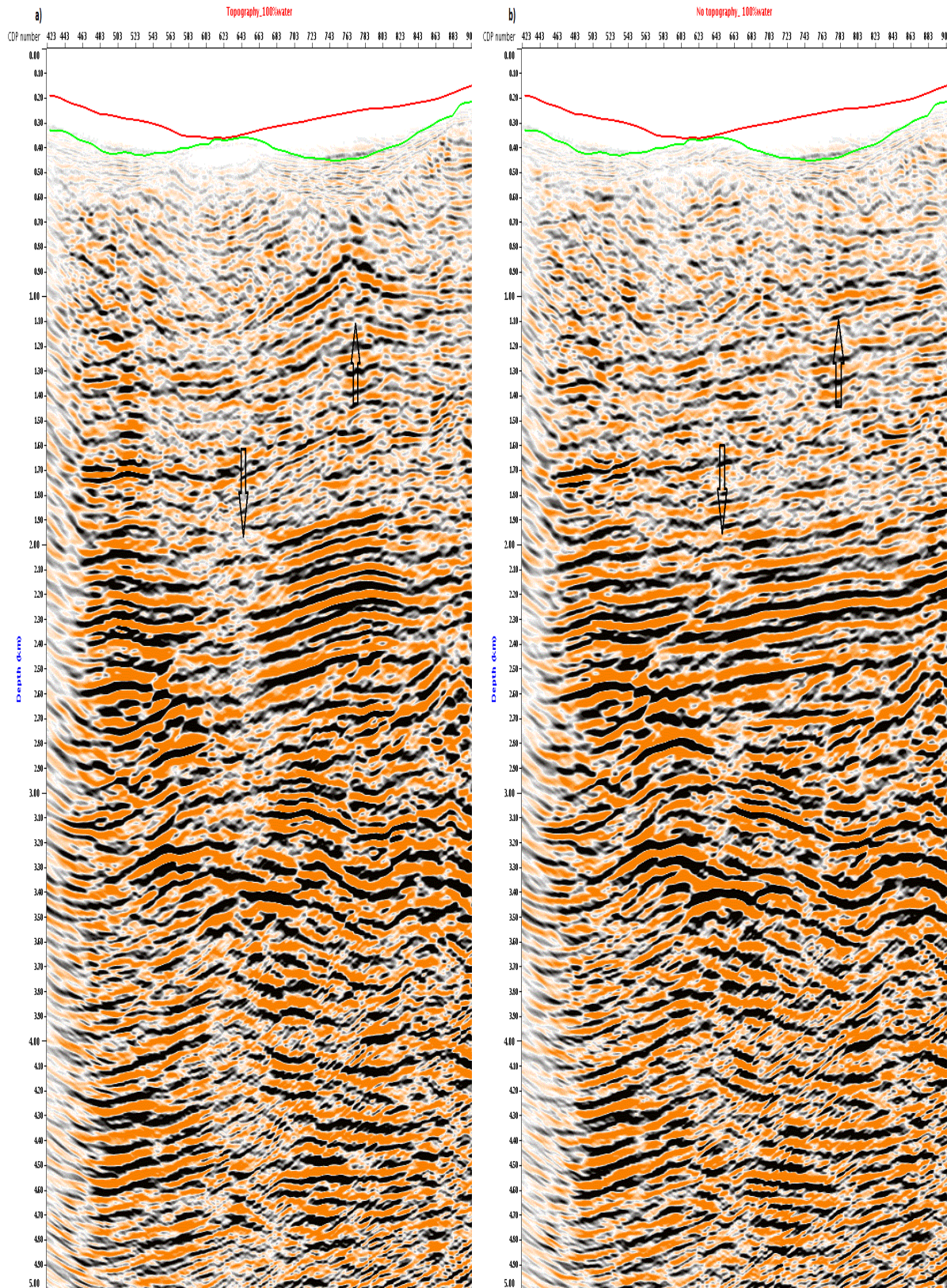


Figure C1: Comparing seismic section when the permafrost distribution a) is included and b) not included for 100% water saturated near-surface sediments. The arrows show the main differences. The red and green line is the top and bottom of the glacier respectively. The main differences are found beneath the thinnest part of the glacier where there is a break in the continuity of the reflections, and beneath the thickest part of the glacier where the strong reflector show ut as a impossible geological structure.

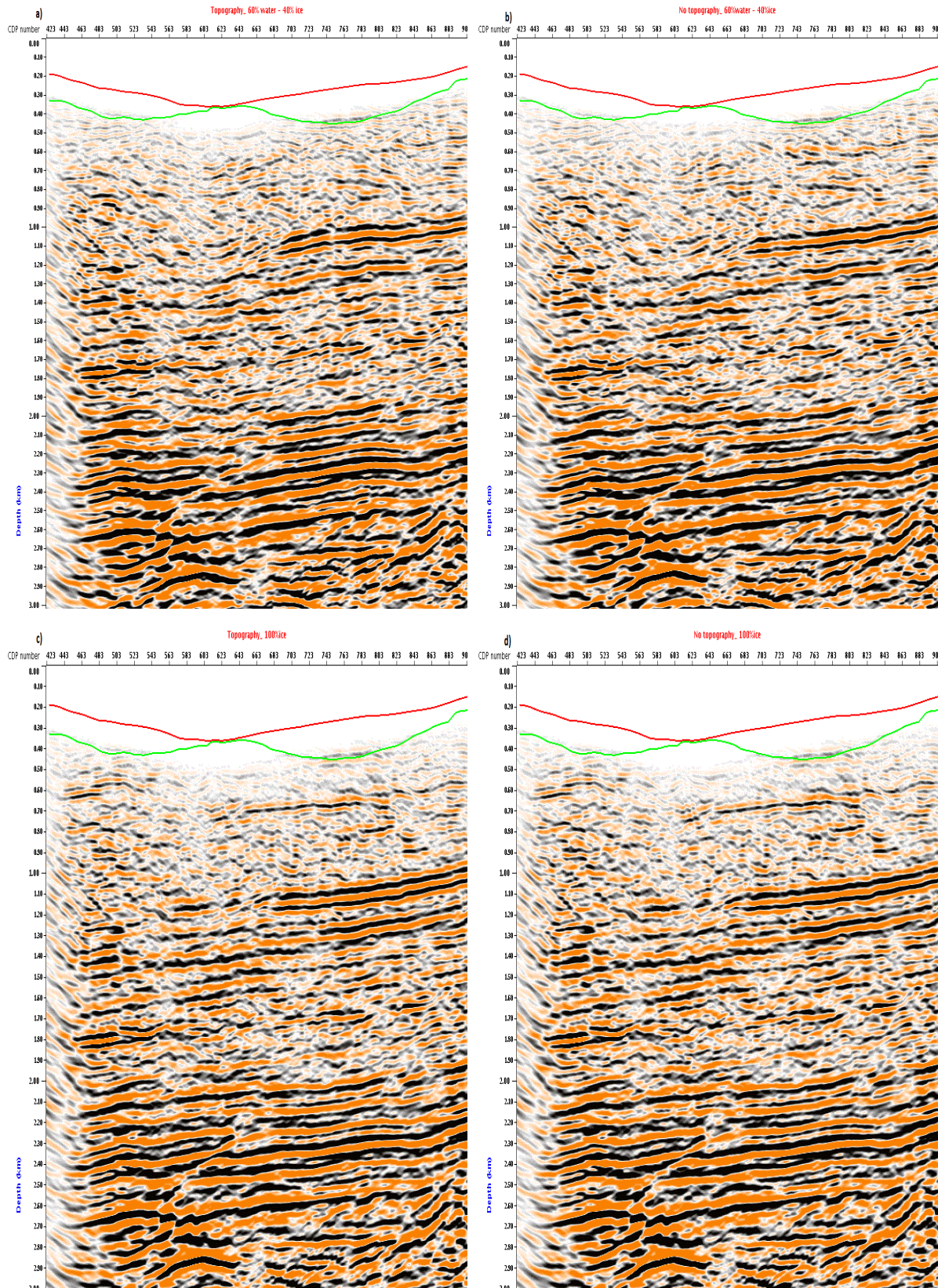


Figure C2: a) and c) show the seismic sections that include the permafrost distribution, while b) and d) show the two that don't include the distribution. a) and b) is the scenario with 40% ice and 60% water saturation, while c) and d) are 100% ice. The differences are insignificant, thus not marked with arrows.